

**AN INTERNATIONAL FORUM FOR THE RAPID PUBLICATION OF
ORIGINAL SCIENTIFIC ARTICLES DEALING WITH SCIENCES AND
RELATED INTERDISCIPLINARY AREAS**



SOUTHERN
JOURNAL OF SCIENCES

ESTABLISHED IN 1993

Formerly known as the Southern Brazilian Journal of Chemistry

VOLUME THIRTY, NUMBER THIRTY-THREE

ISSN: 2764-5967 - E-ISSN: 2764-5959

JUNE– 2022

Former Printed ISSN: 0104-5431 and E-ISSN: 2674-6891

SOUTHERN JOURNAL OF SCIENCES

ISSN: 2764-5967

E-ISSN: 2764-5959

Volume 30

Number 33

2022

Dados Internacionais de Catalogação na Publicação (CIP)

S727 Southern Journal of Sciences [recurso eletrônico] :
interdisciplinary path for scientific divulgation / Dr. D.
Scientific Consulting. – (Fev. 2022). – Dados eletrônicos. –
Nova Prata. : Dr. D. Scientific Consulting, 2022-.

Semestral

Recurso on-line

Descrição baseada em: Vol. 30, n. 33 (JUN. 2022)

Formerly known as: Southern Brazilian Journal of
Chemistry

Modo de acesso: < <https://sjofsciences.com> >.

E-ISSN: 2764-5959

ISSN: 2764-5967

1. Química. 2. Física. 3. Biologia. 4. Ciências Naturais. 5.
Farmacologia. 6. Ciências exatas. 7. Ciências aplicadas. 8.
Ciências. I. Dr. D. Scientific Consulting.

UDC 001

Bibliotecário Responsável

Ednei de Freitas Silveira

CRB 10/1262

Journal E-mail: southbchem@gmail.com

SOUTHERN JOURNAL OF SCIENCES

ISSN: 2764-5967

E-ISSN: 2764-5959

Volume 30

Number 33

2022

Editorial Board

Editor-in-Chief

- Walter José Peláez, Ph.D., walter.pelaez@unc.edu.ar, Argentina, UNC.

Assistant Editors

- Ketevan Kupatadze, Ph.D., ketevan_kupatadze@iliauni.edu, Georgia, ISU.
- Shaima R. Banoon, MsC., shimarb@uomisan.edu.iq, Iraq, University of Misan.
- Cristián Andrés Quintero, Ph.D., cquintero@umaza.edu.ar, Argentina, Universidad Juan Agustín Maza.
- Aline Maria dos Santos, Ph.D., aline.santos@ifrj.edu.br Brazil, IFRJ.
- Cristiane de Souza Siqueira Pereira, Ph.D., cristiane.pereira@universidadedevassouras.edu.br Brazil, Universidade de Vassouras.

General secretary

- Luis Alcides Brandini De Boni, Ph.D., labdeboni@gmail.com, Brazil, TQG;

Scientific Council

- Teresa M. Roseiro Maria Estronca, Ph.D., troseiro@ci.uc.pt, UC, Portugal.
- Rafael Rodrigues de Oliveira, Ph.D., rafa_rdo@yahoo.com.br, Neoprospecta, Brazil.
- Eduardo Goldani, Ph.D., eduardogoldani@gmail.com, Brazil, TQG;
- Marcos Antônio Klunk, Ph.D., marcosak@edu.unisinos.br, UNISINOS, Brazil.
- Francisco José Santos Lima, Ph.D., limafjs@yahoo.com, UFRN, Brazil.
- Monica Regina da Costa Marques, Ph.D., mmarquesrj@gmail.com, UERJ, Brazil.
- Rodrigo Brambilla, Ph.D., kigobrambilla@gmail.com, UFRGS, Brazil.
- Gabriel Rubensam, Me., rubensam_quimico@hotmail.com, PUCRS, Brazil.
- Andrian Saputra, Ph.D., andriansaputra@fkip.unila.ac.id, University of Lampung, Indonesia.
- Zhanar Zhumadilova, Ph.D., zhanar_85@mail.ru, Satbayev University, Kazakhstan.

- Roberto Fernandez, Ph.D., rfernandezm@unicartagena.edu.co, Universidad de Cartagena, Colombia.
- Andrey Vladimirovich Sevbitov, Ph.D., avsevbitov@mail.ru, I. M. Sechenov First Moscow State Medical University, Russian Federation.
- Jorge Fernando Silva de Menezes, Ph.D., jorge_fernando@ufrb.edu.br, UFRB, Brazil.
- Paulo Sergio Souza, Ph.D., Brazil, paulosergio@fosorio.g12.br, Brazil, Fundação Osorio.
- Alessandra Deise Sebben, PhD., adsebben@gmail.com, Brazil
- Fredy Hernán Martínez Sarmiento, PhD., fhmartinezs@udistrital.edu.co, UD-FJC, Colombia.
- Fabiana de Carvalho Fim, PhD., fabianafim@ct.ufpb.br, UFPB, Brazil.
- Mariana Babilone de S. Ferreira, MsC., mariana.babilone@prof.una.br, UNA, Brazil.
- Flavia Maria Pompeia Cavalcanti, MsC., flaviamaria@upf.br, Brazil, UPF.
- Gustavo Guthmann Pesenatto, MD., gustavoggp@gmail.com, Primary Health Care, Brazil.
- Fábio Herrmann, MD., fabioherrmannfh@gmail.com, Santa Casa de Misericórdia de Porto Alegre Hospital, Brazil.
- Marco Antonio Smiderle Gelain, MD., marco_gelain@hotmail.com, Dante Pazzanese Cardiology Institute, São Paulo - Brazil.
- Rene Francisco Boschi Gonçalves, Ph.D., renefbg@gmail.com, Technological Institute of Aeronautics - ITA, Brazil.
- Élcio J. de Oliveira, Ph.D., INNOSPACE, Korea/Brazil
- Ademir Oliveira da Silva, Ph.D., aosquimica@gmail.com, Federal University of Rio Grande do Norte - UFRN, Brazil.
- Francisco José Santos Lima, Ph.D., limafjs@yahoo.com, Federal University of Rio Grande do Norte - UFRN, Brazil.
- Anton Timoshin, Ph.D., anton-timoshin007@yandex.ru, I. M. Sechenov First Moscow State Medical University, Russian Federation.
- Intisar Razzaq Sharba, Ph.D., intisar.sharba@uokufa.edu.iq, University of Kufa, Iraq.
- Paulo Roberto Barros Gomes, Ph.D., prbgomes@yahoo.com.br, Federal Institute of Technical Education of Pará - IFPA, Brazil.
- Ingrid Grazielle Sousa, M.sc., indi.sousa@gmail.com, Ph.D. candidate at Unicamp, Brazil.
- Nicholas Karasavvidis M. Sc., nick.kara014@gmail.com, University of Sydney, Australia.

SOUTHERN JOURNAL OF SCIENCES

ISSN: 2764-5959 (Online)

ISSN: 2764-5967 (Print)

DOI: 10.48141/2764-5959

Digital preservation: Portico

Former Southern Brazilian Journal of Chemistry

Former E-ISSN 2674-6891

Former ISSN 0104-5431

Available at

<https://sjofsciences.com>

Mission

The **SOUTHERN JOURNAL OF SCIENCES** is a double-blind peer review, open access, **multidisciplinary** Journal dedicated to publishing high-quality content and is intended to fill a gap in terms of scientific information for Southern Brazil. We have set high standards for the articles to be published by ensuring strong but fair refereeing by at least two reviewers. The Journal publishes original research articles in all the fields of Engineering, Mathematics, physics, Chemistry, Biology, Agriculture, Natural resource management, Pharmacy, Medicine, and others.

Occasionally the Journal will include review papers, interviews, and other types of communications. It will be published mainly in English, and at present, there are no page charges.

We hope this Journal will provide a forum for disseminating high-quality research in Science and are open to any questions and suggestions.

The responsibility for the articles is exclusive to the authors.

Subjects List

UDC 001

Correspondências

Av. Carlos Tarasconi, 281/202.

Bairro Sagrada Família. CEP: 95320-000

Nova Prata – RS. Brasil.

www.sjofsciences.com

southbchem@gmail.com

INDEX OF THE ISSUE NUMBER 33

ISSN: 2764-5967

E-ISSN: 2764-5959

Volume 30

2022

<p><u>1. Editor note</u></p> <p style="text-align: center;">Argentina</p> <p style="text-align: center;">Dr. Walter Pelaez, UNC.</p> <p>Pg. 01</p>	<p><u>2. Journal news (A)</u></p> <p style="text-align: center;">Brazil / Argentina</p> <p>Introduction of an additional template file, to properly support review manuscripts.</p> <p>Pg. 02</p>
<p><u>3. Journal news (B)</u></p> <p style="text-align: center;">Brazil / Argentina</p> <p style="text-align: center;">New tool to assist the authors in the production of the abstract section. A. M. T.</p> <p>Pg. 05</p>	<p><u>4. Original research paper</u></p> <p>LIMA, Francisco José Santos; PESSOA, Maria José de Oliveira; ARAÚJO, Lucas da Silva; SILVA, Ademir Oliveira da, and PEREIRA, Francisco Claudece.</p> <p style="text-align: center;">Brazil</p> <p style="text-align: center;">MOLECULAR MODELING, REACTIVITY PARAMETERS, AND SPECTROCHEMIC STUDIES OF ϵ-CAPROLACTAM AND <i>o</i>-PHENANTROLINE</p> <p>Pg. 08</p>
<p><u>5. Original research paper</u></p> <p>BABATUNDE, Esther Olubunmi; ADERIBIGBE, Fatai Alade; JOSEPH Isaac Adekunle; ARE, Comfort Temitope; PAUL-LASISI Joshua Oluwatobi</p> <p style="text-align: center;">Nigeria</p> <p style="text-align: center;">SYNTHESIS OF ZIRCONIUM OXIDE CATALYST SUPPORTED ON CARBONIZED MATERIAL FOR THE OPTIMIZATION OF BIODIESEL FROM WASTE VEGETABLE OIL</p> <p>Pg. 18</p>	<p><u>6. Original research paper</u></p> <p>AJALA, Mary Adejoke; ABDULKAREEM, Ambali Saka; KOVO, Abdulsalami Sanni; TIJANI, Jimoh Oladejo; AJALA, Olawale Elijah</p> <p style="text-align: center;">Nigeria</p> <p style="text-align: center;">ADSORPTION STUDIES OF ZINC, COPPER, AND LEAD IONS FROM PHARMACEUTICAL WASTEWATER ONTO SILVER-MODIFIED CLAY ADSORBENT</p> <p>Pg. 28</p>
<p><u>7. Original research paper</u></p> <p>ORYNBEKOV, Yelzhan S.; ZHUMADILOVA, Zhanar O.; SELYAEV, Vladimir P.; NURLYBAEV, Ruslan E.; SANGULOVA, Indira B.</p> <p style="text-align: center;">Kazakhstan</p> <p style="text-align: center;">THE INFLUENCE OF CLIMATIC FACTORS ON THE CHANGE IN THE ELASTIC-STRENGTH INDICATORS OF EPOXY POLYMERS BINDERS USED IN LIQUID THERMAL INSULATION COATINGS</p> <p>Pg. 44</p>	<p><u>8. Original research paper</u></p> <p>PERLBACH, Agostina; ROMANO, Mariana; DINAMARCA, Sofia; BUONFIGLI, Julio; QUINTERO, Cristián Andrés</p> <p style="text-align: center;">Argentina</p> <p style="text-align: center;">SURVEY ON KNOWLEDGE OF SEXUALLY TRANSMITTED INFECTIONS AND GONORRHEA: DO WE KNOW ENOUGH?</p> <p>Pg. 54</p>

9. Original research paper

JOSEPH, Isaac Adekunle; AJALA, Elijah Olawale;
AHMED, El-Imam Amina; AJALA, Mary Ajoke

Nigeria

**OPTIMIZATION AND KINETICS STUDIES
OF THE DISSOLUTION OF DOLOMITE IN
SULPHURIC ACID (H₂SO₄) VIA BOX-
BEHNKEN EXPERIMENTAL DESIGN**

Pg. 69

10. Journal news (C)

Brazil / Argentina

RESULTS OF THE 21SCON.ORG

*Conference to celebrate the 30 years
of the Southern Brazilian Journal of
Chemistry, and its transformation into
the Southern Journal of Sciences*

Pg. 82

For the most updated information, please visit the website of the Journal at
<https://sjofsciences.com/>

EVOLUTION 2022,

Did you know that we are constantly adapting?. Adaptation is a form of evolution. It is a natural process that selects the best of each species and takes it to its maximum expression. This has been happening since time immemorial, and it will always happen, it is an event that ensures the survival of a species by maintaining the characteristics that make its individuals stronger and more resilient, in short, adaptation and evolution ensure subsistence.

This event does not leave scientific journals exempt, where evolution and changes occur not only to give the possibility to all scientists to express themselves and be recognized in the world for their work but also so that knowledge can be shared, disseminated, and used for the general good of all individuals in society.

Because of this, the SOUTHERN BRAZILIAN JOURNAL OF CHEMISTRY has grown up and is now called the SOUTHERN JOURNAL OF SCIENCES. This change leads us to expand and now publish high-impact scientific papers in different fields of Exact Sciences, which as a whole will be a reservoir and source of knowledge of greater utility.

Faced with this event, we should not be afraid, and scientific life is full of changes, we just have to accept that today's reality is different from yesterday's and that to stand out, we have to be able to leave footprints that will serve as a guide for future generations.



Dr. Walter J. Peláez
Editor-in-chief

NEW TEMPLATE FILE FOR REVIEW PAPERS

For the first time in about 30 years, the journal staff has decided to make a new and specific template file. This file is intended to make the publication of review manuscripts more homogeneous. The journal staff is aware that there are several ways to present a review manuscript, and it is not claiming that this is the best format, just that it is a suitable format and allows the readers to have a reasonable understanding of how the authors conducted the review research. The new file was included in the compressed file that the authors downloaded to access the template and the cover letter, and its use will be mandatory for the review papers in the second semester of 2022.

Figure 1 shows the abstract section, with some new sample text highlighted in yellow. In addition, it has a tip with a link to the Abstract Maker Tool.

SOUTHERN JOURNAL OF SCIENCES
ESTABLISHED IN 1993

Review paper

TITLE IN CAPITAL LETTERS (ARIAL, FONT SIZE 12, BOLD)

DE BONI, Luis Alcides Brandini^{1*}; GOLDANI, Eduardo²; CASTILHOS, João³;

^{1,2}University name, Faculty or Institute name, Department name. Country.

³Universidade Federal do Ceará, Instituto de Química, Departamento de Físico-Química. **Brazil, (Example)**

* Corresponding author
e-mail: fulanodetal@tchequimica.iq.br

Received 12 June 2022; received in revised form 30 November 2022; accepted 14 December 2022

ABSTRACT

TIP: Consider using the **Abstract Maker Tool** to create this section. The tool is available at <https://www.sjofsciences.com/Abstract-maker.php>

Background: Introduction and problem statement; identify the need for the research question. Rigorous research may include a hypothesis that is supported or refuted accordingly. What is the subject and relevance of the study? What does it intend to demonstrate or describe? This should be written succinctly; it might be eventually necessary to refer briefly to a context. What is the importance of the research? Why would a reader be interested in the larger work? The background (introduction) must clearly state the problem, the reason for doing the work, the hypotheses or theoretical predictions under consideration, and the essential background. **Aim:** the purpose of the work (objective); What is the aim of the study? The exact question(s) addressed by the article; the primary objective of the review. Begin with a clear, concise statement of the precise objective or question addressed in the manuscript. If more than 1 objective is addressed, the main objective should be indicated, and only key secondary objectives stated. If an a priori hypothesis was tested, it should be stated. Example: This study aimed to...or...The purpose of this study was to... **Methods:** **Name the databases that were used in the research. What were the main terms used in the research?** Criteria for maintaining a manuscript in the research, criteria for exclusion. The basic design of the study; state the duration of follow-up, if any; explain the methods so others can replicate the study. How are the objectives achieved? Include the main method(s) used for the research; data collection - describes the process and points out potential omissions; What is the study method? Show the methodology used, the form of data, and sample collection. If it is a theoretical essay, what is the approach adopted. Provide sufficient details to the reader to understand how the study was performed. **Results and Discussion:** **How many results did the search terms return in the databases? How many results were maintained in the study? Discuss the main results. How many are in agreement?** The purpose of a Results and Discussion section is to present the key results of your research. What are the main results? The main outcomes of the study should be provided and quantified, including confidence intervals or P values. For comparative studies, confidence intervals should relate to the differences between groups. Results should be presented concisely. Point out the significance of the results, and place the results in the context of other work and theoretical backgrounds. It is important to plan this section carefully as it may contain a large amount of scientific data that needs to be presented clearly and concisely. **Conclusions:** Provide only conclusions directly supported by the results; avoid speculation and overgeneralization. Indicate whether additional study is required; Give equal emphasis to positive and negative findings of equal scientific merit; point out things that may have been overlooked, and suggests areas for further research. Summary of your research.

Keywords: Authors should provide appropriate and short keywords that encapsulate the principal topics of the paper. *The maximum number of keywords is 5* not including items appearing in the title. The keywords should be supplied, indicating the scope of the paper. Size 10, italic, justify, only the word Keywords must be bold, left alignment.

1. INTRODUCTION

A review paper can be presented in a wide variety of formats. This template is by far not perfect, but it was created to provide some directions of the minimal components that the authors should include in a review paper to make it relevant, clear, reliable, and verifiable.

SOUTHERN JOURNAL OF SCIENCES
E-ISSN 2764-5959 vol.30 n°33 2022 Established in 1993 © The Author(s) 2022

Figure 1. Abstract section with additional sample text.

The materials and methods section was simplified to just methods (section 2), as presented in Figure 2. Some sample text was introduced to assist the authors in the description of where the research

was conducted. In addition, a suggestion was introduced to present the inclusion and exclusion criteria for the manuscripts.

As the author, you are not forced to follow these orientations, but we are not obligated to publish manuscripts that are considered substandard. So please consider the quality of your research prior to any submission to this journal. This template model structure is mandatory from December 2022 and on.

The spacing between paragraphs should be 0pt, then 6pt, and single spacing between lines.

The body text can be written in Brazilian Portuguese.

The introduction must clearly state the problem, the reason for doing the work, the hypotheses or theoretical predictions under consideration, and the essential background. It should not contain equations or mathematical notation. A brief survey of the relevant literature so that a non-specialist reader could understand the significance of the presented results.

Page size: A4, margins: 2 cm on each side, line spacing: single, font type: Arial. Font size: 11. Please leave headers and footers unchanged since the editors should fill it.

In the text, references should be cited in the APA style (Author, year). Alternatively, the author's surname may be integrated into the text, followed by the year of publication in parentheses. Cite only essential resources, and avoid citing unpublished material. References to papers "in the press" must mean that the article has been accepted for publication. At the end of the paper, list references alphabetically by the last name of the first author. Please, list only those references that are cited in the text and prepare this list as an automatically numbered list. The word References with size 12, bold, capital letters, left alignment.

Examples: Grasslands are regarded as important foraging areas for many insectivores in Europe, such as birds (Vichery, 2001; Barnet *et al.*, 2004) and bats (Güttinger, 1997) or amphibians and reptiles (Langton and Burton, 1997). However, the knowledge of the overall arthropod availability in such grasslands is scarce since many studies about insect populations concentrate on extensive grasslands on poor, dry, or wet soils and include only a few species or systematic groups (Ellsen *et al.*, 1997; Gibson *et al.*, 1992; Hänsel and Plachter, 2004; Manhart *et al.*, 2004; Krüss and Tschamke, 2002a, b; Wingerden *et al.*, 1992; Sjödin, 2007a, b; Perner *et al.*, 2005).

Carbon dioxide produced by the

biodiesel combustion on the greenhouse effect (Könitz, 1999; Agarwal and Das, 2001). In addition, biodiesel has a relatively high flash point (150 °C), which makes it less volatile and safer to transport or handle than petroleum diesel (Krawczyk, 1996).

2. METHODS

Provide sufficient details to permit repetition of the experimental work. The technical description of methods should be given when such methods are new.

Within each main section, three levels of subheadings are available, and the titles must be bold, bold, and italic, italic, respectively. Font size: 10.

2.1. Methods

Present the main methodology used in this section. Remember to include the references to the methods.

(sample text) This research was conducted in the databases of Scopus, WoS, Google Patentes, and the library X....

The keywords or terms used in the search were "A", "b", "c".....

The logical operators used in the search were AND, OR, XOR... In addition, the search used the terms individually and in combination....

2.2.1. Method A...

Criteria to maintain results in the search....

Criteria to exclude the results....

2.2.2. Method B...

2.1. Subheadings

2.1.1 Subheadings

2.1.1.1 Subheadings

Examples:

2.1. Materials or Samples or Participants

Figure 2. New methods section

The section Results and Discussion have also received some sample text to make it easier for the authors to present the research results. The suggested tables in Figure 3 turn the expression of the results straightforward (section 3.1).

And section 3.2, the discussion section, can receive a great amount of content and the authors' review notes regarding the results.

2.2. Groups of Study or Study Design or.....

2.3. Methods or Experimental procedures or....

2.4. Data Collection

2.5. Statistical Analysis or Data Analysis

2.6. Ethics or Ethical Guidelines

2.7. Other items that the authors deem necessary and relevant

Mathematical expressions: In general minimize unusual typographical requirements, use solidus, built-up fractions. Avoid lengthy equations that will take several lines (possibly by defining terms of the equation in separate displays). Please use the Equation Editor of Word for drawing equations, if possible. Make subscripts and superscripts clear. Display only those mathematical expressions that must be numbered for later reference or that need to be emphasized throughout the paper. The numbers should be placed in parentheses to the right of Equation 1 e.g., (Eq. 1).

$$3x^3 + 2x^2 + 5x + 6$$

(Eq. 1)

3. RESULTS AND DISCUSSION

3.1. Results

Results should be presented concisely.

A table is a good way to present the results

Table 1. Example of a simple search result table

Term	Database	Results	Exclusions
"A"	Scopus	1	1
	DOAJ	5	3
	WoS	3	2
"B"	Scopus	6	0
	DOAJ	3	1
	WoS	5	2
"C"	Scopus	8	5
	DOAJ	2	0
	WoS	4	1

Table 2. Example of a combined search result table

Term	Database	Results	Exclusions
"A" AND	ScienceDirect	1	1
	DOAJ	5	3
"B"	WoS	3	2
	ScienceDirect	6	0
"A" AND "C"	DOAJ	3	1
	WoS	5	2
"B" AND "B"	ScienceDirect	8	5
	DOAJ	2	0
	WoS	4	1

3.2. Discussions

Discussion of the results. Point out the significance of the results and place the results in

SOUTHERN JOURNAL OF SCIENCES

Figure 3. New sample text for the "results and discussion" sections.

This new template format will evolve in the next couple of months to provide a better publication experience for the authors. At the same time, it provides a more robust environment for the review papers. Suggestions and comments on this new template can be addressed to the journal e-mail at southbchem@gmail.com.

In addition, the journal staff agrees that this conceptual format of the publication is Open Access, and other journals can freely use it.

This article is licensed under a Creative Commons Attribution 4.0 (CC BY 4.0) International License, which permits use, sharing, adaptation, distribution, and reproduction in any medium or format, as long as you give appropriate credit to the original author(s) and the source, provide a link to the Creative Commons license, and indicate if changes were made. The images or other third-party material in this article are included in the article's Creative Commons license unless indicated otherwise in a credit line to the material. If material is not included in the article's Creative Commons license and your intended use is not permitted by statutory regulation or exceeds the permitted use, you will need to obtain permission directly from the copyright holder. To view a copy of this license, visit <http://creativecommons.org/licenses/by/4.0/>.

Dr. Walter J. Peláez
Editor-in-chief

Dr. Luis A. B. De Boni.
General secretary.

ABSTRACT MAKER TOOL (A. M. T.)

There are different ways that the authors can present the abstract of a manuscript. However, with the evolution of the journal and the passing of time, the Southern Journal of Sciences adopted the structured format of the abstract.

The structured abstract is intended to be comprehensive, providing a logical order for the presentation of scientific communication. It also provides the readers with a summary of the research background, objectives, methods, results, and conclusions. It is not complicated to do, but frequently the authors may forget to include parts of its content; therefore, this tool was developed, so the authors can enjoy the writing of the abstract in a very straightforward way.

When exploring the environment of the A. M. T. (script version 1.0), the authors will initially find a collection of text boxes to include the proper text(background, aims...), as in Figure 1.

The screenshot displays the 'Abstract maker tool' interface. At the top, the title 'Abstract maker tool' is centered. Below it, a message reads: 'Please fill in the boxes below to prepare an abstract. It is easy as 1, 2, and 3! At this time this tool is only available in English.' A red '(Step 1):' label precedes the instruction: 'Please, type the sections of the abstract in the boxes below.' Three text input fields are arranged vertically. The first is labeled 'Background:' and contains the placeholder text 'Describe the Background/Introduction here...'. The second is labeled 'Aims:' and contains 'Describe the Aims of the research here...'. The third is labeled 'Methods:' and contains 'Describe the Methods here...'. Each field has a small green 'G' icon in the bottom right corner, likely representing a Google search or spellcheck integration.

Figure 1. Textfield introduction areas for the abstract maker tool.

If the authors have a browser with a dictionary or spellchecker installed, recommendations for text corrections will be made available instantaneously.

Southern Journal of Sciences recommends that the abstract section should have around 250 and 350 words. The word counter box also allows text edition, making the adjustments faster.

(Step 3). Please copy and paste the text from step 2 in the textbox below to automatically count the words.

A screenshot of a word counter interface. It features a large text area with a blue border and a vertical scrollbar on the right. The text area contains several lines of placeholder text: "Sample dummy text Sample dummy text Sample dummy text", "Sample dummy text Sample dummy text Sample dummy text", "Sample dummy text Sample dummy text Sample dummy text", "Sample dummy text Conclusions: Sample dummy text Sample", "dummy text Sample dummy text Sample dummy text Sample", "dummy text Sample dummy text Sample dummy text Sample", "dummy text Sample dummy text Sample dummy text Sample", "dummy text Sample dummy text Sample dummy text Sample", "dummy text Sample dummy text Sample dummy text Sample", "dummy text Sample dummy text Sample dummy text Sample", "dummy text Sample dummy text Sample dummy text". The text ends with a cursor. To the right of the text area is a vertical scrollbar with up and down arrows and a diagonal line at the bottom.

If the Word Count is among 250 and 350 congratulations, you may have done a great work.

Word Count: 295

Figure 4. Word counter box.

If the authors are satisfied with the results, they can copy and paste the abstract directly into the journal template file. Therefore, this tool assists the authors in the production of a complete, proportional, and structured abstract, making the submission and review process faster. The tool is freely available at <https://www.sjofsciences.com/Abstract-maker.php>.

Dr. Luis A. B. De Boni.
General secretary.

MOLECULAR MODELING, REACTIVITY PARAMETERS, AND SPECTROCHEMIC STUDIES OF ϵ -CAPROLACTAM AND o-PHENANTHROLINE

LIMA, Francisco José Santos*; PESSOA, Maria José de Oliveira; ARAÚJO, Lucas da Silva; SILVA, Ademir Oliveira da, and PEREIRA, Francisco Claudece.

Universidade Federal do Rio Grande do Norte, Centro de Ciências Exatas, Instituto de Química, Brazil

* Corresponding author
e-mail: limafjs@yahoo.com

Received 06 March 2022; received in revised form 22 May 2022; accepted 16 June 2022

ABSTRACT

Background: Recently, research has been carried out to improve the efficiency of electronic devices in general. With the commercial search for consolidated materials and the growth in demand with monitoring of costs, research has sought to minimize these effects with the replacement or functionalization of other substances, which may be applied at lower costs without compromising operating yields already achieved. **Objective:** This work aimed to obtain molecular modeling and reactivity parameters of ϵ -caprolactam and o-phenanthroline to evaluate the interaction capacity in the formation of molecular systems. Conductance measurements were taken to observe the electrolytic behavior. Infrared and UV-visible spectra were recorded to characterize vibrational transitions and evaluate spectrochemical properties. **Methods:** The WebLab[®] program was used to obtain structural data and calculate reactivity parameters. Conductance was obtained in QUIMIS Q-405 equipment. IR spectra were recorded on PERKIN ELMER FRONTIER equipment. UV-vis spectra were recorded in a SHIMADZU equipment 200 – 1000 nm range to record the main transitions. **Results and Discussions:** Electron donor atoms are centered mainly on oxygen and nitrogen, respectively, which are sterically more favorable. The behavior was non-electrolyte. Groups with vibrational transitions sensitive to chemical interactions are comprised of C=N, C-N, and C=O bonds. The ϵ parameter indicates transitions in the 190 – 300 nm region and the near-infrared, and the oscillator strength is typical of molecules used as dyes and sensitizers in optical light-emitting systems or light-to-electricity converters. **Conclusions:** We observed that these ligands have a donor capacity for the formation of complex systems that meet the need for electron transfer in optical pumping devices for the intensification of transitions or radiation converters, which can also be applied in radiation-to-electricity converter systems.

KEYWORDS: oscillator strength, transition dipole moment, spectrochemical properties.

1. INTRODUCTION:

ϵ -caprolactam is a cyclic chain amine that has molecular formula $C_6H_{11}NO$, molar mass 113.16 g/mol, soluble in water (50 mg/mL), which in aqueous solution has a pH between 7.0 - 8.5 (333 g/L) (Sigma-Aldrich, 2021). In the chemical industry, it has been used as a precursor of polymers called nylon 6 (Bomfim *et al.*, 2009). It has also been used in the synthesis of polymeric polyamide composites (Gong and Yang, 2010), in thermodynamic evaluations of uses in photochemical-photovoltaic-thermochemical (CP-PV-T) systems in the use of high-efficiency full-spectrum solar energy (Fang *et al.*, 2010), as well as its derivatives, (N-methyl- ϵ -caprolactam) in the

synthesis of light-emitting compounds (Borges *et al.* 2016). As a ligand in coordination compounds, according to studies, it can be observed that, due to the delocalization of the unbound electron pair from nitrogen, oxygen behaves as a donor group and is the main binding point of the molecule (Alvarez, 1998; Cardoso *et al.*, 2007). Figure 01 illustrates the modeling for ϵ -caprolactam. It is possible to see a specific steric impediment to forming a metal-ligand bond by the unbound electron pair of the nitrogen atom. At the same time, oxygen has two unbound electron pairs and a privileged position in the molecule's boundary orbitals.

O-phenanthroline, also called 1,10-phenanthroline, is a solid, white, organic

heterocyclic compound with the molecular formula $C_{12}H_8N_2$, the molar mass of 180.21 g/mol, and has a solubility of 3.3 g/L (25 °C) in monohydrated form (Merck, 2021) and has been used as a bidentate binder in coordination chemistry, where it is commonly used as a chelating agent for metallic ions (Vogel *et al.*, 1981, Huhey, 1983; Greenwood and Earnshaw, 1986; Cotton and Wilkinson, 1988; Vasconcelos, 2019). The bond strength of o-phenanthroline with metals also comes from its ability as an π electron receptor, which contributes enthalpically to the formation of stable complexes (Maldonado, 2017). In Figure 02, the modeling for orthophenanthroline can be seen. Although 1,10-phenanthroline is widely used for fast, flexible, and reliable analysis with a high scientific reputation in research, other applications are found, such as; using cathodic protective buffer layers as a conventional binder to improve the efficiency of organic solar cells (Sun *et al.*, 2014), in the study of efficacy in the Luminol chemiluminescence system in Fenton reactions (Mitsuhiro *et al.*, 2014), in complex systems with Cu(I) using mixed ligands to amplify luminescent radiative emissions by electron transfer with a high quantum efficiency (Li *et al.*, 2012), in complexes with Cu^{2+} and Pt^{2+} that have antimicrobial properties (Neville *et al.*, 2013), in geomicrobiology as an indicator of Fe^{2+} in microbial activities in terrestrial and interstellar minerals (Notini *et al.*, 2019), among others that enrich the national and international literature.

The importance of molecular modeling of the studied compounds is because it provides relevant structural data and better visualization of the chemical environment around these compounds. In addition, modeling is widely used to interpret experimental results and construct materials with specific properties (Coelho *et al.*, 1999; Lima¹ *et al.*, 2015; Lima² *et al.*, 2015).

The reactivity parameter has also been found to be useful in evaluating and understanding the properties of substances, facts that allow a better understanding of which metals will form more stable coordination compounds, and which location is most likely for the formation of the metal-ligand bond, which can be verified experimentally through spectrochemical studies, in addition to other techniques (Lima¹ *et al.*, 2015; Lima² *et al.*, 2015).

Molar conductivity measurements were obtained for the electrolytic evaluation of these compounds in an aqueous solution to observe what influence they could attribute to the formed complex systems (Geary, 1971; Crockford and

Knight, 1977; Belarmino, 1998; Lima *et al.*, 1998; Costa *et al.*, 2013; Lima¹ *et al.*, 2015; Lima² *et al.*, 2015).

Infrared (IR) spectroscopy is a spectroscopic technique that, in addition to identifying the structure and bonds and recognizing groups of atoms in compounds, is also used in qualitative analysis, mainly in the areas of synthesis, organic transformations, and in the chemistry of natural products (Smith, 1961; Silverstein *et al.*, 2007; Pavia *et al.*, 2010; Marin, 2013; Maciel and Filho, 2015).

The technique of the interaction of electromagnetic radiation as molecules, atoms, or ions, the technique of electronic absorption spectroscopy in the UV-vis region, is used. This technique is based on the absorption of radiation that promotes electrons from a lower energy state to another higher energy state, and it is possible to determine physicochemical properties useful in the field of scientific and technological applications (Vogel *et al.*, 1981; Moore, 1991; Silverstein *et al.*, 2007; Pavia *et al.*, 2010; Levine, 2014; LIMA *et al.*, 2017; Fang *et al.*, 2020). Furthermore, according to the literature, the electronic spectra of molecules allow evaluation of some of their spectral properties, making it possible to calculate the oscillator strength, which aims to quantify the intensity of a transition, and thus evaluate the influence of the chemical environment on the dynamics of the spectra (Drago, 1965; Figgs, 1966. Heslop and Jones, 1976; Lima *et al.*, 1996; Lima *et al.*, 2017).

Given the above, the purpose of this work was to obtain the molecular modeling, define the reactivity parameters of ϵ -caprolactam and orthophenanthroline, obtain measurements of molar conductivity, record infrared and UV-visible spectra, evaluate the spectrochemical properties related to the oscillator strength and the induced dipole moment, to sequence the investigation of their functionalities as electron donor species in compounds applied in radiation converter systems or light-to-electricity converters.

2. MATERIALS AND METHODS:

2.1 Molecular Modeling and Reactivity Parameters

Molecular modeling, theoretical reactivity parameters, electrostatic potential cloud, bonding distances, bonding angles, and partial charges were obtained from the WebLab ViewerPro©

program. The parameters were calculated using the following expression (Lima *et al.*, 2020):

$$\mathfrak{R} = \frac{\int q_i d\tau}{\sum_{i=1}^n \left| \int q_i d\tau \right|} \quad (\text{Eq. 01})$$

2.2 Conductance, Conductivity, and Molar Conductivity

Molar conductivity measurements were performed for aqueous solutions of millimolar concentration using a QUIMIS Q-405 conductivity meter at a temperature of 25.0 ± 1 °C, after calibration of the cell constant with freshly prepared standard solutions millimolar of NaCl and KCl. The molar conductivity was calculated using the expression below:

$$\Lambda_M = \frac{(L_{\text{sol}} - L_{\text{solv}}) \cdot Kc \cdot 10^3}{M} = \frac{(k_{\text{sol}} - k_{\text{solv}}) \cdot 10^3}{M}, \quad (\text{Eq. 02})$$

Table 01 – Comparative values of the type of electrolyte with acceptable ranges of molar conductivities in aqueous solution for solutions of concentration $M = 1.00 \times 10^{-3}$ mol L⁻¹ (Belarmino *et al.*, 1998; Lima *et al.*, 1998; Costa *et al.*, 2013; Lima *et al.*, 2020).

Λ_M S cm ² mol ⁻¹	Type of electrolyte $x\text{A}^+ : y\text{B}^-$ $\text{A}_x\text{B}_y \leftrightarrow x\text{A}^+ + y\text{B}^-$	Species predominant
0 - 100	Não eletrólito	A_xB_y
100 - 200	1:1	$\text{A}^+ + \text{B}^-$
200 - 300	1:2 or 2:1	$\text{A}^+ + 2\text{B}^-$ or $2\text{A}^+ + \text{B}^-$
300 - 500	1:3 or 3:1	$\text{A}^+ + 3\text{B}^-$ or $3\text{A}^+ + \text{B}^-$
500 - ?	1:4 or 4:1	$\text{A}^+ + 4\text{B}^-$ or $4\text{A}^+ + \text{B}^-$

2.3 Spectroscopy in the Infrared Region

The infrared spectra of the two samples were recorded in a PERKIN ELMER FRONTIER

equipment, in KBr pellets, in the range of 700 – 4000 cm⁻¹ and resolution of 4 cm⁻¹.

2.4 Spectroscopy in the UV-Visible Region

The UV-vis spectra were recorded in a SHIMADZU UV model spectrophotometer in the range of 200 - 1000 nm, quartz cuvette with a 1 cm optical path for aqueous ϵ -caprolactam solutions (1.18×10^{-2} mol L⁻¹), aqueous o-Phenanthroline (1.15×10^{-2} mol L⁻¹) and ethanolic o-Phenanthroline (1.01×10^{-2} mol L⁻¹). Samples needed to be diluted. The oscillator strength f was calculated by Drago's and Figs method and described methodologies (Lima *et al.*, 2020) according to the expressions:

$$\text{DRAGO: } f = 4,6 \times 10^{-9} \int \epsilon_{(\sigma)} d\sigma \quad (\text{Eq. 03})$$

$$\text{FIGGS: } f = 4,32 \times 10^{-9} \int \epsilon_{(\sigma)} d\sigma \quad (\text{Eq. 04})$$

The area under the absorption band =

$$\int A_{(\sigma)} d\sigma = A_{\text{máx}} \cdot (1/\lambda_1 - 1/\lambda_2) \quad \text{Eq. 05}$$

The importance of using the oscillator force in evaluating optical properties in spectroscopy is that there is a theoretical connection with the initial and final state wave functions of a chemical system involved in an electronic transition. The μ_{if} transition dipole, generally, is a complex vector quantity that includes some phase factors associated with the two states. The direction of its magnitude guides the polarization of a transition, which has the consequence of determining the interaction of the system with an electromagnetic wave of a certain polarization, and the square of its magnitude indicates the strength of this interaction due to the distribution of charge in the system. In a way, it is related to the initial states ψ_i and final states ψ_f , and is defined unidimensionally as:

$$\mu_{if} = \int \psi_i^* \cdot \mu_x \cdot \psi_f dx, \quad (\text{Eq. 06})$$

where

$$\mu_x = \sum_{i=1}^n e_i \cdot x_i \quad (\text{Eq. 07})$$

and e_i , it is (or are) the electron(s) involved in the transition, and x_i the displacement performed in the space provided by the system, being a measure of the dipole moment associated with

the charge displacement when there is a redistribution of an electron into a configuration, brought about by the interaction between electromagnetic radiation and matter. The oscillator strength f is associated with the three-dimensional dipole moment through the equation below,

$$f = \frac{8\pi^2 \cdot M_e \nu}{3he^2} [\mu_{xif}^2 + \mu_{yif}^2 + \mu_{zif}^2],$$

(Eq. 08)

Where M_e is the electron mass, ν the transition frequency, h the Planck constant, e the electron charge and μ_{if} the transition dipole moment in three dimensions (Kauzmann, 1957; Drago, 1965; Pitzer, 1965; Figgis, 1966; Atkins, 1990; Atkins and Friedman, 2011; Levine, 2014).

Rearranging variables and writing the transition dipole moment variation in a more simplified way for an isotropic approximation, we will have:

$$\mu_{if}^2 = \frac{3he^2}{8\pi^2 \cdot M_e \nu} \cdot f \rightarrow$$

$$\mu_{if} = 8,422 \times 10^{-22} (\text{m s}^{-1/2} \text{C}) \cdot \sqrt{\frac{f}{\nu}} \quad (\text{C m})$$

(Eq. 09)

This expression allows, in these terms, to evaluate the experimental transition dipole moment from the oscillator strength and the transition frequency corresponding to the maximum of the absorption band (or the transition barycenter) and certainly takes with it the contributions of the transfer mechanisms of charge (electric dipole moment, magnetic dipole and electric quadrupole), which contribute to its occurrence.

One of the direct applications mentioned in the literature of the dipole moment is that it can be related to; (1) the extent to which an intramolecular bond is polarized and (2) with a more detailed understanding of the geometry of molecules, as mentioned by some researchers (Moore, 1991). In the case of this work, the induced dipole moment can guide us concerning the reactivity of the binding groups that we intend to manipulate in the formation of complex chemical systems, especially the lower energy transitions that certain molecules present in their

spectra, which reveals, in some magnitude, the ease or difficulty of polarizing its electrons situated in the molecule's boundary orbitals, where the most important chemical interactions that precede bond formation or electron transfer in electronic devices usually occur.

From the UV-vis electronic spectra of solutions of ϵ -caprolactam and o-phenanthroline compounds, the oscillator strength is calculated by the Gaussian (or half-band) method and by applying the expressions described by Drago and Figgs (Drago, 1965; Figgs, 1966; Barrow, 1982), it was possible to evaluate the transition dipole moment, also called the induced dipole moment, for the transitions resolved in the electronic absorption bands, recorded and shown in Figure 05. This magnitude reveals the connection that exists with the system's wave functions, modified by the interaction of electromagnetic radiation with the chemical environment of the compounds under the influence of the solvents chosen for this study in the first analysis, and indeed, the same ones that will be used in the synthesis of the alleged complexed systems in the adducts, to assess their understanding in the chemical modification of the spectroscopic properties of these and others similar, with potential application in light-emitting devices and radiation-to-electricity converters, such as those mentioned in the literature.

3. RESULTS AND DISCUSSION:

3.1 Molecular modeling, obtaining structural data and reactivity parameters.

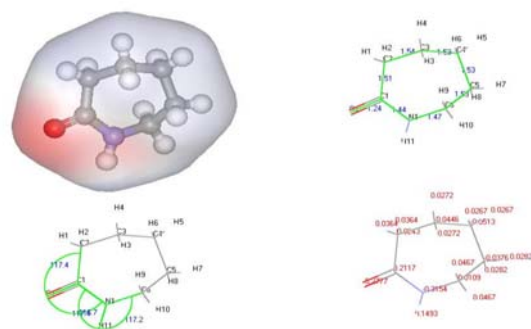


Figure 01 - Modeling obtained for ϵ -Caprolactam, $C_6H_{11}NO$, using the WebLab ViewerPro program®.

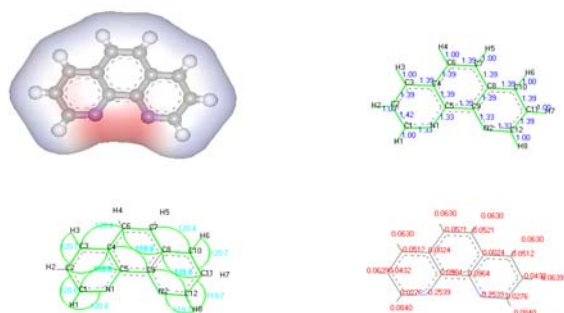


Figure 02 - Modeling obtained for o-Phenanthroline, $C_{12}H_8N_2$, using the WebLab ViewerPro program®.

Table 02 - Partial charges and PRM for ϵ -Caprolactam, $C_6H_{11}NO$. (main atoms)

Atoms	Partial charges		PRM	
	δ^-	δ^+	\mathcal{R}^-	\mathcal{R}^+
O ₁	-0,2777		-0,3822	
C ₁		0,2117		0,2913
H ₁		0,0364		0,0501
H ₁₀		0,0467		0,0643
N ₁	-0,3154		-0,4341	
H ₁₁		0,1493		0,2054

PRM - Molecular Reactivity Parameters

Table 03 - Partial charges and PRM for o-Phenanthroline, $C_{12}H_8N_2$. (main atoms)

Atoms	Partial charges		PRM	
	δ^-	δ^+	\mathcal{R}^-	\mathcal{R}^+
C ₁		0,0276		0,0345
C ₁₂		0,0276		0,0345
C ₅		0,0964		0,1204
C ₉		0,0964		0,1204
N ₁	-0,2539		-0,3171	
N ₂	-0,2539		-0,3171	

PRM - Molecular Reactivity Parameters

3.2 Conductivity measurements and the associated electrolyte type.

Table 04 – Conductivities obtained for millimolar aqueous solutions at $25.0 \pm 1^\circ C$.

	k $\times 10^{-6}$	M Mol/L	Λ_M	Type of electrolyte
H ₂ O	17,6	55,5	$31,7 \times 10^{-5}$	n-electrol
NaCl	121	0,001	103,4	1:1
KCl	150	0,001	132,4	1:1
ϵ -capro	34,4	0,001	16,8	n-electrol
o-fen	33,0	0,001	15,4	n-electrol

Units: k ($S\ cm^{-1}$); Λ_M ($S\ cm^2\ mol^{-1}$)

3.3 Spectra in the infrared region.

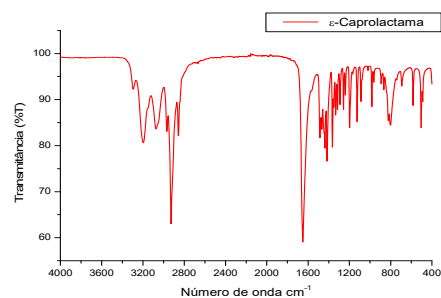


Figure 03 - Infrared spectrum of ϵ -Caprolactam

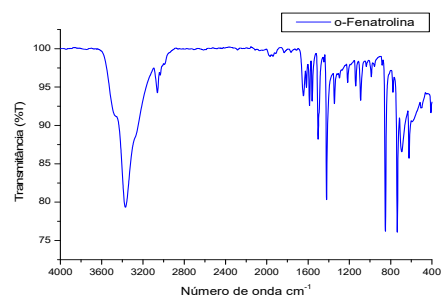


Figure 04 - Infrared spectrum of o-Phenanthroline

Table 05 - Vibrational transition assignments for ϵ -Caprolactam (main)

vib. modes	Silverstein 2007	Pavia 2010	Cardoso <i>et al</i> 2017	Exper
N-H	3350 3180	3300 3100		3294 w 3197 m 3073 m
C=O	1720 1706	1680 1630	1663	1652 s
C-N			1461	1467 m
C-N		1400		1417 m

w (weak); m (medium); s (strong)

3.4 Spectra in the UV-Visible region in aqueous and ethanolic solution.

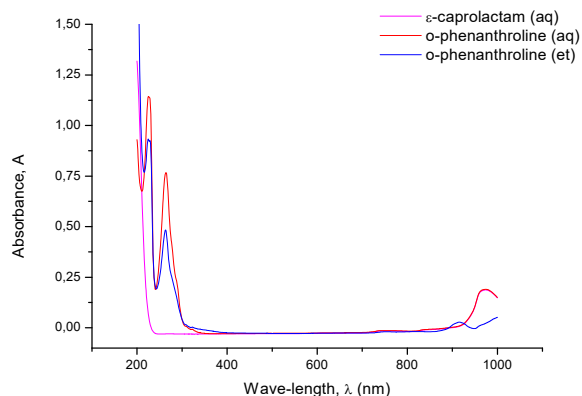


Figure 05 - UV-vis spectrum of ϵ -caprolactam and o-phenanthroline.

Table 06 - Vibrational transition assignments for o-Phenanthroline (main)

vib. modes	Smith, 1961	Martins 2010	Maciel 2015	Exper
ν C=N	1616			1616 m
ν_{sim} C=C			1600	
ν C=N	1585 1558			1586 w 1561 m
ν CC	1508			
		1501		1503 s
ν C=C	1418			
ν CN		1419		1421 s
C-N _{arom}	1340			1345 w
δ C=N		621		622 m

w (weak); m (medium); s (strong)

Table 07 - Oscillator strength and ligand transition dipole moment.

Ligand	Range Spectral (nm)	f ($\times 10^{-3}$) (adim)		μ_{if} ($\times 10^{-30}$) C m (Debye)	
		D	F	D	F
ϵ -cap (aq)	948-999	3,9	3,68	3,0 (0,90)	2,91 (0,872)
	217-234	1,5	1,44	28 (8,4)	27,7 (8,30)
o-phe (aq)	251 -278	1,2	1,11	27 (8,1)	26,4 (7,91)
	948-1000	42	39,2	9,8 (2,9)	9,50 (2,85)
o-phe (et)	215-234	1,6	1,50	29 (8,7)	28,3 (8,48)
	249-278	0,91	0,852	24 (7,2)	23,0 (6,89)
	900-930	4,5	4,22	3,1 (0,93)	3,22 (0,905)

D – Drago; F – Figgs; 1 Debye = $3,336 \times 10^{-30}$ C m (aq) aqueous solution, (et) ethanolic solution.

4. CONCLUSIONS:

Molecular modeling, partial charge δ and reactivity parameters \Re for elements with higher negative densities corroborate that these species have a Lewis base characteristic, which can function as electron donor molecules in systems that are deficient in pumping electrons, to enhance the inductive and resonance effects, to optimize preconceived chemical systems that have optical properties.

Molar conductivity measurements confirmed the non-electrolyte behavior for the compounds in an aqueous solution of ϵ -caprolactam and o-phenanthroline, as described in Table 04. These analyzes are intended to evaluate further the influence of these species on the electrochemical behavior of complex systems.

The spectra in the infrared region accurately identify these species and are presented with good resolution, which allows the characterization of these molecules present in new chemical environments to be analyzed. The transitions that occur for ϵ -caprolactam NH, C=O, CN, $CC_{(axial)}$ and $CC_{(ang)}$ at 3294, 3073, 1652, 1467, 1437, 1417, 1365, 1351, 1333, 1257, 1198, 1125, 803, 505 and 490 cm^{-1} , identified in Table 05, are particularly useful in recognizing these species for the free molecule and in complex systems. In the spectrum of orthophenanthroline, the transition at 3369 cm^{-1} is attributed to the water molecule of the o-phenanthroline monohydrate, and the transition at 3060 cm^{-1} is attributed to the ν_{sym} C-H transition. Its main C=N, CN, and C=C transitions that occur around 1645, 1616, 1421, 1420, 1345, 1217, 1139, 778, 736 cm^{-1} , shown in Table 06, are also of particular interest in recognition spectral for the free molecule as well as indicative when bound in other compounds.

The UV-vis spectra clearly show that both ϵ -caprolactam and o-phenanthroline do not absorb in the visible between 400 - 760 nm, which can be interesting in certain situations, and therefore they are white compounds in solid-state, and their solutions are colorless. However, they absorb with great intensity in the ultraviolet region in the range of 200 - 280 nm and with less intensity in the near-infrared region, in the range of 940 - 1000 nm, which can provide these species with a tendency to act as pumpers of electrons in optical devices and in complex systems, mainly due to the values obtained for

their spectrochemical parameters of molar absorptivity ϵ_{max} , oscillator strength f and transition dipole moment μ_{if} .

We observed that in these evaluated concentrations, which allowed the adequate resolution to detect the best resolution of the spectrum, the values of the induced dipole moment, obtained through the oscillator force by the half-band method using the expressions of Drago and Figgs (Drago, 1965; Figgs, 1966), guided us to state that the boundary electrons in o-phenanthroline in aqueous solution have higher values (2,9 – 2,85 Debye), than when compared to the same o-phenanthroline in solution ethanolic (0,93 – 0,905 Debye) and ϵ -caprolactam in aqueous solution (0,90 – 0,872 Debye). It is possible to conclude, based on the behavior of o-phenanthroline, that the solvent change will not only influence the dynamics of the transitions and intensities of the dipole moment but especially the chemical interactions, which may favor the application of the dipole moment of transition, as an additional or alternative parameter, for the choice of ligands and solvents, to facilitate the efficiency of electron transfer and the energy performance of some reactions, as well as help in the choice of pairs (solvents/ligands), that contribute to the formation of chemical interactions and bonds in complex systems that show more excellent stability.

5. DECLARATIONS

5.1. Study Limitations

No limitations were known at the time of the study.

5.2. Acknowledgements

Our thanks to the Institute of Chemistry at UFRN for supporting the infrared and UV-visible equipment.

5.3. Funding source

The authors funded this research

5.4. Competing Interests

There are no conflicts of interest in this work that we are aware of currently.

5.5. Open Access

This article is licensed under a Creative Commons Attribution 4.0 (CC BY 4.0) International License, which permits use, sharing, adaptation, distribution, and reproduction in any medium or format, if you give appropriate credit

to the original author(s) and the source, provide a link to the Creative Commons license, and indicate if changes were made. The images or other third-party material in this article are included in the article's Creative Commons license unless indicated otherwise in a credit line to the material. If material is not included in the article's Creative Commons license and your intended use is not permitted by statutory regulation or exceeds the permitted use, you will need to obtain permission directly from the copyright holder. To view a copy of this license, visit <http://creativecommons.org/licenses/by/4.0/>.

6. REFERENCES:

- Alvarez, H. A., (1998) - Síntese, Caracterização, Estudos Espectroscópicos e Termoanalíticos de Compostos de Adição de Trifluorometanossulfonatos de Lantanídeos (III) Com o Ligante ϵ -Caprolactama. . 125 f. Tese (Doutorado) - Curso de Química Inorgânica, Instituto de Química, USP, São Paulo, 1998.
- Atkins, P. W., (1990) – Physical Chemistry, 4^a Ed. Oxford Press, printed in the Great Britain.
- Atkins, P. W., Friedman, (2011) - Molecular Quantum Mechanics, 5^a Ed., Oxford University Press, Printed in Great Britain.
- Barrow, G. M., (1982) – Físico-Química – Editora Reverté Ltda, Rio de Janeiro.
- Belarmino, L. D., (1998) – Caracterização e Estudos Condutimétricos e Espectroquímicos dos Compostos $K_2Cr_2O_7$ e $[Cr(H_2O)_4Cl_2]Cl$ – Estágio Supervisionado, Monografia apresentada ao Departamento de Química da UFRN, sob a orientação do Prof. Dr. Francisco José Santos Lima.
- Bomfim, M. V. J.; Abrantes, S. de M. P.; Zamith, H. P. S., (2009) - Estudos Sobre a Toxicologia da ϵ -Caprolactama. *Brazilian Journal of Pharmaceutical Sciences* vol. 45, n. 1, jan/mar.
- Borges, A. S., Caliman, E. V., Dutra, J. D. L., Silva, J. G. DA, AND Araújo, M. H., (2016) - Structure and Luminescent Investigation of New Ln(III)-TTA Complexes Containing N-Methyl- ϵ -Caprolactam as Ligand - *Journal of Luminescence* V. 170, Part 2, 654-662.
- Cardoso, M. C. C.; Belarmino, L. D.; Zukerman-Schpector, J., (2007) - Estudo Termoanalítico de Compostos de Lantanídeos Contendo ϵ -Caprolactama - *Trabalho apresentado no XLVII Congresso Brasileiro de Química* 17 a 21 de setembro, consulted in: <http://www.abq.org.br/cbq/2007/trabalhos/2/2-303-504.htm>
- Coelho, L. W., Junqueira, G. M. A., Herrera, J. O. M. e Machado, S. de P., (1999) – Aplicação de Mecânica Molecular em Química Inorgânica - *Química Nova*, 22(3), 396-404.
- Costa, L. H. M.; Lima, F. J. S. e Silva, A. O., (2013) - Síntese, Complexometria, Análise Térmica e Condutância Molar dos Cloretos de Lantânio, Neodímio e Érbio Hidratados, *Periódico Tche Química*, vol. 10 (19), pag 38-45.
- Cotton, F. A., and Wilkinson, F. R. S., (1988) - Advanced Inorganic chemistry. A comprehensive text. - 5a Ed., Ch.20, 955-79 (Ln) e Ch. 21, 980-1017 (An), Wiley-Interscience Publication, New York.
- Crockford, H. D. and Knight, S. B., (1977) – Fundamentos de Físico-Química. Livros Técnicos e Científicos Editora S.A., Rio de Janeiro, Brasil.
- Drago, R. S., (1965) - Physical Methods in Inorganic Chemistry - Van Nostrand Reinhold Company, printed Holland.
- Fang, J., Wu, H., Liu, T., Zheng, Z., Lei, J., Liu, Q., Jin, H., (2020) - Thermodynamic evaluation of a Concentrated Photochemical-Photovoltaic-Thermochemical (CP-PV-T) System in the Full-Spectrum Solar Energy Utilization, *Applied Energy*, Volume 279.
- Figgis, B. N., (1966) - Introduction to Ligands Fields – Interscience

- Publishers, New York, NY.
16. Geary W. J., (1971) - The Use of Conductivity Measurements in Organic Solvents for the Characterization of *Coordination Compounds – Coord. Chem. Rev.*, 7, 81-122.
 17. Gong, Y., Liu A. Yang, G., (2010) - Polyamide Single Polymer Composites Prepared Via in situ Anionic Polymerization of ϵ -Caprolactam, Composites Part A: *Applied Science and Manufacturing* Volume 41, (8), 1006-1011.
 18. Greenwood, N. N. and Earnshaw, A., (1986) - Chemistry of The Elements - Ch.20, 1102-10, 3a Ed., Pergamon Press, Printed in Great Britain.
 19. Heslop, R. B. and Jones, K., (1976) – Química Inorgânica 2ª Ed., Fundação Calouste Gulbenkian, Lisboa.
 20. Huhey, J. E., (1983) - Inorganic Chemistry, Principles of Structure and Reactivity - Ch.16, 795-820, 3a Ed., Harper International SI Ed., New York.
 21. Kauzmann, W., (1957) – Quantum Chemistry – Academic Press, Inc., New York.
 22. Levine, I. N., (2014) - Quantum Chemistry, 7ª Ed., Pearson Education, Inc. Copyright, Boston.
 23. Li, X. L., Ai, Y. B., Yang, B., Chen, J., Tan., M., Xin, X. L., Shi, Y. H., (2012) - Syntheses, structures and photophysical properties of a series of luminescent copper(I) mixed-ligand complexes, *Polyhedron*, 35 (1), 47-54.
 24. Lima, F. J. S., Brito, H. F., Silva, A. G. Silva, A. O. Braga, C. C. M, Lima, A. J. P., Cardoso, M. C. C., (1996) - O Uso da Força do Oscilador na Avaliação de Intensidades Espectrais - *Anais da Associação Brasileira de Química*, 45 (1), 31-35.
 25. Lima, F. J. S.; Silva, A. G.; Melo, D. M. A.; Belarmino, L. D., (1998) - Caracterização e Estudos Condutimétricos e Espectroquímicos dos Compostos $K_2Cr_2O_7$ e $[Cr(H_2O)_4Cl_2]Cl$. In: 50ª Reunião Anual da SBPC, 1998, Natal - RN. *Livro de Resumos do 50ª. Reunião Anual da SBPC*, v. 01. p. 1079-1079.
 26. Lima¹, F. J. S.; Costa, L. H. M.; Silva, A. O., (2015) - Estudo Térmico e Estereoquímico do Acetato de Urânio Di-Hidratado. *Periódico Tche Química*, vol. 12(23), 66 -73.
 27. Lima², F. J. S.; Costa, L. H. M.; Silva, A. O. Azevedo, D. M., (2015) - Parâmetros de Reatividade Molecular e a Correlação com Condutividades Molares da Quinolina-N-Óxido, Nicotinamida-N-Óxido e a 2,2-Dithiobispiridina-N-Óxido. 1º *Simpósio Nordestino de Química*, Natal/ RN, 27-29 de Abril.
 28. Lima, F. J. S.; Costa, L. H. M.; Silva, A. O.; Pereira, F. C., (2017) - Espectroscopia de Absorção Molecular na Região do Uv-Vis Para os Ligantes Quinolina-N-Óxido, Nicotinamida-N-Óxido e 2,2-Dithiobispiridina-N-Óxido. *Periódico Tche Química*, vol. 15 (29).
 29. Lima, S. G. M.; Cruz, T. J. T. ; Pereira, F. C.; Silva, A. O.; Lima, F. J. S., (2020) - Modelagem Molecular, Medidas Condutimétricas e Espectros Uv-Vis do Ácido Ascórbico Para Formação de Sistemas Químicos Complexos, *Periódico Tche Química*, vol. 17(35), 203-215.
 30. Maciel, J. W O. and Filho, N. C. V., (2015) - Síntese, Caracterização por Infravermelho e Uv-Visível do Composto $[Fe(Cn)_3(Phen)(OH_2)]^{-1}$, 55º *Congresso Brasileiro de Química*, 02 a 06 novembro, Goiânia, GO.
 31. Maldonado, I. A. V., (2017) - Síntese e Caracterização de Complexos de Fenantrolina-Cobre(II).2017. 75 f. TCC (Graduação) - Curso de Química, Centro De Ciências Matemáticas e da Natureza – CCMN, Instituto De Química – IQ, Universidade Federal do Rio de Janeiro, Rio de Janeiro.
 32. Marin, E. P., (2013) - Espectroscopia de Infravermelho e Suas Aplicações - Trabalho de Conclusão de Curso (Bacharelado - Física) - Universidade Estadual Paulista, Instituto de Geociências e Ciências Exatas, 2013. Disponível em: <http://hdl.handle.net/11449/119826> consulted in: 22 aug de 2019.
 33. Martins, E. P. S., (2010) - Síntese e

- Estudo Termodinâmico em Adutos de Trihaletos de Antimônio e Bismuto Com 2,2'-Bipiridina e 1,10-Fenantrolina, Masters dissertation, UFPB, João Pessoa - PB – Brasil.
34. Merck, (2021) - Informações de Propriedades Físico-Químicas da 1,10-Fenantrolina - https://www.merckmillipore.com/BR/pt/product/110-Phenanthroline-monohydrate,MDA_CHEM-107225#anchor_PDP_OverviewTab_Product_Physico_Chemical_Info_Solubilidade – consulted in 30/11/2021
 35. Mitsuhiro W., Hiroaki K., Rie I., Talal A. A., Suleiman M. A., Naotaka K., AND Kenichiro N., (2014) - In Vitro Screening Of Fe²⁺ - Chelating Effect By A Fenton's Reaction–Luminol Chemiluminescence System - *Luminescence*, 29: 955–958.
 36. Moore, W. J., (1991) - Físico-Química, Vol. 2 , 4ª Ed., Ed. Edgard Blucher, SP.,pg. 394-399.
 37. Neville, S. N., Leverett P., Hibbs D. E., Yang Q., Bulanadi J. C., Wua M. J. AND Aldrich-Wright, J. R., (2013) - The antimicrobial properties of some copper(II) and platinum(II)1,10-phenanthroline Complexes, *Dalton Trans.*, 42, 3196–3209.
 38. Notini, L., Byrne, J. M., Tomaszewski, E. J., Latta, D. E., Zhou, Z., Scherer M. M., and Kappler, A., (2019) - Mineral Defects Enhance Bioavailability of Goethite toward Microbial Fe(III) Reduction - *Environ. Sci. Technol.* , 53, 15, 8883–8891.
 39. Pavia, D. L., Lampman, G. M., Kriz, G. S., Vyvyan, J. R., (2010) – Introdução a Espectroscopia, Cengage Learning Ed., Ltda.
 40. Pitzer, K. S., (1965) – Quantum Chemistry, Pretince-Hall, Inc., 7ª Ed.
 41. Silverstein, R. M.; Webster, F. X.; Kiemle, D. J., (2007) - Identificação Espectrométrica de Compostos Orgânicos. 7. ed. Rio de Janeiro: Lct., Tradução de: Spectrometric Identification of Organic Compounds.
 42. Sigma-Aldrich, (2021) - Ficha de Informação de Segurança Sigma-Aldrich, <https://www.sigmaaldrich.com/BR/pt/sds/aldrich/c2204>, consulted in 30/08/2021.
 43. Smith, R. C., (1961) - Infrared Spectra of Substituted 1,10-Phenanthrolines, - *Retrospective Theses and Dissertations*. 2419. <https://lib.dr.iastate.edu/rtd/2419>
 44. Sun, C., Wu, Y., Zhang W., Jiang N., Jiu T., and Fang J., (2014) - Improving Efficiency by Hybrid TiO₂ Nanorods with 1,10-Phenanthroline as a Cathode Buffer Layer for Inverted Organic Solar Cells, *ACS Appl. Mater. Interfaces*, 6(2), 739–744.
 45. Vasconcelos, N. M. S., (2019) - Fundamentos de Química Analítica Quantitativa - 2ª edição, Fortaleza – Ceará.
 46. Vogel, A., Basset, J., Denney, R. C., Jeffery, G. H., Mendham, J., (1981) - Análise Inorgânica Quantitativa 4ª Ed., Ed Guanabara Dois.

SYNTHESIS OF ZIRCONIUM OXIDE CATALYST SUPPORTED ON CARBONIZED MATERIAL FOR THE OPTIMIZATION OF BIODIESEL FROM WASTE VEGETABLE OIL

BABATUNDE, Esther Olubunmi^{1*}; ADERIBIGBE, Fatai Alade¹; JOSEPH Isaac Adekunle¹; ARE, Comfort Temitope²; PAUL-LASISI Joshua Oluwatobi¹

¹ Chemical Engineering Department, University of Ilorin, Ilorin, Kwara State, Nigeria.

² Prince Abubakar Audu University, Chemistry Department Anyigba, Kogi State, Nigeria.

* Corresponding author

e-mail: babatunde.eo@unilorin.edu.ng

Received 16 April June 2022; received in revised form 26 May 2022; accepted 14 June 2022

ABSTRACT

Background: In line with the current global energy crisis, there is an urgent need to seek cheap energy sources. This study has utilized waste materials for synthesizing biodiesel, an environmentally friendly alternative energy. **Aim:** This study aimed to prepare low-cost carbon-based zirconium impregnated heterogeneous catalysts using wood dust to produce biodiesel from waste vegetable oil (WVO). **Methods:** Response Surface Methodology via Central Composite Design (RSM-CCD) optimized the biodiesel production process. The physico-chemical properties of waste vegetable methyl ester were determined following the American Standard Testing of Materials (ASTM). In addition, the catalyst morphology and elemental composition were determined using Scanning Electron Microscopy (SEM) and Energy-Dispersive X-ray (EDX), respectively. **Results and Discussion:** The optimum conditions were observed to be 8:1 methanol/oil ratio, 5 wt% catalyst loading, 55 °C temperature, and 3 hours of reaction time. The corresponding response was observed to be 98.39%. **Conclusions:** The experimental analysis confirmed that the synthesized catalyst from wood dust under optimized conditions transesterified the waste vegetable oil into biodiesel with properties that comply with American Standard Testing of Materials.

Keywords: Optimization, Waste Vegetable Oil, Zirconium, Carbonized material, Transesterification.

1. INTRODUCTION

The prospect of a fossil fuel shortage (Olutoye and Hameed, 2011; Adepoju *et al.*, 2020) and the pollution that comes with it prompted researchers to search for alternatives to petroleum derivatives. The discovery from the research gave rise to “biodiesel” as an alternative fuel. Biodiesel is a biofuel that is similar to fossil diesel (Gashaw and Teshita, 2014). Vegetable oil, animal oil/fats, tallow, and waste cooking oil can produce biodiesel. Transesterification is the chemical reaction used to convert these oils into biodiesel (Yildiz *et al.*, 2015; Babatunde *et al.*, 2020a). Oil crops such as rapeseed, palm, and soybean provide the largest possible source of suitable vegetable oil (Yildiz *et al.*, 2015; Dhawane *et al.*, 2017). In the UK, rapeseed provides the highest potential for biodiesel production. Most biodiesel synthesis comes from waste vegetable oil supplied from restaurants, chip shops, and industrial food processing.

Although oil directly from the agricultural industry has the greatest potential, biodiesel has not been commercialized because of the high cost of raw materials. (Yildiz *et al.*, 2015; Dhawane *et al.*, 2018, Chaveanghong *et al.*, 2018).

Biodiesel is one of several alternative fuels designed to extend the life and cleanliness of diesel engines with the following advantages; low exhaust emissions, renewability, non-toxic, biodegradable, and sustainability—reduced reliance on foreign oil and economic development. (Sumit *et al.*, 2016; Kamakar *et al.*, 2020, babatunde *et al.*, 2020a;). Research into biofuel production is currently on in Nigeria. However, there are challenges such as competition between edible vegetable oil consumption and biofuel production, long-term sustainability to meet industry demands and the high cost of virgin vegetable oil, and environmental contamination from the indiscriminate discharge of used alkali catalyst

(Ramachandra *et al.*, 2013; Erum *et al.*, 2014; Shaaban *et al.* 2015). Therefore, in this paper, wood dust which poses environmental pollution, was utilized to synthesize heterogeneous catalysts to produce biodiesel.

This study aimed to develop low-cost carbon-based zirconium impregnated heterogeneous catalysts using wood dust to synthesize biodiesel from WVO.

2. MATERIALS AND METHODS

2.1 Materials

Wood dust abundantly found in Tanke Iledu, Ilorin, Kwara State, Nigeria, was chosen as a precursor for preparing catalyst support. The waste vegetable oil (WVO) was obtained from Oke-odo frying fish sellers Ilorin, Kwara State, Nigeria. Methanol, potassium hydroxide (KOH), Petroleum ether, and zirconium oxide are all analytical grades obtained from Central Research Laboratory, Ilorin, Kwara State, Nigeria.

2.2 Methods

2.2.1 Determination of Physicochemical Properties

The physicochemical properties of the waste Vegetable oil and produced biodiesel were analyzed according to ASTM D6751-02 (Babatunde *et al.*, 2020b).

2.2.2 Catalyst preparation

Wood dust was pretreated by washing, oven-dried at a temperature of 120 °C for 24 hours, and sieved. Next, the catalyst support was prepared by carbonizing the pretreated wood dust at a temperature of 500 °C for one hour to obtain activated carbon. The zirconium oxide was later anchored on the surface of the activated carbon by the wet impregnation method. After that, the mixture was calcined at 500 °C and kept in a desiccator to avoid moisture.

2.2.3 Catalyst Characterization

The catalyst was characterized by Scanning Electron Microscopy (SEM), which was used to view the surface morphology of the catalysts. Energy Dispersive Spectroscopy (EDS), used to determine the elemental analysis of the sample and the quantitative composition of the catalyst, X-ray diffraction analysis (XRD) equipped with K α and Cu radiation source, Fourier transform infrared spectroscopy (FTIR), used to confirm the presence of the functional group. Brunauer-Emmett-Teller (BET) isothermal sorption

(QUANTACHROME, 1 KE) was used to determine the surface area of the catalyst through N₂-adsorption.

2.2.4 Design of Experiment using Central Composite Design of Response Surface Methodology

The experimental conditions were designed via the application of Central Composite Design (CCD) in Design-Expert software (version 10.0.1). Table 1 shows the process input parameters, viz. methanol to oil ratio (6:1–9:1), reaction temperature (50–70 °C), reaction time (1–4 h), and catalyst loading level (0.5–2.0 wt%) investigated for maximum yield. The CCD was used to produce 30 experimental runs. The terms of the quadratic polynomial models of the variables were fitted through multiple regressions. The model was established through various statistical analyses such as ANOVA and significance test at a 95% confidence level. Equation (2) describes the fitted second-order mathematical regression model. (Babatunde *et al.*, 2020a; Betiku *et al.*, 2019; Joseph, 2014).

Table 1: Independent variables and levels used for RSM

Symbols	Variables	Levels		
		-1	0	1
A	Methanol/oil ratio(v/v)	6:01	7.5:1	9:01
B	Temperature (°C)	50	60	70
C	Time (h)	1	2	3
D	Catalyst loading (w%)	0.5	1.25	2

2.2.5 Transesterification of Waste Vegetable Oil

The transesterification reaction was carried out in 100 mL conical flasks on magnetic stirrers. First, 10 g of waste vegetable oil was measured into the conical flasks. A calculated amount of methanol was added to a known amount of catalyst (0.5, 1.25, 2.00, and 2.75 per weight of oil) to ease miscibility and speed up the reaction rate. The mixture of methanol to oil ratios of 6:1, 7.5:1, and 9:1) was stirred vigorously at constant agitation speed, reaction temperature (50 °C, 55 °C, 60 °C, and 65 °C), and reaction

time (1, 2, 3, and 4 h). The effects of alcohol-oil ratio, reaction time, reaction temperature, and catalysts concentration were investigated according to the experimental runs in Table 2. At the end of the transesterification reaction, 30 ml of distilled water was added to the products; biodiesel and glycerol gave rise to two distinct phases separated using a separating funnel through a filter paper to prevent catalyst loss. The glycerol was dispersed in the water phase (lower layer) while the biodiesel was above (upper layer). The biodiesel yield was calculated using Equation 1.

$$\text{Biodiesel Yield (\%)} = \frac{\text{Mass of biodiesel}}{\text{Mass of WVO}} \times 100 \quad (\text{Eq. 1})$$

3. RESULTS AND DISCUSSION

3.1. Determination of Physicochemical properties of Waste Vegetable Oil

The physicochemical properties of the waste vegetable oil and produced biodiesel are presented in Table 2.

3.2. Characterization of Synthesized Catalyst

3.2.1. Morphology Elemental Analysis

The SEM images are shown in Figure 1:

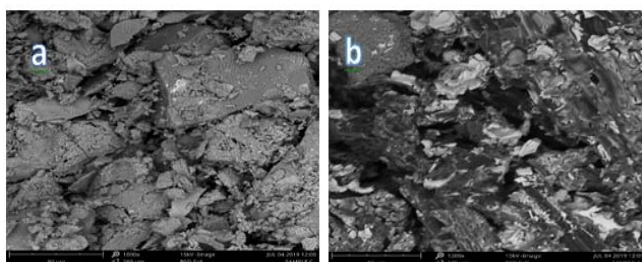


Figure 1: SEM images of (a) carbonized wood dust and (b) synthesized catalyst

The morphological features of the wood – dust were studied using SEM. Micrographs (a and b) in Figure 1 depict the SEM images for carbonized wood dust and (b) synthesized catalyst. It can be seen that Figure 1a shows an irregular porous morphology, while SEM image obtained in Figure 1b illustrates the spongy and porous nature of the particles, which are characterized by increased particle agglomeration. Furthermore, the calcination of the wood-dust sample led to smaller aggregates

of the particles with high fibrous and mesoporous nature. Hence, zirconium was successfully adsorbed on the support, which also confirmed the result of Energy Dispersive Spectroscopy.

3.2.2. Elemental Analysis

Energy Dispersive Spectroscopy (EDS) analysis was used to carry out quantitative chemical analysis (elemental composition) on the catalyst preparation. Figure 2 shows that zirconium (66.06 %) is the major element, followed by calcium (16.83 %). In contrast, others such as S, Mg, Al, Si, Fe, Na, Cr, and Ti are traces in the material. The 66.06 % zirconium shows the highest composition, confirming its successful incorporation into the support (wood-dust).

The statistical significance of the designs was confirmed by the F-test for analysis of variance (ANOVA), as shown in Table 4. For any model or variable to be significant, the P-value must be less than 0.05. Thus, catalyst concentration (D) is the most significant value with a p-value of 0.0008, followed by time (C) with a p-value of 0.0056 and methanol to oil ratio (A) with a p-value of 0.0565. This implies that three of the selected single effect factors significantly influenced the zirconium catalyzed conversion of Waste Vegetable oil to biodiesel. The analysis was also significant for the interactive effect of temperature * time (BC) with a p-value of 0.0330 and Catalyst concentration² (C²) with a p-value of 0.0187. The coefficients were identified for the full model by means of regression analysis. The quadratic polynomial Equation 2 is significant with a p-value of 0.038; this implies that the model can be used to navigate the design space.

The model was therefore reduced to Equation 2 with significant terms only:

$$\text{Biodiesel Yield} = 91.08 - 26.16 * A - 1.50 * C - 6.33 * D - 0.36 * B * C + 2.34 * C^2 \quad (\text{Eq. 2})$$

3.3. Analysis of Waste Vegetable Oil and produced Biodiesel

The results in Table 5 show significant improvement on the fuel properties of the produced biodiesel compared with the waste vegetable oil (WVO). The properties of the biodiesel produced in this study are within the acceptable ASTM standard for biodiesel.

3.3.1. Fatty Acid Methyl Ester (FAME) Analysis

Figure 3 and Table 6 show GC-MS analysis of the biodiesel produced and FAME profile. This was carried out to identify the various methyl esters in the biodiesel.

In Table 6, the major component of the waste vegetable oil biodiesel is n-Hexadecanoic acid (54.19 %), followed by dimethylmalonic acid (22.32 %), while the least component is tetradecanoic acid (2.08 %). As specified by ASTM, the total FAME composition (97.39 %) is greater than 96.5 % minimum composition required for good biodiesel. The FAME profile consists of 54.19 % unsaturated, and 45.91 % saturated fatty acids.

3.4. Reusability study of the synthesized catalyst

The extent of reusability of the synthesized catalyst was studied to check its activity under the optimum conditions. The experiments were carried out, and the yield was estimated after five completed cycles and compared with the yield obtained using fresh catalyst at optimal conditions presented in Table 7 and Figure 4. The decrease in biodiesel yield after five cycles by 2.18 – 2.22 % is due to bond breaking.

Table 7. Comparison of biodiesel yield for fresh and reused catalyst

		Yield (%)			
Fresh catalyst	First reuse	2nd reuse	3rd reuse	4th reuse	
98.39	96.04	95.36	93.66	90.62	

4. CONCLUSIONS

The impregnation method of synthesizing catalysts is fast and suitable for synthesizing a low-cost carbon-based catalyst. Characterization of the synthesized catalyst by SEM and EDS confirmed the presence of zirconium in the synthesized catalyst, which was uniformly dispersed on the support material (carbonized wood-dust) synthesized by the impregnation method. The synthesized catalyst was suitable for producing biodiesel with a maximum yield of 98.39 % at a methanol to oil ratio of 9:1, 5% catalyst concentration concerning the weight of oil, reaction temperature of 55 °C, and reaction

time of 3 h. The physicochemical properties of the waste vegetable oil biodiesel showed that it meets the ASTM standards. The GC-MS FAME profile further confirmed the quality of the biodiesel.

5. DECLARATIONS

5.1. Study Limitations

“No limitations were known at the time of the study”.

5.2. Acknowledgements

The Authors appreciate the Department of Chemical Engineering, University of Ilorin, Nigeria, for providing all the equipment used in this research.

5.3. Funding source

The authors funded this research.

5.4. Competing Interests

The authors declare that there are no competing interests.

5.5. Open Access

This article is licensed under a Creative Commons Attribution 4.0 (CC BY 4.0) International License, which permits use, sharing, adaptation, distribution, and reproduction in any medium or format, as long as you give appropriate credit to the original author(s) and the source, provide a link to the Creative Commons license, and indicate if changes were made. The images or other third-party material in this article are included in the article's Creative Commons license unless indicated otherwise in a credit line to the material. Suppose material is not included in the article's Creative Commons license, and your intended use is not permitted by statutory regulation or exceeds the permitted use. In that case, you will need to obtain permission directly from the copyright holder. To view a copy of this license, visit <http://creativecommons.org/licenses/by/4.0/>.

6. REFERENCES:

- 1 Babatunde E. O., Saka H. B., Olutoye M. A., Akpan U.G. and M. Auta. (2020a). Synthesis of fatty acid methyl esters from used vegetable oil using activated anthill as a catalyst. *Nigerian Journal of Technology (NIJOTECH)*, 39, (1),140-147.
- 2 Babatunde. E.O., Bisheswar K., Olutoye M.A., Akpan U.G., Manase A. and Gopinath H. (2020b): Parametric optimization by Taguchi L9 approach towards biodiesel production from restaurant waste oil using Fe-supported anthill catalyst. *Journal of Environmental Chemical Engineering*, 8(5):104288.
- 3 Betiku, E., Omilakin, O.R and Ajala, S.O. (2014). Mathematical modelling and process parameters optimization studies by artificial neural network and response surface methodology: A case of non-edible neem (*Azadirachta indica*) seed oil biodiesel synthesis. *Energy*, 72, 266-273.
- 4 Chaveanghong, S., Smith, S. M., Smith, C. B., Luengnaruemitchai, A., and Boonyuen, S. (2018). Simultaneous transesterification and esterification of acidic oil feedstocks catalyzed by heterogeneous tungsten loaded bovine bone under mild conditions. *Renewable Energy*, 126, 156–162. <https://doi.org/10.1016/j.renene.2018.03.036>
- 5 Dhawane, S.H., Bora, A.P., Kumar, T and Halder, G. (2017). Parametric optimization of biodiesel synthesis from rubber seed oil using iron-doped carbon catalyst by Taguchi approach. *Renewable Energy*, 105, 616-624.
- 6 Dhawane, S. H., Karmakar, B., Ghosh, S., and Halder, G. (2018). Parametric optimization of biodiesel synthesis from waste cooking oil via Taguchi approach. *Journal of Environmental Chemical Engineering*, 6,(4),3971–3980. <https://doi.org/10.1016/j.jece.2018.05.053>
- 7 Erum, Z., Rehana, S., Mehwish, A. H., and Anjum, Y. (2014). Study of physicochemical properties of edible oil and evaluation of frying oil quality by Fourier Transform-Infrared (FT- IR) Spectroscopy. *Arabian Journal of Chemistry*,3870–3876. <https://doi.org/10.1016/j.arabjc.2014.05.025>
- 8 Gashaw, A., and Teshita, A. (2014). Sustainable Energy Production of biodiesel from waste cooking oil and factors affecting its formation: A review. *International Journal of Renewable and Sustainable Energy*, 3(5), 92– 98. <https://doi.org/10.11648/j.ijrse.20140305.12>
- 9 Ismail S. A. A. and Ali R. F. M. (2015). Physicochemical properties of biodiesel manufactured from waste frying oil using domestic adsorbents. *Science and Technology of Advanced Materials*. doi:10.1088/1468-6996/16/3/034602
- 10 Joseph I. A. (2016). Production and optimization of biolubricant from jatropha curcas oil. B.Eng. Thesis submitted to the Department of Chemical Engineering. Federal University of Technology, Minna, Niger State.
- 11 Olutoye, M. A. and Hameed, B. H. (2011). Synthesis of fatty acid methyl ester from used vegetable cooking oil by solid reusable $Mg_{1-x}Zn_{1+x}O_2$ catalyst. *Bioresource Technology*, 102, 3819-3826.
- 12 Ramachandran, K., Suganya, T., Gandhi, N. N., and Renganathan, S. (2013). Recent developments for biodiesel production by ultrasonic assist transesterification using different heterogeneous catalyst: a review. *Renewable and sustainable energy reviews*, 22, 410-418
- 13 Shaaban, W., Elkady, M. F., and Ohshima, M. (2015). Investigation of Factors Affects Biodiesel Production in Microreactor with T-Mixer, 88, 2–3. <https://doi.org/10.7763/IPCBEE>.
- 14 Sumit H. D, Tarkeshwar K. and Gopinath H. (2016). Biodiesel synthesis from hevea brasiliensis oil employing carbon-supported heterogeneous catalyst: Optimization by Taguchi method. *Renewable Energy*, 89, 506-514
- 15 Taufiq-Yap, Y. H., Teo, S. H., Rashid, U., Islam, A., Hussien, M. Z., and Lee, K. T. (2014). Transesterification of Jatropha curcas crude oil to biodiesel on calcium lanthanum mixed oxide catalyst: Effect of stoichiometric composition. *Energy Conversion and Management*. <https://doi.org/10.1016/j.enconman.2013.12.075>
- 16 Van Setten, B. A. A. L., Makkee, M., and Moulijn, J. A. (2001). Science and technology of catalytic diesel particulate filters. *Catalysis Reviews-Science and*

- Engineering*. <https://doi.org/10.1081/CR-120001810>
- 17 Yildiz, G., Ronsse, F., Venderbosch, R., Duren, R. van, Kersten, S. R. A., and Prins, W. (2015). Effect of biomass ash in fast catalytic pyrolysis of pine wood. *Applied Catalysis B: Environmental*. <https://doi.org/10.1016/j.apcatb.2014.12.044>
- 18 Yusuff, A. S and Owolabi J.O. (2019). Synthesis and characterization of alumina-supported coconut chaff catalyst for biodiesel production from waste frying oil. *South African Journal of Chemical Engineering*, 30,42-49. <https://doi.org/10.1016/j.sajce.2019.09.001>

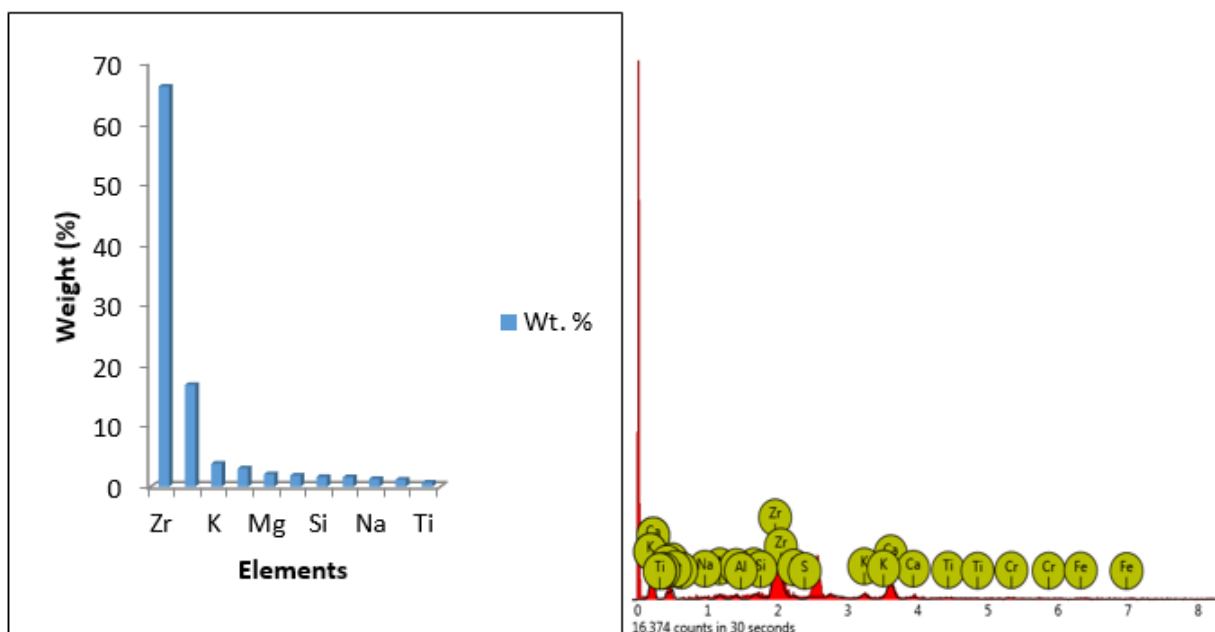


Figure 2: Energy Dispersive Spectroscopy (EDS) pattern of the synthesized catalyst

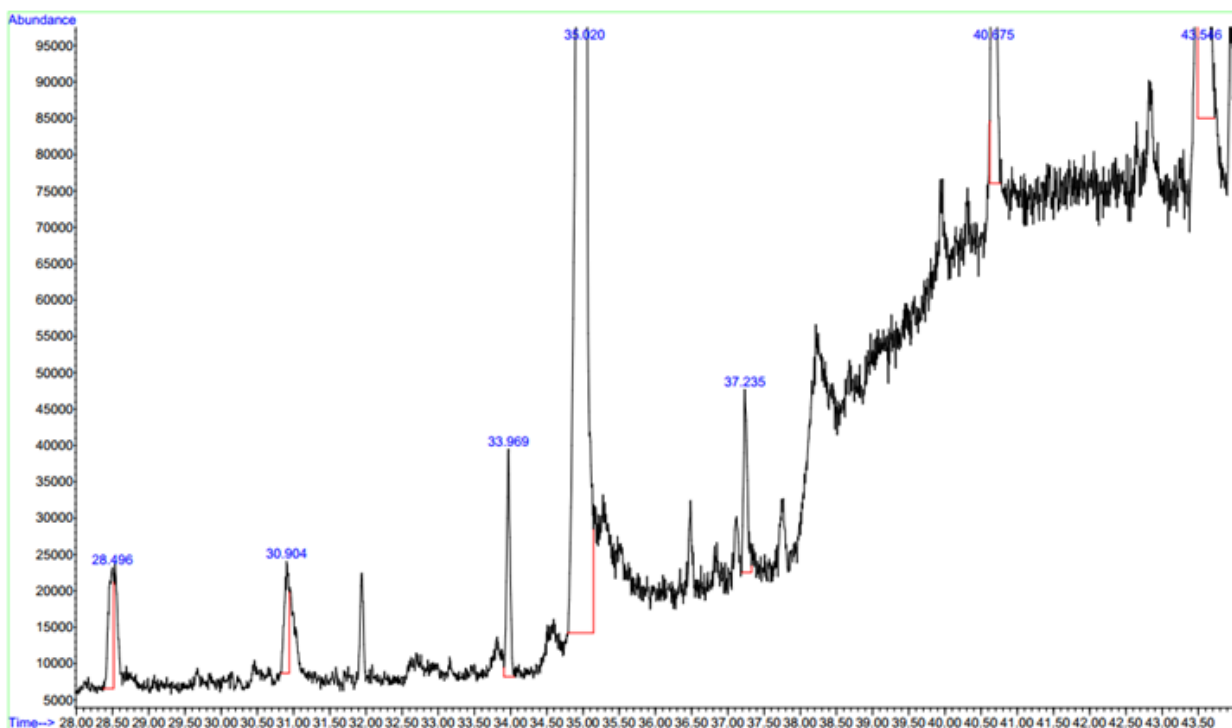


Figure 3: GC-MS of the waste vegetable oil biodiesel

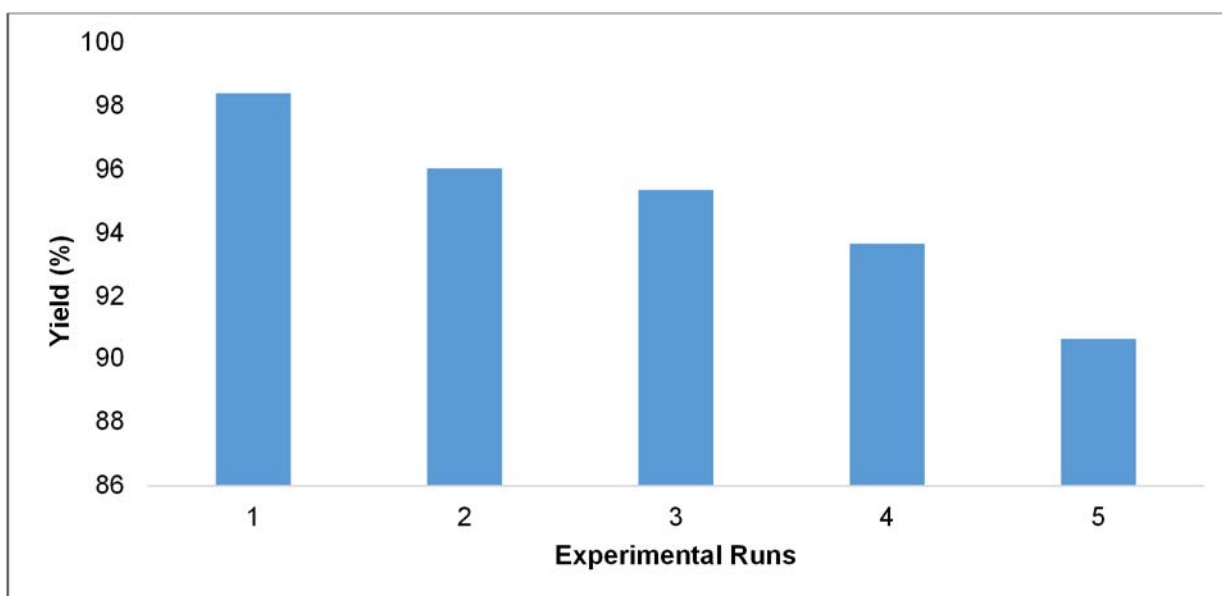


Figure 4: Reusability test of the synthesized catalyst

Table 2: Physicochemical Properties of Waste Vegetable Oil and produced Biodiesel

Fuel properties (units)	WVO	Waste Vegetable oil Biodiesel	ASTM standard for biodiesel	ASTM Method
Density at 15°C (g/cm ³)	0.937	0.887	0.860 to 0.900	ASTM D1298
Flash point (°C)	224	173	≥130	ASTM D92
Acid value (mg KOH/g)	3.366	0.435	≤0.80	ASTM D664
Cloud point (°C)	21	-2	-3 to -12	ASTM D2500
FFA	1.683	0.218	-	-
Viscosity @ 40 °C/(mm ² /s)	20.50	4.52	-	-
Saponification Value	185.32	165	-	-

Table 3: CCD Experimental design and biodiesel yield

Run	Methanol/oil ratio	Temperature (°C)	Catalyst loading (w%)	Time (h)	Yield (%)
1	9.00	60.00	1.25	2.00	66.40
2	8.00	65.00	0.50	3.00	84.10
3	7.00	60.00	1.25	4.00	91.23
4	8.00	55.00	2.00	1.00	53.60
5	8.00	55.00	0.50	3.00	98.39
6	6.00	55.00	2.00	3.00	88.70
7	6.00	55.00	0.50	3.00	87.41
8	8.00	65.00	0.50	1.00	66.22
9	7.00	60.00	1.25	2.00	68.88
10	7.00	60.00	1.25	1.00	53.20
11	6.00	65.00	0.50	3.00	76.65
12	7.00	60.00	2.75	2.00	74.82
13	6.00	55.00	2.00	1.00	68.29
14	7.00	60.00	1.25	2.00	68.88

15	6.00	55.00	0.50	1.00	86.92
16	8.00	55.00	0.50	1.00	79.87
17	6.00	65.00	2.00	3.00	83.12
18	7.00	50.00	1.25	2.00	57.09
19	7.00	60.00	1.25	2.00	68.88
20	6.00	65.00	0.50	1.00	74.31
21	7.00	60.00	1.25	2.00	68.88
22	7.00	60.00	1.25	2.00	68.88
23	7.00	60.00	1.25	2.00	68.88
24	8.00	55.00	2.00	3.00	81.05
25	8.00	65.00	2.00	3.00	81.23
26	6.00	65.00	2.00	1.00	75.35
27	7.00	70.00	1.25	2.00	82.31
28	5.00	60.00	1.25	2.00	67.35
29	7.00	60.00	0.25	2.00	63.54
30	8.00	65.00	2.00	1.00	71.35

Table 4: Analysis of variance (ANOVA)

-Source	Sum of Squares	Df	Mean Square	F Value	p-value Prob > F
Model	2274.27	14	162.45	2.06	0.0387
A-MeOH: Oil	30.02	1	30.02	0.38	0.0565
B-Temp.	14.32	1	14.32	0.18	0.0261
C-Time	34.13	1	34.13	0.43	0.0056
D-Cat. Conc.	1362.03	1	1362.03	17.27	0.0008
AB	8.82	1	8.82	0.11	0.7427
AC	62.09	1	62.09	0.79	0.3889
AD	114.06	1	114.06	1.45	0.2478
BC	312.58	1	312.58	3.96	0.0330
BD	52.56	1	52.56	0.67	0.4271
CD	43.16	1	43.16	0.55	0.4709
A²	27.75	1	27.75	0.35	0.5619
B²	80.40	1	80.40	1.02	0.3287
C²	68.65	1	68.65	0.87	0.3656

D²	150.29	1	150.29	1.91	0.0187
Residual	1183.07	15	78.87		
Lack of Fit	1183.07	10	118.31		
Pure Error	18.60	5	9.96		
Cor Total	3457.35	29			

Table 5: Physicochemical Properties of Waste Vegetable Oil and Synthesized Biodiesel

Fuel properties (units)	WVO	Waste Vegetable oil Biodiesel	ASTM standard for biodiesel	ASTM Method
FAME content (%m/m)	-	98.39	≥96.5	—
Density at 15°C (g/cm³)	0.873	0.873	0.860 to 0.900	ASTM D1298
Flash point (°C)	159	224	≥130	ASTM D92
Acid value (mg KOH/g)	3.366	0.4354	≤0.80	ASTM D664
Cloud point (°C)	-	-2	-3 to -12	ASTM D2500
FFA	1.683	0.2177		—
Viscosity	5.360	4.68	-	-
Saponification Value	125.3208	125.7	-	-

Table 6: Methyl esters composition of waste vegetable oil Biodiesel

Peak No.	Retention time	Methyl esters	Composition (%)
1	30.904	Tetradecanoic acid	2.08
2	33.969	Methyl palmitate	3.21
3	35.020	n-Hexadecanoic acid	54.19
4	37.235	7-Octadecanoic acid 6-Octadecanoic acid	2.93
5	40.675	Hexadecanedioic acid	12.66
6	43.546	Dimethylmalonic acid	22.32

ADSORPTION STUDIES OF ZINC, COPPER, AND LEAD IONS FROM PHARMACEUTICAL WASTEWATER ONTO SILVER-MODIFIED CLAY ADSORBENT

AJALA, Mary Adejoke^{1,2,4*}; ABDULKAREEM, Ambali Saka^{2,4}; KOVO, Abdulsalami Sanni^{2,4}; TIJANI, Jimoh Oladejo^{3,4}; AJALA, Olawale Elijah¹¹ Department of Chemical Engineering, University of Ilorin, Ilorin, Kwara State, Nigeria.² Department of Chemical Engineering, Federal University of Technology, Minna.³ Department of Chemistry, Federal University of Technology, Minna, Niger State, Nigeria.⁴ Nanotechnology Research Group, Centre for Genetic Engineering and Biotechnology (CGEB), Federal University of Technology, P.M.B 65, Bosso, Minna, Niger State, Nigeria.

* Corresponding author

e-mail: ajala.ma@unilorin.edu.ng;

Received 12 April 2022; received in revised form 30 May 2022; accepted 14 June 2022

ABSTRACT

Background: Industrial wastewater contains pollutants that are detrimental to human health in varied proportions. Among the pollutants are heavy metals, including Zn^{2+} , Pb^{2+} , and Cu^{2+} found in a characterized pharmaceutical wastewater. Several techniques have been proposed for the heavy metal sequester. However, they are with attendant challenges. The adsorption techniques using clay-metal oxide modified adsorbent/composite such as silver-clay adsorbent is considered suitable for an effective sequestering process. **Aims:** To develop and characterize Ag/clay adsorbent for pharmaceutical wastewater treatment. **Methods:** The Ag nanoparticles were synthesized using *Parkia biglobosa* aqueous leaves extract in an optimization study. The raw clay was beneficiated and doped with silver nanoparticles via the wet impregnation method. The silver-clay adsorbent was characterized using FTIR, XRD, SEM, and EDS characterization tools. The developed adsorbent was used for the batch adsorption process of the heavy metal ion removal from the wastewater. **Results and Discussion:** The phytochemical analysis and FTIR results of the *P. biglobosa* showed that the leaf contains phenol, tannin, and flavonoids which acts as reducing, capping, and stabilizing agent required for synthesizing the silver nanoparticles. The prepared silver nanoparticles modified clay adsorbent Ag/clay, have evenly distributed stacks of pseudo-hexagonal plates, are rich in silica, possess silver nanoparticles in the frameworks, and contain functional groups suitable for binding heavy metals. The adsorptions of Zn^{2+} , Pb^{2+} , and Cu^{2+} from pharmaceutical wastewater onto the silver-modified clay were studied as a function of adsorbent dosage and contact time. The percentage removal results obtained showed that the adsorbent had up to 99.96%, 99.5%, and 99.44% removal efficiency for Zn^{2+} , Pb^{2+} , and Cu^{2+} , respectively, which are better compared with previous studies. The adsorption process was feasible, spontaneous, and exothermic, with Langmuir and Pseudo-second-order models as best fits for the process. **Conclusions:** The adsorption of selected heavy metal ions onto the green synthesized silver-modified clay adsorbent (Ag/clay) was feasible, spontaneous, and exothermic in the order $Zn^{2+} > Pb^{2+} > Cu^{2+}$ with Langmuir and Pseudo-second-order model best fitted for the process. These show that the synthesized silver oxide nanoparticles supported on local clay can be used as a potentially low-cost adsorbent to remove heavy metal ions from industrial wastewater.

Keywords: Green synthesis, *Parkia biglobosa*, Silver oxide, Nanoadsorbent, heavy metals.

1. INTRODUCTION

The pharmaceutical industry is a major producer of wastewater effluents containing pollutants such as heavy metals (zinc (Zn), copper (Cu), and lead (Pb)), microbes (bacteria), and dyes (yellow). The pollutants reduce the photosynthetic activity of aquatic life and could

poison certain forms of aquatic life (Bashir *et al.*, 2020). Zn, Cu, and Pb ions are part of pollutants in pharmaceutical wastewater, which are hazardous and harmful to human health. Although Zn is an essential element in humans because it could serve as a food supplement, its excess is extremely dangerous as it may cause paralysis

and neurological problems. Excess Zn may also lead to a state of depression and other unwanted effects such as dizziness, breathing problems, and chest pain (Kaur and Sharma, 2017). More so, the WHO guidelines gave the maximum admissible concentration of Zn in an aqueous solution as 5.0 mg/l (WHO, 2019). Also, Cu has been reported to have adverse effects on human health. These include mental disorders, anemia, arthritis/rheumatoid arthritis, hypertension, and liver enlargement (Lakherwal, 2014). Furthermore, the WHO gave the maximum admissible concentration of Cu in an aqueous solution as 0.05 mg/l (Bankole *et al.*, 2019). On the other hand, lead is responsible for lung dysfunction, liver damage, reduced pulmonary function, and cardiovascular dysfunction (Balali-Mood, Naseri, Tahergorabi, Khazdair, and Sadeghi, 2021). Hence, Zn, Cu, and Pb removal from pharmaceutical wastewater are essential for human and aquatic survival.

Several conventional techniques such as photocatalytic oxidation, chemical coagulants, bioremediation, ion-exchange resins, reverse osmosis, membrane filtration, solvent extraction, and electrolysis have been reported for the removal of various heavy metals from wastewater (Dave and Chopda, 2014). However, they are found to be inadequate with some challenges and drawbacks, such as cost-effectiveness, disposal after use, efficiency, and lack of eco-friendliness of the technological processes (Dutta, Borah, and Puzari, 2021). Therefore the need for more research on some other methods such as adsorption.

The adsorption technique is advancing in removing heavy metals, colors, and microbes from wastewater. Since the process is highly efficient, adsorbate-specific, cost-effective, easy to handle, and eco-friendliness (Dutta *et al.*, 2021). Adebayo *et al.* (2020) (Adebayo, Adegoke, and F., 2020), however, justified the use of nanomaterial as a good adsorbent for the removal of heavy metals. Furthermore, it was reported that nanomaterials have appropriate adsorption surfaces and possess unique characteristics vis-à-vis a very high surface-area-to-volume ratio. These advantages give a tremendous driving force for diffusion, especially at high temperatures (Lakherwal, 2014).

Several nanomaterials have been used for the removal of heavy metals from wastewater, and such research includes that of Mustapha *et al.* (2019), who utilized modified kaolinite clay to remove Zinc and Chromium ions from tannery wastewater (Mustapha *et al.*, 2019). In another

research, a silver-clay composite was tested for iodine-129 retention and found suitable (Sadasivam and Rao, 2016). Also, Choudhury *et al.* (2021) used Montmorillonite-silver(MMT/Ag) composite to absorb methylene blue. The outcome of the findings revealed that layered, sheet-like morphology of MMT/Ag nanocomposite was synthesized and found suitable for MB adsorption from wastewater (Choudhary *et al.*, 2021). Clay/copper/silver composite was successfully synthesized by Asamoah *et al.* (2020) (Asamoah, Yaya, Nbelayim, Annan, and Onwona-Agyeman, 2020). However, the suitability of the composite was only tested against bacterial strains and not heavy metals. Kariim *et al.* (2020) used a developed nano-adsorbent to treat pharmaceutical wastewater, focusing on removing metronidazole and levofloxacin from the wastewater (Kariim, Abdulkareem, and Abubakre, 2020).

Therefore, this study investigated the development of Ag/clay adsorbent using a green synthesis approach to remove Zn, Cu, and Pb ions from pharmaceutical wastewater. The process's isothermal, kinetics, and thermodynamic parameters were investigated for an effective sorption study of the sorbate onto the adsorbent surface.

2. MATERIALS AND METHODS

2.1. Preparation procedures

2.1.1 Beneficiation of clay

The ball clay collected from Akerebiata, Ilorin in Kwara State, Nigeria, was soaked in water for 48 h to allow the clustered clay to dissolve. It was then sieved to ease the removal of the sand particles and later allowed to sediment to get the fine particles of the clay. The fine particles obtained were sun-dried, oven-dried at 100 °C pulverized, and then sieved with a sieve mesh of < 0.2 µm.

2.1.2 Preparation of leaf extract

The leaves extract was prepared according to the method of Ajala *et al.* (Ajala, Abdulkareem, Tijani, and Kovo, 2022) following; fresh leaves of *Parkia biglobosa* were washed with clean water and air-dried for two weeks at room temperature

to prevent the destruction of the Thermo labile constituents present in the plant by direct sun rays. The room-dried leaves were then pulverized, and the phytochemical analysis of the plants was carried out. Next, 100 mL of deionized water was added to 5g of the pulverized leaf, and the solution was then boiled at 60 °C for 30min to extract the reducing and stabilizing agents. Finally, the aqueous extract was filtered using a muslin cloth and filter paper (Whatman no.1). The filtrate was kept in a refrigerator for the biosynthesis of silver nanoparticles.

2.1.3 Green synthesis of silver nanoparticles

The silver nanoparticles were synthesized by adopting the method of Dhand (Dhand *et al.*, 2016). *P.biglobossa* leaves were dried and pulverized. About 5g of the pulverized leaves was added to 100 mL of deionized water, boiled at 60 °C, and stirred continuously for 30 min using a magnetic stirrer to extract the reducing and stabilizing agents. The solution was filtered using a muslin cloth and filter paper (Whatman no.1). The varied volume of leaf extract was added to the varied volume of 1mM AgNO₃ solution following the data gotten from the factorial design of the Design Expert. The solution was allowed to stand for 20 minutes. The pH of the resultant solution was adjusted between pH 4 and pH 10 with either 2 M NaOH or HCl. The color change from green to brown indicates the formation of nanoparticles. The solutions were characterized using a UV-Visible spectrophotometer.

2.1.4 Silver/Clay loading procedure

Forty grams (40 g) of the beneficiated clay was weighed on an analytical balance and added to a flask containing 400 mL of 1 mM AgNO₃. After that, 20 mL of the *P. biglobossa* leaves extract was added under continuous stirring for a few minutes (The amount of leaf extract added was obtained from the earlier synthesis of Ag nanoparticles carried out). The flask was sealed and shaken at room temperature for 24 hours in a thermostatic water bath shaker (SHA-C). The suspension was filtered using a filter paper (Whatman no.1) and washed several times with deionized water to remove residual Ag⁺ ions. The residual suspension was dried in an oven at 50 °C for 12 hours.

2.1.5 Characterisation of the synthesized titanium dioxide

The prepared adsorbents were characterized using; Ultraviolet-visible spectroscopy (Uv-vis), Fourier Transform Infrared spectroscopy (FTIR), X-ray diffraction (XRD), High-Resolution Scanning Electron Microscopy (HRSEM), and Electron Diffraction Spectroscopy (EDS) to determine the microstructure, morphology, chemical composition, surface area, phase structure, and optical properties of the prepared Ag/clay adsorbent.

2.2 Batch Adsorption Studies

The investigations were carried out in batches to determine the effects of contact time, adsorbent dosage, and pH to check the nature of the adsorption process. The metal ions removed from the wastewater were determined in prior physicochemical parameter investigations of the pharmaceutical wastewater in previous research (Ajala *et al.*, 2022). For the batch experiment, 25 mL of the wastewater of known concentrations was poured into Ag/clay adsorbent (0.1-0.5 g dosage) in a 100 mL flat bottom flask. The mixture was shaken at a varied time (30- 240 min) and designated temperature (30-50 °C), the supernatant was filtered through Whatman Filter Paper No. 1, and the wastewater was analyzed using AAS. The isotherm, kinetics, and thermodynamics governing the adsorption were also determined via batch experiments. The amount of Zn²⁺, Pb²⁺, and Cu²⁺ ions adsorbed at the time (q_t), equilibrium (q_e), and the percentage removal was calculated by the Equations 1-3:

$$q_t = \frac{(C_o - C_t)V}{m} \quad (\text{Eq. 1})$$

$$q_e = \frac{(C_o - C_e)V}{m} \quad (\text{Eq. 2})$$

$$\text{Removal (\%)} = \frac{C_o - C_t}{C_o} \times 100\% \quad (\text{Eq. 3})$$

Where C_o and C_e are the initial and the final (equilibrium) metal ion concentration (mg·L⁻¹), V is

the water sample volume (L), m is the mass (g) of adsorbent used, C_o , C_t and C_e are the initial, final (at a designated time) and equilibrium metal ion concentration ($\text{mg}\cdot\text{L}^{-1}$) respectively (López-Luna *et al.*, 2019).

$$\frac{C_e}{q_e} = \frac{1}{q_o K_L} + \frac{C_e}{q_o} \quad (\text{Eq. 6})$$

Freundlich isotherm;

2.2.1. Adsorption kinetic models

$$\ln q_e = \ln K_F + \frac{1}{n_F} \ln C_e \quad (\text{Eq. 7})$$

The kinetics of Zn^{2+} , Pb^{2+} , and Cu^{2+} adsorption onto Ag/clay nano adsorbent was analyzed using the pseudo-first-order (PFO) (Miyah *et al.*, 2017) and pseudo-second-order (PSO) (Ho and McKay, 1999) kinetic models. The PFO and PSO model is expressed mathematically as Equations 4 and 5:

Temkin isotherm;

$$q_e = \frac{RT}{b_T} \ln A_T + \frac{RT}{b_T} \ln C_e \quad (\text{Eq. 8})$$

The pseudo-first-order model:

D–R isotherm;

$$\ln(q_e - q_t) = q_e - k_1 t \quad (\text{Eq. 4})$$

$$\ln q_e = \ln q_o - K_{ad} \varepsilon^2 \quad (\text{Eq. 9})$$

The pseudo-second-order model:

$$\frac{dq_t}{dt} = k_2 (q_e - q_t)^2 \quad (\text{Eq. 5})$$

Where q_e (mg/g) = adsorbed amounts of metal ion at equilibrium, q_t (mg/g) = adsorbed amounts of each metal ion at time t (min), k_1 (min^{-1}) and k_2 (mg/g min) are the pseudo-first-order and the pseudo-second order rate constants.

where q_e (mg/g) is the quantity of metal ion adsorbed at equilibrium, q_m (mg/g) represents maximum adsorption capacity for monolayer coverage on the surface of the adsorbent, and C_e (mg/L) represents metal ions concentration at equilibrium. k_L (L mg^{-1}) is the Langmuir equilibrium adsorption constant. K_F (mg/g) and n_F is the Freundlich adsorption isotherm constant which denotes the adsorption capacity of the adsorbent and the heterogeneity of the adsorption process, respectively. A_T (L/g) and b_T (kJ/mol) are Temkin constants related to the heat of adsorption and maximum binding energy. T ($^{\circ}\text{C}$) is the temperature, while R (8.314 J/mol.K) is the universal gas constant, q_{ad} and q_s are constant related to adsorption mean free energy and D–R adsorption capacity at monolayer saturation, while ε is a Polanyi potential.

2.2.2. Adsorption isotherm model

The isotherm models are employed in adsorption process analysis to investigate the distribution of adsorbate molecules at the solid/liquid interface. For the adsorption of Zn^{2+} , Pb^{2+} and Cu^{2+} onto Ag/clay nano adsorbent, four isotherm models, namely; Langmuir (Langmuir, 1918), Freundlich (Miyah *et al.*, 2017), Temkin (Egbosiuba *et al.*, 2019) and Dubinin–Radushkevich (D–R) (Ayawei, Ebelegi, and Wankasi, 2017; Dubinin, 1969) were applied.

2.7.3. Adsorption thermodynamics

The mathematical representation of the models is given by the Equations 6-9:

The thermodynamics studies of Zn^{2+} , Pb^{2+} , and Cu^{2+} onto Ag/clay nano adsorbent were carried out at 30, 40, and 50 $^{\circ}\text{C}$, respectively. These were carried out to understand the energy changes of the process. Enthalpy change (ΔH°), Gibbs free energy change (ΔG°), and entropy change (ΔS) as the major thermodynamics parameters were evaluated using Equations 10 to 15.

Langmuir isotherm;

$$\Delta G_{ads} = \Delta G^{\circ} + RT \ln Q \quad (\text{Eq. 10})$$

The Gibbs energy change (ΔG , kJ/mol) of the metal ion(s) adsorption process was determined by Equation 10 and analyzed using Equations 11-13 in which Q describes the quotient of reaction, which relates to the metal ion concentrations of a system that is not in equilibrium. However, at equilibrium $\Delta G_{\text{ads}} = 0$. Hence Equation 10 is reduced to Equation 11:

$$\Delta G^\circ = -RT \ln K_d \quad (\text{Eq. 11})$$

$$K_d = \frac{q_e}{C_e} \quad (\text{Eq. 12})$$

$$\ln K_d = -\frac{\Delta G^\circ}{RT} = \frac{\Delta S}{R} - \frac{\Delta H^\circ}{RT} \quad (\text{Eq. 13})$$

Where K_d is the equilibrium parameter represented by Equation 15, the values of ΔH° and ΔS° values are obtained from the slope and intercept of the Van't Hoff plots of $\ln K_d$ against $1/T$ (Bankole *et al.*, 2019).

2.7.4 Analysis of error

All the figures obtained from each experiment and analysis were duplicated to remove or minimize errors in the results. The constants of the isotherm and kinetics studies were determined using Origin 2019 software at a 95% confidence level. To determine the isotherm and kinetic model fitness to the experimental data in this work, the linear determination coefficient (R^2), the non-linear Chi-square test (X^2), and the sum of square error (SSE) statistical error analysis tests were performed (Ngakou, Anagho, and Ngomo, 2019). The mathematical equations are represented in Equations 14 and 15.

$$X^2 = \sum((q_{e,exp} - q_{e,cal})^2 / q_{e,cal}) \quad (\text{Eq. 14})$$

$$SSE = \sum(q_{e,exp} - q_{e,cal})^2 \quad (\text{Eq. 15})$$

3. RESULTS AND DISCUSSION

3.1 Characterization result

3.1.1 FTIR of *Parkia Biglobosa*, Clay and Ag-clay

The structural exposition and macromolecules of *Parkia biglobosa* were evaluated using the FTIR technique (Figure 1), and the FTIR spectra showed characteristic peaks of hydrogen-bonded O-H stretch at 3533.71, 3417.98, 3363.97, and 3271.38 cm^{-1} , the peak at 3055.35 cm^{-1} indicates C=C-H asymmetric stretch. The peaks at 3417.98, 3363.97, 3271.38, and 3055.35 cm^{-1} also indicate N-H stretch. Peaks of H-C-H asymmetric and symmetric stretch were shown at 2924.18 and 2862.46 cm^{-1} , while 2746.73 cm^{-1} indicates C-H stretch off C=O; the peak at 2345.52 cm^{-1} is a result of C≡N stretch. The peaks at 1728.28 and 1627.97 cm^{-1} indicate C=O stretch; 1535.39 and 1442.80 cm^{-1} are due to H-C-H bend and C-C=C asymmetric stretch. The peaks at 1373.36, 1327.07, and 1026.16 cm^{-1} indicate the C-O stretch. The presence of the O-H stretch, which is related to phenol, serves as a reducing and stabilizing agent in the formation of the silver nanoparticles.

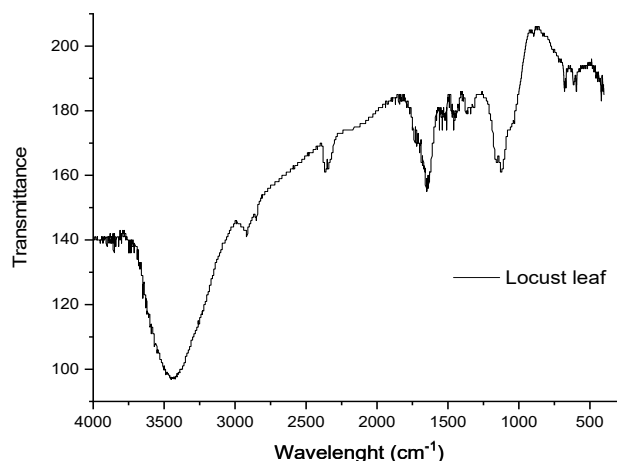


Figure 1. FTIR spectrum of *Parkia biglobosa*

The Fourier transform infrared (FTIR) spectroscopy of the clay was evaluated, as shown in Figure 2a. The characteristic peaks at 3701.70 and 3615.89 cm^{-1} represent the O-H stretch of alcohols and phenolic group, the peak at 1111.01 cm^{-1} represents the C-O stretch of esters, while the C-O stretching peak at 1004.77 cm^{-1} is of ethers. The peaks at 914.87, 792.28, and 706.47 cm^{-1} are attributed to the silicate clay's Si-

O-Si and Al-O-Si bonds. The FTIR spectra of the silver clay in Figure 2b shows several peaks indicating the functional groups embedded in the adsorbent. The characteristic peak of hydrogen-bonded O-H stretch, at 3305.86 cm^{-1} is that of the phenolic and alcohol group. Bonded O-H of carboxylic acids is observed at 2928 cm^{-1} , and the peaks at 1621 and 1600 are attributed to the C=O stretch of carbonyl and ketones. Other peaks at 1298 cm^{-1} , 1251 cm^{-1} , and 1186 cm^{-1} depict C-O stretch attributed to esters and ethers, indicating a shift from the previously observed in unmodified clay likely due to the chemical modification (Dhand *et al.*, 2016). Si-O-Si and Al-O-Si bonds of silicate clay are at 910 cm^{-1} , 800.24 cm^{-1} , and 700 cm^{-1} . New peaks, which deviated entirely from those on the clay spectral, are observed at 534.78 cm^{-1} , 462.34 cm^{-1} , and 432.66 cm^{-1} are attributed to Ag loading, similar to the findings of Krishnan and Mahalingam (2017).

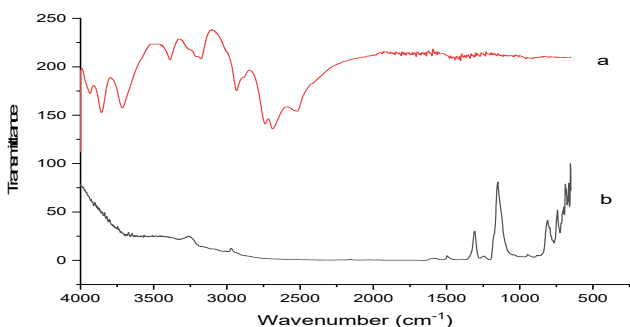


Figure 2. FTIR spectrum of (a) Raw clay and (b) Ag/clay Adsorbent

3.1.2 XRD results

The XRD result of the raw clay and Ag/clay are presented in Figures 3 (a) and (b). The diffraction pattern illustrates the presence of major peaks at 2Θ values and crystal planes at 12.31° (001), 19.80° (020), 35.92° (002), and 73.53° (-261), corresponding to the kaolinite (k) clay mineral peaks which agrees with the JCP library 01-079-1570. Silicon oxide in the form of quartz (q) was observed at 20.91° (100), 26.80° (101), 40.22° (111), and 60.01° (211), 67.60° (212), 73.77° (014) (JCP-01-083-0539) (Ajala *et al.*, 2022), while the scanty short peaks at 24.94° , 28.56° are Albite (a) (Na_{1.09}(Al_{1.09}Si_{2.91}O₈)) peaks. The Microcline (m) peaks in Figure 3(b) are the transformations of the kaolinites due to hydrolysis. Other peaks are at 76.42° and 82.02° , synchronized to calcite-magnesian peaks (c) (MgO.CaO.CO₃) as impurities in the clay source. The calcite peaks in

Figure 3(a) were observed absent in Figure 3(b), this is attributed to the beneficiation and modification processes carried out on the clay. The presence of high-intensity peaks in Figure 3(a) was reduced to low intensity in Figure 3(b), and there was the total disappearance of the calcite peaks earlier observed in Figure 3(a). This improvement suggests that the immobilization of the silver nanoparticles in the clay surface has led to the changes observed. This agrees with previous literature (Alaya-Ibrahim, Kovo, Abdulkareem, Adeniyi, and Yahya, 2019).

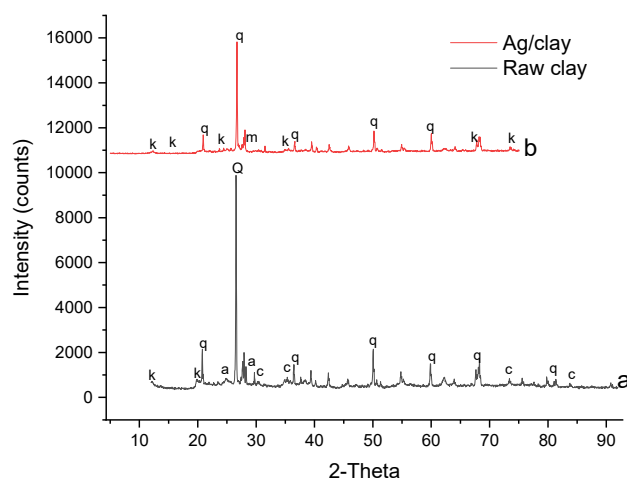


Figure 3. XRD of the Silver/clay Adsorbent

3.1.3 Morphology and Structure

The Scanning Electron Microscope was used to examine the surface morphology of the prepared adsorbent. Figure 4 reveals an evenly distributed arrangement of spherical nanocomposites. The flat-lying stacks are pseudo-hexagonal in a structure having curved edges, which are the characteristics of kaolinite clays. The even arrangement may imply polydispersity and intercalation of the silver nanoparticles into the clay structure. The EDS result in Figure 5 shows that the clay is truly rich in silica at 24.9%, bonded oxygen is up to 48.68% of the entire weight, and titanium and iron elements have low weight percent of 0.46 and 2.39%, respectively. After the beneficiation process and reduction of silver nanoparticles into the clay, the percentage weight of silicon in the Ag/clay became 13.97%, Aluminium, 11.71%, which further revealed the kaolinite nature of the clay (Al: Si equals 1:1). The EDS result also confirmed the successful immobilization of the silver nanoparticles on the clay with 0.74% of Ag present in the prepared adsorbent. Ti and Fe were also retained on the

Ag/clay composite at reduced percentages compared to the unmodified clay.

3.2. Adsorption studies

3.3.1 Effect of contact time on the removal of the heavy metals using silver-clay adsorbent

The influence of contact time on the removal of Zn^{2+} , Pb^{2+} , and Cu^{2+} ions was studied between 30 to 240 min, keeping other parameters constant (Temperature; 30 °C, dosage; 0.5 g, concentration; 100mg/L, pH; 7). Figure 6 shows the effect of contact time on the adsorption of Zn^{2+} , Pb^{2+} , and Cu^{2+} ions. From the figure, as the adsorption time increased from 30 to 240 min, the percentage removal of the metal ion (Zn^{2+} , Pb^{2+} , and Cu^{2+}) increased. Arising steadily from 92.3%, 81.2%, and 80.1% at 30 min to 97.82%, 85.83%, and 85.39% at 90 min, respectively, remained constant afterward. Rapid metal ion uptake of the metal ion may be linked to available surface adsorption sites on the Ag-clay adsorbent (Adebayo, Adegoke, and Sidiq, 2020). Equilibrium was attained at 90 min of the adsorption process, linked to the surface coverage of the adsorbent per time and adherence to functional groups on the adsorbent until no further adsorption occurs.

3.3.2 Effect of adsorbent dose on the removal of the heavy metals

The effect of adsorbent dosage on Zn^{2+} , Pb^{2+} , and Cu^{2+} removal from the wastewater was investigated, and the results are presented in Figure 7. From the figure, increasing the amount of adsorbent from 0.1 g to 0.3 g increases Zn^{2+} , Pb^{2+} and Cu^{2+} percentage removal from the aqueous solution. However, there was no further increment in the percentage adsorbed beyond 0.3 g, as shown in Figure 7. This is because there is no more exposure of the metal ion to the available binding sites due to small adsorbate in the medium, causing less metal ion per gram adsorption (Ajala *et al.*, 2022). In addition, with the increase in adsorbent dosage, aggregation of particles occurs due to the low volume of solution, and as a result, removal efficiency and adsorption of Zn^{2+} , Pb^{2+} , and Cu^{2+} decreases.

3.3.3 Effect of pH on the removal of the heavy metals

In the adsorption process of metal ions from aqueous solutions, the pH of the solution plays an important role. It is apparent from the results represented in Figure 8 that, with the increase in pH, the adsorption of metals increased gradually. Maximum adsorption (99.94%, 99.55, and 99.44% for Zn^{2+} , Pb^{2+} , and Cu^{2+} , respectively) was observed between pH 7 and pH 10, while adsorption of the metal ions was inhibited at lower pH (2–6). The Maximum removal efficiency obtained at high pH was because deprotonation takes place due to the presence of too many OH^- ions produced in the solution, making the surface of Ag/clay become negatively charged. (Hajjaji *et al.*, 2018). Also, higher pH may have improved the electrostatic interaction between negatively charged adsorbent surface and heavy metal ions, which are positively charged, boosting the adsorption of Zn^{2+} , Pb^{2+} and Cu^{2+} onto Ag-Clay composites. Hence the removal efficiency increases with an increase in pH.

3.3.4 Effect of temperature on the removal of the heavy metals

The solution temperature plays a vital role in the adsorption of Zn^{2+} , Pb^{2+} , and Cu^{2+} metal ions onto Ag-clay, as presented in Figure 9. The percentage removal of the three ions was found to increase with the increase in the solution temperature. The adsorption rate of Zn^{2+} , Pb^{2+} , and Cu^{2+} by the Ag-clay nanocomposite rapidly reached a maximum of 97.00%, 88.50%, and 88.33%, respectively, at 40 °C as shown in Figure 9. This phenomenon indicates that the adsorption process of the metal ions onto the nanoparticles may be described as chemisorption or process (Bankole *et al.*, 2019). It can be explained that, at the temperature of 40 °C, the activation of the adsorbent surfaces is enlarged, facilitating more active sites for the adsorption of the metal ions. Moreover, easy mobility and enhanced accessibility of metal ions from the bulk solution to the adsorbent active sites could also be the reason for the maximum adsorption of metal ions at higher temperatures. Also, from the obtained graph, the adsorption for Zn^{2+} , Pb^{2+} , and Cu^{2+} was not so favorable at a temperature higher than 40 °C for the Cu^{2+} ion. Therefore, optimum multi-ion adsorption may not go beyond 40 °C temperature.

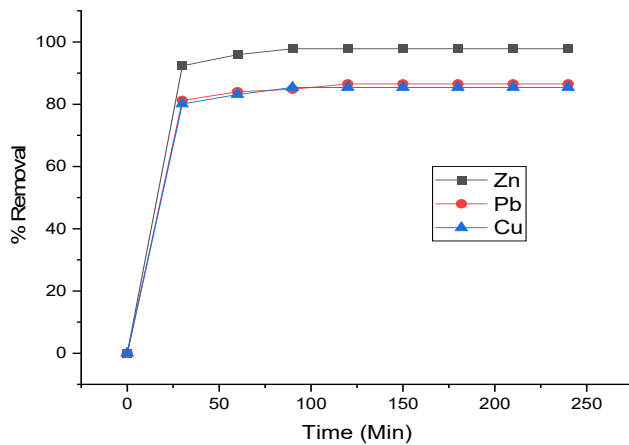


Figure 6. Effect of contact time on % removal

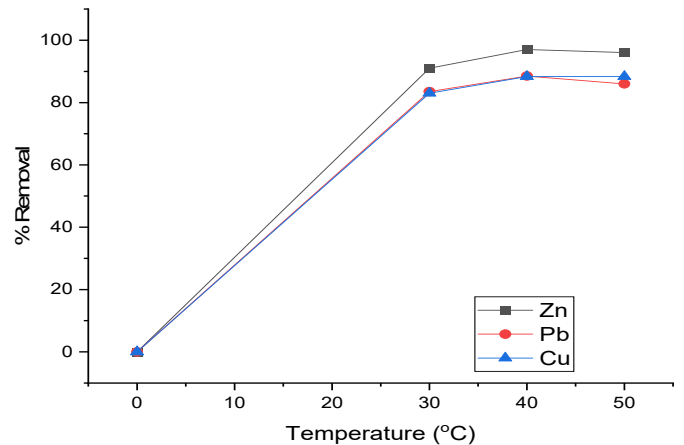


Figure 9. Effect of Temperature on % removal

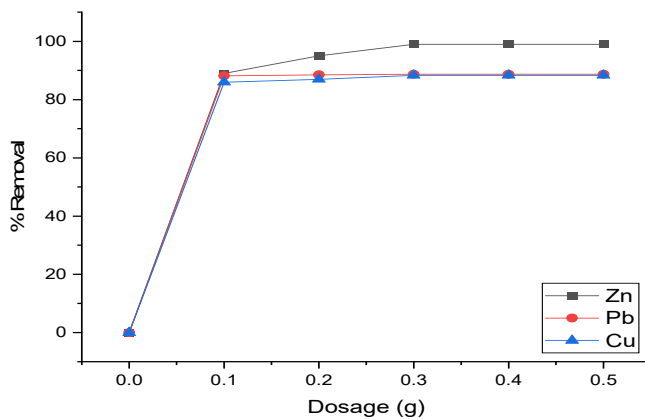


Figure 7. Effect of adsorbent dosage on % removal

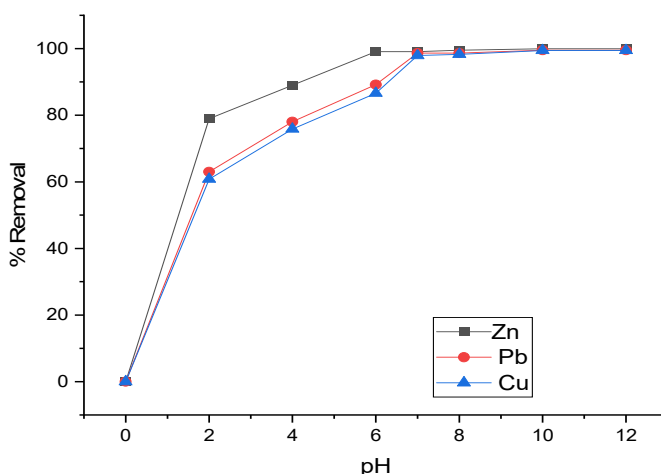


Figure 8. Effect of pH on % removal

3.4 Adsorption Isotherm Studies

The equilibrium adsorption isotherms are essential data sources to design, understand, and optimize the adsorption process. The data expresses the intrinsic properties and interaction between adsorbate and adsorbent. The data can be used to compare the adsorptive capacities of the adsorbent for different pollutants. Isotherm models investigated for the adsorption of Zn^{2+} , Pb^{2+} , and Cu^{2+} onto Ag/Clay are; Langmuir, Freundlich, Temkin, and Dubinin–Radushkevich, and the result is presented in Table 1. From the table, the Langmuir isotherm has the correlation coefficients (R^2) of 0.976, 0.994, and 0.964 for Zn^{2+} , Pb^{2+} , and Cu^{2+} respectively, which are the highest of the four isotherm models tested. The results show that the Langmuir model is suitable to explain the sorption behavior of the adsorption of the heavy metal ions onto the prepared adsorbent. The Langmuir theory (Langmuir 1918) suggests that the sorbent surface is homogeneous, and there is no interaction in-between the molecules adsorbed during the formation of a monolayer surface coverage. The R_L value calculated for the three ions is between 8.162×10^{-5} and 3.110×10^{-4} , which are less than 1. These values suggest that the adsorption of the ions onto the adsorbents was favorable in all the conditions investigated. Also, from Table 1, the magnitude of the Freundlich isotherm constant K_F suggests that the sorption capacity of the experimented metal ions was in $Zn^{2+} < Cu^{2+} < Pb^{2+}$ order. The value of $N_F > 1$ for Zn^{2+} , Cu^{2+} and Pb^{2+} suggest heterogeneity of the adsorbent surface, and that the metal ions are favorably and intensively adsorbed by silver clay under the experimental conditions. Temkin isotherm constant (b_T), otherwise known as the equilibrium binding factor, was calculated from the Temkin

isotherm expression and shown in Table 1. As shown in Table 1, Pb^{2+} has the highest equilibrium binding constant at low temperatures. The low values of the Temkin adsorption potential, A_T in the range of 3.418 to 0.115 (L/mg), indicate a lower sorbent-metal ion potential. The Dubinin–Radushkevich (D-R) isotherm was applied to distinguish the physical and chemical adsorption of metal ions with its mean free energy. The D-R isotherm has the lowest regression values plots are 0.891, 0.443, and 0.651 for Zn^{2+} , Pb^{2+} , and Cu^{2+} , respectively. The apparent free energy (E) values obtained less than ($<$) 40 kJ/mol, which signifies that the nature of the adsorption mechanism is physisorption (Ayawei *et al.*, 2017). Comparing the average error functions (X^2 and SSE), it was reported that the closer to zero the values of the error functions are, the suitability of the model reported (Egboosiuba *et al.*, 2020). Therefore from Table 1, out of the four isotherms, the Langmuir isotherm has the lowest error values, which are closer to zero than those of the Freundlich, Temkin, and Dubinin–Radushkevich isotherms. These results further confirmed the suitability of the Langmuir isotherm model for the description of the adsorption process, which means; the adsorption of Zn^{2+} , Cu^{2+} and Pb^{2+} is based on single-layer coverage on the adsorbent surface which depicts a monolayer formation.

3.5 Adsorption Kinetics Studies

The kinetic data are essential to understanding the rate and nature of adsorption onto the adsorbents. In addition, the data can be used to compare the kinetics of the adsorbent for different pollutants. Figures 10 and 11 show the Pseudo-first-order (PFO) and Pseudo-second-order (PSO) plots for the adsorption of Zn^{2+} , Pb^{2+} , and Cu^{2+} onto the Ag/clay adsorbent from which the kinetics parameters in Table 2 was obtained. The PFO is based on multi-layer adsorption on the adsorbent surface, explained by the forces such as the Van der Waals (Ngakou *et al.*, 2019). From the table, the regression coefficients (R^2) for the heavy metal ions are 0.839, 0.917, and 0.935 for the PFO. This result suggests that the experimental data support the PFO model to describe adsorption kinetics of the three metal ions, most especially for Cu^{2+} .

However, the differences between the modeled adsorptive capacity values, ($q_{e, cal}$) and the experimental values ($q_{e, exp}$) are very high. This refers to the fact that both the metal ions and adsorbents were involved in the adsorption

process (Meitei and Prasad, 2014). Therefore, from the residual plot and the error functions, it is suggested that the pseudo-first-order model does not describe the kinetic sorption of the process sufficiently, over the range of experimental time considered. Also from Table 2 presented, it was noted that the regression coefficients for the three ions are high in the order; Cu^{2+} (0.982) > Pb^{2+} (0.969) > Zn^{2+} (0.968) which implies good correlation of the model. Considering the modeled and the experimental values of the adsorptive capacities ($q_{e, cal}$, and $q_{e, exp}$), the obtained values are closer unlike that of the PFO that are wide apart. Moreover, the error function values (SSE and X^2) for PSO are lower compared with the PFO. This suggests that the PSO kinetic model fits the adsorption process better. This interaction implies that there is a mono-layer coverage between the adsorbed and the adsorbent, with π - π bond interactions as the major bonds formed (Bello, Chris, Oluwakemi, and Olatunde, 2020; Ngakou *et al.*, 2019) in the Zn^{2+} , Pb^{2+} , and Cu^{2+} adsorption onto the Ag/clay surface.

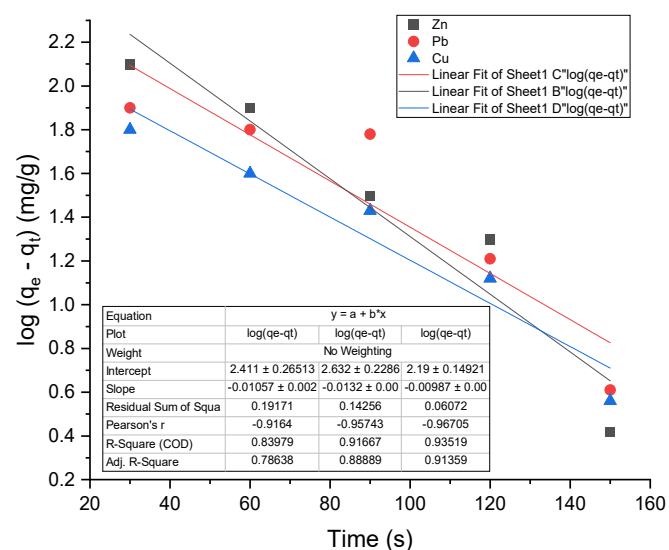


Figure 10. Pseudo-first-order plots

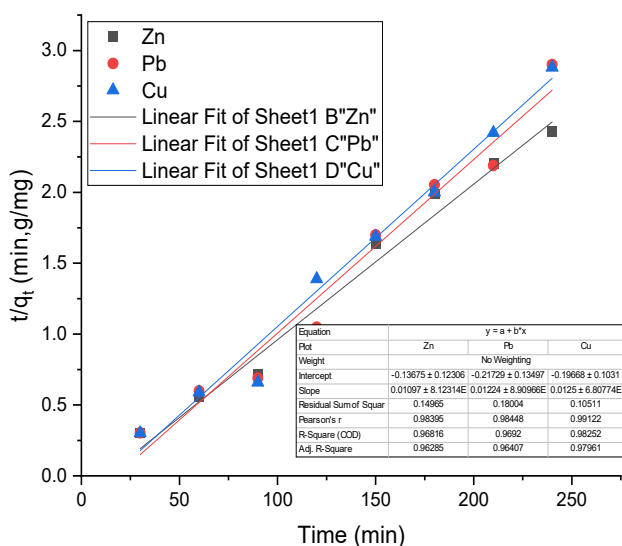


Figure 11. Pseudo-second-order plots

To justify the Zn^{2+} , Pb^{2+} , and Cu^{2+} adsorption from pharmaceutical wastewater, the results obtained in this study were compared with the percentage removal of pollutants by other adsorbents. The result of the findings for another pollutant removal by silver and clay-formulated adsorbents is presented in Table 3. The data in Table 3 showed that the percentage removal of Zn^{2+} , Pb^{2+} and Cu^{2+} ions using the Ag/clay adsorbent was higher than that of acid-activated Bentonite clay for the removal of similar heavy metal ions (Budsaerechai, Kamwialisak, and Ngernyen, 2012). In another research where Ag/kaolinite was used to remove an Acid cyanine dye, about 90% removal percentage of the dye was reported (Hashemian and Shahedi, 2013). Other composites/adsorbents such as AgNPs/TAC (Trinh *et al.*, 2020), Ag/TiO₂ (Demirci *et al.*, 2016), Clay/ZnO/Ag (Demirci *et al.*, 2016) do not compare efficiently with the 99.96%, 99.5%, and 99.44% removal efficiency obtained for Zn^{2+} , Pb^{2+} , and Cu^{2+} in the present study. This indicated that Ag/clay is a potentially effective and efficient adsorbent for removing heavy metal ions from aqueous solutions.

3.6. Thermodynamics

The adsorption thermodynamics was fitted by Vant Hoff's linear plot of $\ln K_d$ versus $1/T$ in Figure 12. From the figure, thermodynamics parameters; Gibb's free energy (ΔG°), enthalpy (ΔH°), and entropy (ΔS°) values were obtained as shown in Table 4. The negative Gibb's free energy (ΔG°) value obtained for the three ions at various temperatures revealed the adsorption of Zn^{2+} , Pb^{2+} , and Cu^{2+} ions onto Ag/clay adsorbents was

feasible and spontaneous. The obtained ΔH° values at 313, 323, and 333 K temperatures are negative, this shows that the adsorption process is exothermic. Also in Table 4, the enthalpy values obtained for Zn^{2+} , and Cu^{2+} (II) were greater than 40 kJ/mol, suggesting that the process is more chemically controlled than physically controlled, similar to previous research (Khulbe and Matsuura, 2019). The negative ΔS° implied that there is a reduction in the degree of randomness at the Ag/clay and Zn^{2+} , Pb^{2+} , and Cu^{2+} interfaces during the sorption process.

4. CONCLUSIONS

A new adsorbent was synthesized using local clay from Akerebiata, Ilorin modified with silver nanoparticles. The synthesis of Ag nanoparticles in a green process confirms the suitability of *Parkia biglobosa* leaf extract as a reducing, capping, and stabilizing agent. The local clay was also confirmed kaolinite in nature, rich in silica, and contains functional groups capable of binding metal ions to themselves. The adsorption of selected heavy metal ions; Zn^{2+} , Pb^{2+} , and Cu^{2+} onto the silver-modified clay was affected by contact time, pH, adsorbent dosage and temperature with equilibrium attained at 90 min. The Langmuir isotherm and Pseudo-second-order kinetics model best modeled the adsorption process. It was feasible, spontaneous, and exothermic in the order $Zn^{2+} > Pb^{2+} > Cu^{2+}$. The silver-clay adsorbent is, therefore, suitable and efficient for removing heavy metal ions from an aqueous solution.

5. DECLARATIONS

5.1. Study Limitations

No limitations were known at the time of the study.

5.2. Acknowledgements

The authors would like to thank the University of Ilorin, Ilorin Nigeria for providing enabling environment for this research.

5.3. Funding source

The authors funded this research.

5.4. Competing Interests

No potential conflict of interest exists in this publication.

5.5. Open Access

This article is licensed under a Creative Commons Attribution 4.0 (CC BY 4.0) International License, which permits use, sharing, adaptation, distribution, and reproduction in any medium or format, as long as you give appropriate credit to the original author(s) and the source, provide a link to the Creative Commons license, and indicate if changes were made. The images or other third-party material in this article are included in the article's Creative Commons license unless indicated otherwise in a credit line to the material. Suppose material is not included in the article's Creative Commons license, and your intended use is not permitted by statutory regulation or exceeds the permitted use. In that case, you will need to obtain permission directly from the copyright holder. To view a copy of this license, visit <http://creativecommons.org/licenses/by/4.0/>.

6. REFERENCES:

1. Adebayo, G. B., Adegoke, H. I., and F., S. (2020). Adsorption of Cr(VI) ions onto goethite, activated carbon and their composite: kinetic and thermodynamic studies. *Applied Water Science*, 10, 213-231. doi:10.1007/s13201-020-01295-z
2. Adebayo, G. B., Adegoke, H. I., and Sidiq, F. (2020). Adsorption of Cr(VI) ions onto goethite, activated carbon and their composite: kinetic and thermodynamic studies. *Applied Water Science*, 10, 213-231. doi:10.1007/s13201-020-01295-z
3. Ajala, M. A., Abdulkareem, A. S., Tijani, J. O., and Kovo, A. S. (2022). Adsorptive behaviour of rutile phased titania nanoparticles supported on acid-modified kaolinite clay for the removal of selected heavy metal ions from mining wastewater. *Applied Water Science*, 12(19), 1-24. doi:10.1007/s13201-021-01561-8
4. Ajala, M. A., Ajala, E. O., Tayo-Alabi, A., Sodiq, H. K., Abdulkareem, A. S., Kovo, A. S., and Tijani, J. O. (2022). Development of Titanium Dioxide Pillared Clay Adsorbent for Removal of Lead (II), Zinc (II), and Copper (II) ions from Aqueous Solution. *UNIOSUN Journal of Engineering and Environmental Sciences*, 4(1), 264-280. doi:10.36108/ujees/2202.40.0172
5. Alaya-Ibrahim, S., Kovo, A. S., Abdulkareem, A. S., Adeniyi, O. D., and Yahya, M. D. (2019). Development of nano-silver doped zeolite Asynthesized from Nigerian Ahoko kaolin for treatment of wastewater of a typical textile company. *Chemical Engineering Communications*, 9, 1-25. doi:10.1080/00986445.2019.1641490
6. Asamoah, R. B., Yaya, A., Nbelayim, P., Annan, E., and Onwona-Agyeman, B. (2020). Development and Characterization of Clay-Nanocomposites for Water Purification. *Materials (Basel, Switzerland)*, 13(17), 3793. doi:10.3390/ma13173793
7. Ayawei, N., Ebelegi, A. N., and Wankasi, D. (2017). Modelling and Interpretation of Adsorption Isotherms. *Journal of Chemistry*, 2017, 3039817. doi:10.1155/2017/3039817
8. Balali-Mood, M., Naseri, K., Tahergorabi, Z., Khazdair, M. R., and Sadeghi, M. (2021). Toxic Mechanisms of Five Heavy Metals: Mercury, Lead, Chromium, Cadmium, and Arsenic. 12(227). doi:10.3389/fphar.2021.643972
9. Bankole, M. T., Abdulkareem, A. S., Mohammed, I. A., Ochigbo, S. S., Tijani, J. O., Abubakre, O. K., and Roos, W. D. (2019). Selected heavymetals removal from electroplating wastewater by purifiedand polyhydroxybutyrate functionalized carbon nanotubesadsorbents. . *Scientific Report*, 9, 1-19. doi:10.1038/s41598-018-37899-4
10. Bashir, I., Lone, F. A., Bhat, R. A., Mir, S. A., Dar, Z. A., and Dar, S. A. (2020). Concerns and Threats of Contamination on Aquatic Ecosystems. In K. R. Hakeem, R. A. Bhat, and H. Qadri (Eds.), *Bioremediation and Biotechnology: Sustainable Approaches to Pollution Degradation* (pp. 1-26). Cham: Springer International Publishing.
11. Bello, O., Chris, T., Oluwakemi, C. A., and Olatunde, A. (2020). Sequestering a non-steroidal anti-inflammatory drug using modified orange peels. *Applied Water Science*, 10. doi:10.1007/s13201-020-01254-8
12. Budsareechai, S., Kamwialisak, K., and Ngernyen, Y. (2012). Adsorption of lead, cadmium and copper on natural and acid activated bentonite clay. *KKU Research*

- Journal*, 17(5), 800-810.
13. Choudhary, N., Yadav, V. K., Yadav, K. K., Almohana, A. I., Almojil, S. F., Gnanamoorthy, G., . . . Jeon, B. H. (2021). Application of Green Synthesized MMT/Ag Nanocomposite for Removal of Methylene Blue from Aqueous Solution. *Water*, 13(3206). doi:10.3390/w13223206
 14. Dave, P., and Chopda, L. (2014). Application of Iron Oxide Nanomaterials for the Removal of Heavy Metals. *Journal of Nanotechnology*, 2014(1), 1-14. doi:10.1155/2014/398569
 15. Demirci, S., Dikici, T., Yurddaskal, M., Gultekin, S., Toparli, M., and Celik, E. (2016). Synthesis and characterization of Ag doped TiO₂ heterojunction films and their photocatalytic performances. *Applied Surface Science*, 390, 591-601. doi:https://doi.org/10.1016/j.apsusc.2016.08.145
 16. Dhand, V., Soumya, L., Bharadwaj, S. G., Chakra, S., Bhatt, D., and Sreedhar, B. (2016). Green synthesis of silver nanoparticles using Coffea arabica seed extract and its antibacterial activity. *Materials science and engineering. C, Materials for biological applications*, 58, 36-43. doi:10.1016/j.msec.2015.08.018
 17. Dubinin, M. M., 1969. (1969). The potential theory of adsorption of gas theory of adsorption of gases and vapour. *Chem. Rev.*, 60, 235-241
 18. Dutta, D., Borah, P. J., and Puzari, A. (2021). Iron oxide coated hollow poly(methylmethacrylate) as an efficient adsorption media for removal of arsenic from water. *RSC Advances*, 11, 13376-13385. doi:10.1039/D0RA10801D
 19. Egbosiuba, T. C., Abdulkareem, A. S., Kovo, A. S., Afolabi, E. A., Tijani, J. O., Auta, M., and Roos, W. D. (2019). Ultrasonic enhanced adsorption of methylene blue onto the optimized surface area of activated carbon: Adsorption isotherm, kinetics and thermodynamics. *Chemical Engineering Research and Design*, 153, 315-336. doi:10.106/j.cherd.2019.10.016
 20. Egbosiuba, T. C., Abdulkareem, A. S., Kovo, A. S., Afolabi, E. A., Tijani, J. O., and Roos, W. D. (2020). Enhanced adsorption of As(V) and Mn(VII) from industrial wastewater using multi-walled carbon nanotubes and carboxylated multi-walled carbon nanotubes. *Chemosphere*, 254(126780). doi:10.1016/j.chemosphere.2020.126780
 21. Hajjaji, W., Andrejkovičová, S., Pullar, R. C., Tobaldi, D. M., Lopez-Galindo, A., Jammousi, F. and Labrincha, J. A. (2018). Effective removal of anionic and cationic dyes by kaolinite and TiO₂/kaolinite composites. *Clay Minerals*, 51(1), 19-27. doi:10.1180/claymin.2016.051.1.02
 22. Hashemian, S., and Shahedi, M. R. (2013). Novel Ag/Kaolin Nanocomposite as Adsorbent for Removal of Acid Cyanine 5R from Aqueous Solution. *Journal of Chemistry*, 2013, 285671. doi:10.1155/2013/285671
 23. Ho, Y. S., and McKay, G. (1999). Pseudo-second order model for sorption processes. 34, 451-465. *Process Biochemistry*, 34(5), 451-465. doi:10.1016/S0032-9592(98)00112-5
 24. Kariim, I., Abdulkareem, A. S., and Abubakre, O. K. (2020). Development and characterization of MWCNTs from activated carbon as adsorbent for metronidazole and levofloxacin sorption from pharmaceutical wastewater: Kinetics, isotherms and thermodynamic studies. *Scientific African*, 7(2020). doi:10.1016/j.sciaf.2019.e00242
 25. Kaur, A., and Sharma, S. (2017). Removal of Heavy Metals from Waste Water by using Various Adsorbents- A Review. *Indian Journal of Science and Technology*, Vol 10(34), DOI: , September 2017, 10(34). doi:10.17485/ijst/2017/v10i34/117269
 26. Khulbe, K. C., and Matsuura, T. (2019). Removal of heavy metals and pollutants by membrane adsorption techniques. *Applied Water Science*, 8(19), 1-30. doi:10.1007/s13201-018-0661-6
 27. Korolkova, S. V., Volovicheva, N. A., Vezentsev, A. I., Gorbunova, N. M., and Nurasyil, T. E. (2020). Sorption of Cu²⁺ ions and Fe³⁺ with alkaline forms of montmorillonite containing clay. *European Journal of Molecular and Clinical Medicine*, 7(2), 5586-5597
 28. Lakherwal, D. (2014). Adsorption of Heavy Metals: A Review. *International Journal of Environmental Research and Development*, 4(1), 41-48

29. Langmuir, I. (1918). The Constitution and Fundamental properties of Solids and Liquids. *Journal of American Chemical society.*, 38, 2221-2295
30. López-Luna, J., Ramírez-Montes, L. E., Martínez-Vargas, S., Martínez, A. I., Mijangos-Ricardez, O. F., González-Chávez, M. A., . . . Vázquez-Hipólito, V. (2019). Linear and nonlinear kinetic and isotherm adsorption models for arsenic removal by manganese ferrite nanoparticles. *SN Applied Sciences*, 1(950), 1-19. doi:10.1007/s42452-019-0977-3
31. Meitei, M. D., and Prasad, M. N. V. (2014). Adsorption of Cu (II), Mn (II) and Zn (II) by *Spirodela polyrhiza* (L.): Equilibrium, Kinetic and Thermodynamic studies *Ecological Engineering*, 71, 308–317
32. Miyah, Y., Lahrichi, A., Idrissi, M., Boujraf, S., Taouda, H., and Zerrouq, F. (2017). Assessment of adsorption kinetics for removal potential of Crystal Violet dye from aqueous solutions using Moroccan pyrophyllite. *Journal of the Association of Arab Universities for Basic and Applied Sciences*, 23, 20-28. doi:10.1016/j.jaubas.2016.06.001
33. Mustapha, S., Ndamitso, M. M., Abdulkareem, A. S., Tijani, J. O., Mohammed, A. K., and Shuaib, D. T. (2019). Potential of using kaolin as a natural adsorbent for the removal of pollutants from tannery wastewater. *Heliyon*, 5(e02923), 1-17. doi:10.1016/j.heliyon.2019.e02923
34. Ngakou, C. S., Anagho, G. S., and Ngomo, H. M. (2019). Non-linear Regression Analysis for the Adsorption Kinetics and Equilibrium Isotherm of Phenacetin onto Activated Carbons. *Current Journal of Applied Science and Technology*, 36(4), 1-18
35. Sadasivam, S., and Rao, S. (2016). Characterization of silver—kaolinite (AgK): An adsorbent for long-lived 129I species. *SpringerPlus*, 5. doi:10.1186/s40064-016-1855-8
36. Trinh, V. T., Nguyen, T. M., Van, H. T., Hoang, L. P., Nguyen, T. V., Ha, L. T., . . . Nguyen, X. C. (2020). Phosphate Adsorption by Silver Nanoparticles-Loaded Activated Carbon derived from Tea Residue. *Scientific Reports*, 10(3634), 1-13. doi:10.1038/s41598-020-60542-0
37. WHO. (2019). WHO Guidelines for Drinking Water Quality: First Addendum to the Fourth Edition. In J. A. Cotruvo (Ed.), (Vol. 109, pp. 44-51). Washington, DC, USA: American Water Works Association.

Table 1.: Adsorption isotherm model parameters for the metal ion adsorption onto silver oxide nanoparticles modified clay

Model	Parameter	Metal ions		
		Zn ²⁺	Pb ²⁺	Cu ²⁺
Langmuir	q _m (mg/g)	10.030	22.222	6.803
	K _L	1.231	3.214	12.250
	R _L	8.117x10 ⁻⁴	3.110x10 ⁻⁴	8.162x10 ⁻⁵
	R ²	0.980	0.973	0.960
	X ²	0.003	6.85x10 ⁻⁶	4.725x10 ⁻⁵
	SSE	0.012	2.73x10 ⁻⁵	1.890x10 ⁻⁴
Freundlich	K _F (mg/g)	0.509	1.000	1.000
	N	1.56	0.651	1.073
	R ²	0.955	0.933	0.916
	X ²	0.006	0.049	0.023
	SSE	0.022	0.194	0.091
Temkin	A _T (L/g)	0.115	3.418	0.627
	b _T (kJ/mol)	0.126	0.180	0.097

D-R	R ²	0.815	0.611	0.843
	X ²	128.647	445.907	178.410
	SSE	514.587	8.842	713.640
	E(kJ/mol)	0.354	0.354	0.360
	K _{ad}	3.977	3.982	3.867
	R ²	0.892	0.443	0.651
	X ²	0.071	0.515	0.208
	SSE	0.285	2.060	0.813

Table 2. Kinetics parameter of the metal ions adsorption onto Ag/clay adsorbent

Model	Parameter	Metal ions		
		Zn ²⁺	Pb ²⁺	Cu ²⁺
PFO	q _{e,exp} (mg/g)	97.800	97.000	96.400
	q _{e,cal} (mg/g)	11.145	13.902	8.935
	k ₁ (min ⁻¹)	0.011	0.013	0.010
	R ²	0.839	0.917	0.935
	SSE	0.192	0.143	0.061
	X ²	0.064	0.048	0.020
	PSO	q _{e,exp} (mg/g)	97.800	97.000
q _{e,cal} (mg/g)		90.910	83.330	76.92
k ₂ (min ⁻¹)		0.001	0.001	0.002
R ²		0.968	0.969	0.982
SSE		0.149	0.108	0.011
X ²		0.024	0.030	0.018

Table 3. Comparison of Ag/clay removal capacity with other adsorbents for pollutants removal

Adsorbent	Pollutants removed	Adsorptive conditions	Removal capacity %	Reference
Acid activated bentonite clay	Cu ²⁺ , Cd ²⁺ and Pb ²⁺	t=36 h, Co =2000 mg/L, d=1g	36.68, 57.88, 92.85%	Budsareechai <i>et al.</i> (2012)
Montmorillonite clay	Cu ²⁺ , Fe ³⁺	t=42 h, T=25°C, d=2g	0.358, 0.189 mmol/g	Korolkova, Volovicheva, Vezentsev, Gorbunova, and Nurasyil (2020)
Kaolin	Methylene blue	t=20 min	90%	Hajjaji <i>et al.</i> (2018)
Ag/kaolin nanocomposite	Acid cyanine dye	pH 3, t=60 min	90%	Hashemian and Shahedi (2013)
AgNPs/TAC	Phosphate	pH 3, t=150 min, Co=30 mg/L	78.0% (13.62 mg/g)	Trinh <i>et al.</i> (2020)
Clay/CuO/Ag	<i>E. coli</i>	t=48 h	90%	Asamoah <i>et al.</i> (2020)
Clay/ZnO/Ag	<i>S. aureus</i>	t=48 h	>90%	Asamoah <i>et al.</i> (2020)

Ag/TiO ₂	Methylene blue	Co=3 mg/L	54.13%	Demirci <i>et al.</i> (2016)
Ag/clay	Zn ²⁺ , Pb ²⁺ , and Cu ²⁺	d=0.3 g, 90 min, Co =100 mg/L	>95%	This study

Co= Initial concentration, t=contact time, d=Adsorbent dosage, pH, T=temperature

Table 4. Thermodynamics parameters for Zn²⁺, Pb²⁺ and Cu²⁺ adsorption onto the Ag/clay

Adsorbate	ΔH° (kJ/mol)	ΔS° (kJ/mol.K)	ΔG° (kJ/mol)			R ²
			303K	313K	323K	
Zn ²⁺	-59.986	-2.562x10 ⁻³	-2.071	-3.877	-6.082	0.999
Pb ²⁺	-28.101	8.384 x10 ⁻²	-1.007	-1.866	-2.890	0.998
Cu ²⁺	-70.46	2.119 x10 ⁻¹	-2.136	-3.929	-6.821	1.000

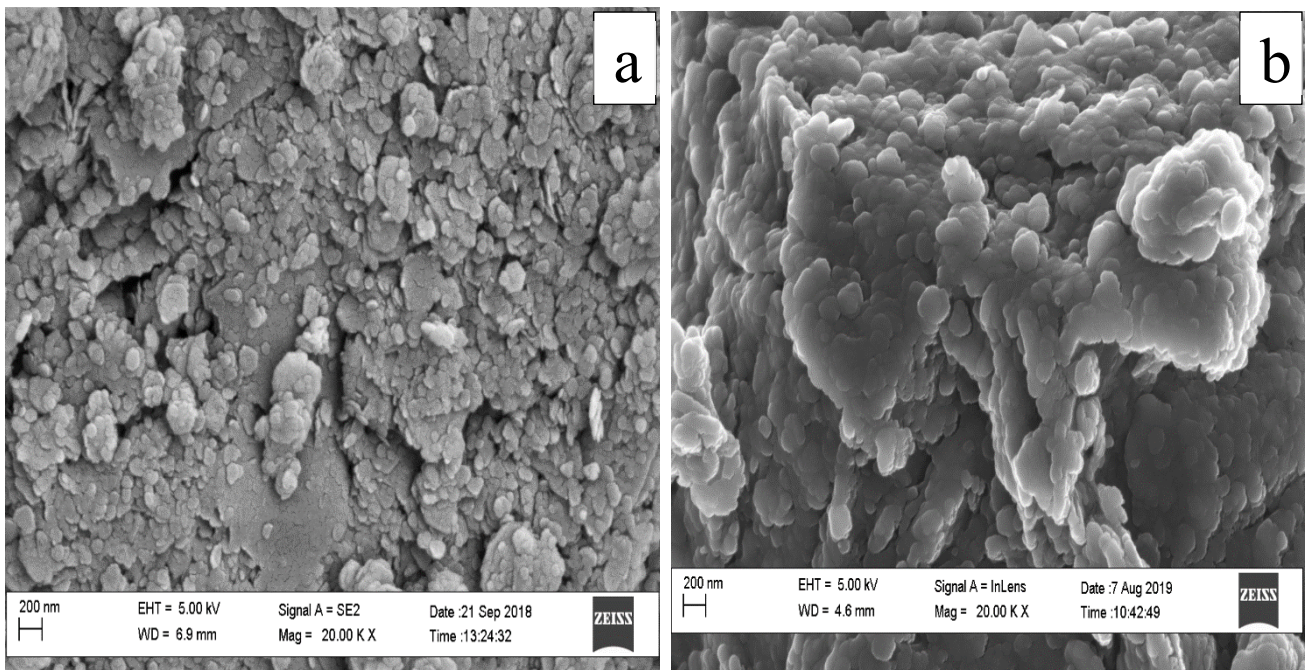


Figure 4. SEM Image of (a) Raw clay (b) Silver/clay adsorbent

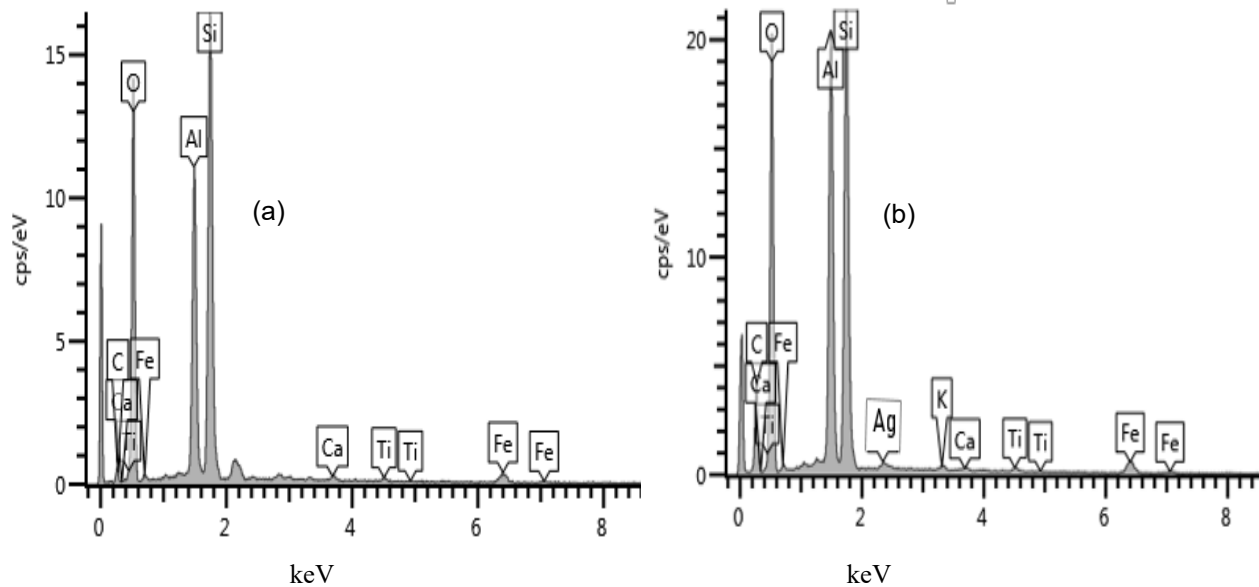


Figure 5. EDS of the (a) Raw-clay and (b) Silver-Clay Adsorbents

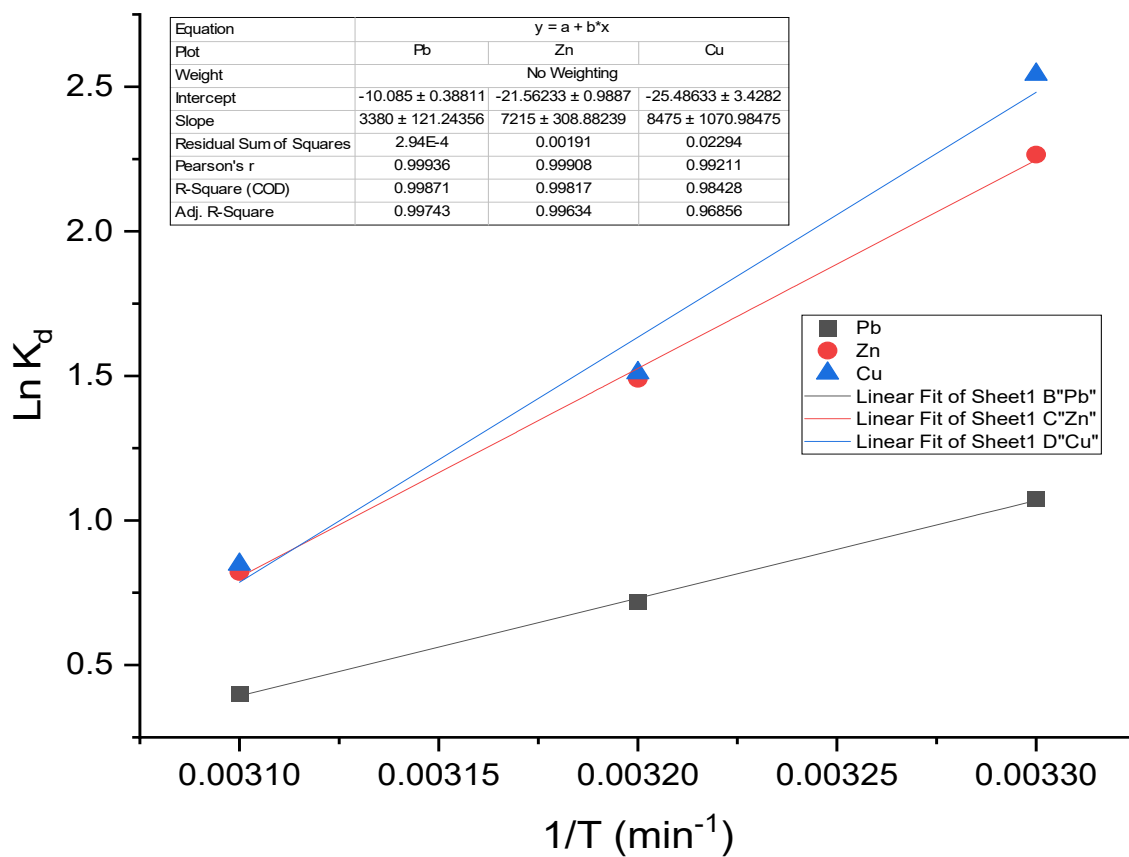


Figure 12. Vant Hoff's plot for Zn^{2+} , Pb^{2+} , and Cu^{2+} adsorption onto the Ag/clay

THE INFLUENCE OF CLIMATIC FACTORS ON THE CHANGE IN THE ELASTIC-STRENGTH INDICATORS OF EPOXY POLYMERS BINDERS USED IN LIQUID THERMAL INSULATION COATINGS

ORYNBEKOV, Yelzhan S.¹, ZHUMADILOVA, Zhanar O.^{2*}; SELYAEV, Vladimir P.³;
NURLYBAEV, Ruslan E.⁴; SANGULOVA, Indira B.⁵

^{1,2,5} Satbayev University, Institute of Architecture and Civil Engineering, Almaty, Kazakhstan

³ Ogarev Mordovia State University, Department of Building Constructions, Saransk – Republic of Mordovia, Russia

⁴ LLP SAVENERGY, Industrial zone, Almaty, Kazakhstan

* Corresponding author
e-mail: zhanar_85@mail.ru

Received 20 November 2021; received in revised form 30 November 2021; accepted 14 December 2021

ABSTRACT

Introduction: Thermal insulating coatings are increasingly being introduced into construction practice for internal and external finishing enclosing structures and pipelines. Thermal insulation coatings are usually made based on polymer binder and mineral fillers. The durability and stability of the properties of heat-insulating materials depend on the type of binder. As a rule, polymers are used as a binder: epoxy resin; silicone rubber; urea-formaldehyde resins; aqueous dispersed polymers - styrene-butadiene, polyvinyl acetate, and acrylate (acrylic and styrene-acrylic). The quality indicator of binders can be assessed by the influence of the seasonality of climatic impact, and as a result, the best elastic strength characteristics of binders can be established after one month to a year of field tests. **Aim:** To determine the influence of climatic factors on the change in the elastic-strength indicators of epoxy polymers binders used in liquid thermal insulation coatings. **Methods:** A tensile testing machine of the AGS-X series with the TRAPEZIUM X software was used for mechanical tests. The tests were carried out in accordance with GOST 11262-2017 (ISO 527-2: 2012) "Plastics. Tensile test method". **Results and Discussion:** The paper discusses the results of experimental studies of the compositions of polymer binders and their resistance to various climatic factors, which will later be used as a polymer binder for thermal insulation coatings based on fine mineral granular systems. **Conclusions:** When analyzing the changes in the characteristics of polymer samples after exposure to climatic factors, it was found that compositions based on Etal-247 epoxy resin, cured with amine hardeners Etal-1440N, Etal-1460, Etal-1472, and Etal-45M, demonstrate the best elastic strength characteristics after one year of full-scale tests. The high stability of the indicators under consideration allows us to conclude that the use of Etal-247 resin as a base leads to creating of the most climate-resistant epoxy coatings.

Keywords: *Durability, temperature, elongation, tensile strength of samples, modified resin.*

1. INTRODUCTION:

The influence of climatic factors on the durability of polymer coatings was investigated and considered in the works of authors (Kablov, 2010; Kablov *et al.*, 2010; Kablov *et al.*, 2011; Startsev, Krotov and Golub, 1998; Startsev, 2009; Kablov, 2018; Selyaev, 2018; Nizina *et al.*, 2016; Selyaev *et al.*, 2020). Furthermore, based on experimental studies of field observations, the following main influencing factors were

established and identified:

- solar radiation, its component in the ultraviolet range;
- the temperature of the ambient air and the temperature of the outer layers of the products;
- the amplitude of daily fluctuations in the temperature of both the air and the surface of the outer layers of the samples;
- relative air humidity and the amplitude of daily fluctuations in air and product humidity;
- average wind speed;

- the duration of exposure to positive and negative temperatures;
- the content of chemically active oxides in the air.

The action of the above environmental factors leads to the degradation of the polymer material, which is accompanied by the accumulation of damage and destruction of products, structures, buildings and structures.

Under the influence of climatic factors, the mechanisms of material degradation can be different: destruction; erosion; corrosion; plasticization; swelling and shrinkage; sorption and desorption; chemical interaction.

Under the influence of these factors, changes in the structure, the shape of the product, stress-strain state occur, internal stresses appear, strength, deformability (embrittlement) decrease. Cracks appear in the coating, it peels off, changes color and geometric parameters.

2. MATERIALS AND METHODS:

An AGS-X series tensile testing machine with TRAPEZIUM X software was used to carry out mechanical tensile testing of polymer composites compositions. The frequency of fixing the values of stresses and strains was 0.01 s. The tests were carried out in accordance with GOST 11262-2017 (ISO 527-2:2012) "Plastics. Tensile test method" at a temperature of 23 ± 2 °C and relative humidity of $50 \pm 5\%$ (GOST 11262-2017 (ISO 527-2: 2012), 2018). The spreading speed of the jaws of the tensile testing machine was 2 mm/min. In parallel, at least 6 samples were tested, having the shape of "eights" (type 2 according to GOST 11262).

GOST 11262-2017 (ISO 527-2:2012) - A test specimen is stretched along its main longitudinal axis at a constant speed, during stretching, the specimen withstands the load, and the elongation of the specimen is measured, and the specified indicators are determined. A testing machine capable of measuring the load with an error of less than 1% of the measured value when the specimen is stretched, and a constant rate of expansion of the clamps within limits is required by this standard.

2.1. Experimental studies of the influence of climatic factors on the change in the elastic-strength indicators of binders

Joint analysis of changes in strength

characteristics and weight gain of epoxy polymers Etal-247 + Etal-45M specimens at the initial stage of exposure allows us to put forward several hypotheses regarding the physical-chemical processes occurring in the structure of the polymer matrix (Figure 1) (Kablov, 2010; Kablov *et al.*, 2010; Kablov *et al.*, 2011; Startsev, Krotov and Golub, 1998; Startsev, 2009; Kablov, 2010; Kablov *et al.*, 2010; Kablov *et al.*, 2011; Startsev, Krotov and Golub, 1998; Startsev, 2009; Selyaev *et al.*, 2020). Analysis of the data presented in Figure 1a, indicates that the relative humidity of samples at the age of 3 months is practically independent of the time of the beginning of the exposure. In this case, the change in the strength indicators of the samples for each of the series of samples is different (Figure 1b), which indicates the absence of a direct relationship between the weight gain and the ultimate tensile strength.

The discrepancy in strength indicators depending on the moment of the beginning of exposure can be described based on the main acting environmental factors (Kablov *et al.*, 2010; Kablov *et al.*, 2011; Startsev, Krotov and Golub, 1998). In particular, although the solar radiation levels in the spring and autumn periods are almost identical, in the first case, there is a slight increase, and in the second, a decrease in strength indicators.

The reason for this is probably the difference in the surface temperature of polymeric materials and the duration of its exposure. Since, among the spring months, only May is characterized by high "activity", as opposed to three months of the summer period, it can be assumed that mainly relaxation processes of the initial structural disequilibrium take place in the first case. At the same time, high levels of solar radiation, combined with temperatures above the glass transition temperature of the polymer binder, during the summer period, could lead to partial surface degradation of the polymer matrix.

The invariability of strength indicators at the end of the autumn period may indicate the equilibrium of the processes of hydrolysis of active, unreacted groups and desorption of low molecular weight reaction products as a result of several successive cycles of moistening and drying (Kablov, 2018; Selyaev, 2018; Nizina *et al.*, 2016). Since the winter months are characterized mainly by negative temperatures in combination with the minimum values of solar radiation, plasticization of the structure of the polymer matrix with atmospheric moisture should be considered as the main reason for the

decrease in strength indicators at this stage.

Analyzing the change in the strength characteristics of specimens of the composition Etal-247 + Etal-45M of various series relative to the common time axis (Figure 2), it should be noted that, despite the same external effect, the change in the properties of specimens of this composition is multidirectional in almost all areas. Taking into account the fact that under prolonged exposure to load, temperature, and moisture, a certain limiting state of the epoxy polymer is reached, characterized by a constant value of strength, it can be argued that the stabilization of properties for the series of samples exposed from March 1 and June 1 was never achieved. The maximum reduction in strength for specimens of these series was 30%. For epoxy polymers exhibited from September 1, the decrease in strength did not exceed 10%; from January 1 - the maximum decrease in strength (about 20%) was recorded in the first three months of aging, while no significant changes were recorded in the remaining time interval. Probably, the stabilization of properties in volume for samples of the "autumn" series occurred at the early stages of exposure, which led to the preservation of properties throughout the experimental study. Since the final seasons of exposure for this series of samples are "spring, summer, and autumn", with a high degree of confidence, one can assume a strong destructive effect of solar radiation on the properties of the epoxy polymer. Nevertheless, due to a large amount of atmospheric precipitation in the spring-autumn time interval of 2021 in combination with the equally high level of solar radiation "summer", it is likely that at this stage, there is also a balance of hydrolytic and desorption processes. The greatest decrease in strength (6%) was recorded for the spring period, which can be explained by the destruction of the surface layer of polymer samples. The change in the properties of the "winter" series samples is inherently close to the course of climatic aging of samples exposed in natural conditions since 2021. The saturation of the samples of this series with moisture at the initial stage, in the absence of a significant effect of solar radiation, despite further drying during the spring season, led to a significant decrease in the strength properties. Apparently, the prevailing role of drying the prevailing role of drying made it possible to compensate for the negative effect of thermal and moisture aging and prevent a further decrease in strength.

Summarizing the data obtained, it can be argued with a high degree of confidence that for

the first incomplete 10 months of exposure, the samples of the compositions under consideration did not transition to the ultimate stable state, characterized by an almost unchanged value of strength indicators. The absence of sharp changes in the strength indicators of epoxy polymers Etal-247 + Etal-45M for less than 10 months of exposure may indicate sufficient stability of the material properties over time.

Let us analyze the climatic resistance of compositions containing the aliphatic diluent Etal-1 (Figure 3). The data obtained for the unmodified composition ED-20 + Etal-45M confirm the previously put forward hypothesis about seasonal differences in the course of structural relaxation processes and the elimination of the initial disequilibrium. So, for compositions, the initial period of exposure of which fell on the seasons with a high level of solar radiation "spring and summer", a sharp drop in strength (more than two times) was recorded after three months. At the same time, the decrease in the strength indicators of the series of samples corresponding to the other two seasons, "winter and spring" occurred more evenly - by 15÷25% per season. Despite the differences in the rate of change in tensile strength, after 10 months of exposure, the strength of all series of samples, without exception, decreased by 60–65% from the initial value. Moreover, if for the epoxy polymers compositions of the "spring" and "summer" series this level was achieved after 6 months of exposure, for the "winter" series - after 9 months, then for the "autumn" series - only by the end of the experimental study, which also suggests the key role of solar radiation in the aging process of the epoxy composition ED-20 + Etal-45M.

The change in the strength of samples of epoxy composition modified with 10% Etal-1 for the "spring" and "summer" series practically does not differ from the control composition. A similar decrease in the absolute value of strength to the level of 20–25 MPa was recorded already after 3 months from the beginning of the exposure. In the future, there are only minor deviations from the obtained values - no more than 6% of the initial value.

For the compositions of other series, changes at the initial stage occur by analogy with the composition Etal-247 + Etal-45M. So, for samples of the "winter" series, there is a decrease in strength caused by the plasticization of intermolecular bonds. However, in the future, due to the effect of solar radiation, there is first a restoration of strength indicators, which is not

typical for an unmodified composition, and then their decrease. Consequently, the introduction of Etal-1 into the composition of ED-20 + Etal-45M leads to a change in the structure of the polymer matrix, in particular, to an increase in the degree of influence of atmospheric moisture on the properties of the epoxy polymer (Startsev, 2009; Kablov, 2018; Selyaev, 2018). Specimens of the "autumn" series, on the other hand, do not undergo significant changes in strength at the initial stage. Nevertheless, by analogy with the composition of ED-20 + Etal-45M, the main decrease in strength takes place precisely during the spring and summer seasons.

The composition (75% ED-20 + 25% Etal-1) + Etal-45M deserves special attention. By analogy with other compositions, at the initial stage, depending on the season of exposure, both an increase and a decrease in strength indicators are observed. At the same time, unlike other modified compositions, a drop in strength over the first 3 months of exposure was recorded only for samples of the "summer" series; in other cases, there is a slight change in properties. It should be noted that regardless of the start of exposure, a sharp drop in strength indicators is observed exclusively in the summer months, which is confirmed by the graphs in Figure 3. As in the case with the samples of the composition (90% ED-20 + 10% Etal-1) + Etal-45M, the recovery of the strength parameters of the epoxy polymers was recorded mainly during the autumn months.

A likely reason for this may be the high proportion of hydroxyl bonds in the composition of the polymer matrix and, accordingly, their increased contribution to the resulting strength value. Consequently, at elevated levels of solar radiation, a number of hydroxyl bonds are destroyed, and the subsequent desorption of low molecular weight components of the polymer matrix takes place. Consequently, at elevated levels of solar radiation, a number of hydroxyl bonds are destroyed, and the subsequent desorption of low molecular weight components of the polymer matrix takes place, leading to a decrease in strength indicators. The increased level of precipitation, in turn, activates the interaction between reactive bonds, leading to additional cross-linking of macromolecules. In total, this change in indicators makes it possible to characterize the properties of the composition under consideration as unstable. Nevertheless, it was found that the greatest change is observed during the relaxation of the initial disequilibrium, that is, hydrolysis of the residues of uncured

binder components and the subsequent desorption of low molecular weight reaction products upon drying. As the number of cycles increases, the change in properties slows down.

2.1.1. Change in elastic-strength and sorption characteristics of polymers during natural climatic aging

It is known that the properties of polymers and their durability during exposure are largely determined by the type of curing system, which makes it extremely important to assess the climatic resistance of polymeric materials with the identification of the most effective resins and hardeners.

The beginning of full-scale exposure at the test site - from December 1, 2020, to September 2021, samples of epoxy polymers were exposed, the compositions of which are shown in Table 1 (except for compositions No. 3, 11, 13, and 14). The change in the elastic-strength parameters of epoxy polymers was recorded after 45, 90, 180, 270, and 300 days of climatic exposure.

According to the results of the tests carried out, it was found that the greatest, almost monotonic, decrease in properties over 180 and 270 days is observed for polymers based on ED-20 epoxy resin, cured, respectively, by Etal-1460 and Etal-45M amine hardeners (Figure 4a). After one year of full-scale exposure, the decrease in strength indicators for the composition cured by Etal-45M reaches 60%, Etal-1460 - 69%. After 10 months of climatic action in a temperate continental climate, the highest stability of properties was recorded for a polymer cured by Etal-1440N. The decrease in tensile strength, in this case, did not exceed 34%. Exposure of this composition for 45 days led to an increase in strength indicators by 13%.

Natural exposure of polymers based on ED-20 epoxy resin is accompanied by a significant decrease in deformative characteristics, which is primarily associated with the embrittlement of the compositions (Figure 4b). The greatest decrease in the relative elongation of polymers is observed up to 180 - 270 days with the stabilization of indicators in the subsequent time interval. For polymers cured, Etal-1460 and Etal-45M, the elongation at maximum load decreases by 7.7 and 3.6 times. For samples cured with Etal-1440N amine hardener, the maximum reduction in tensile deformability does not exceed 2.4 times.

3. RESULTS AND DISCUSSION:

3.1. Results

Analysis of the sorption parameters of epoxy polymers based on ED-20 showed (Figure 5a) that under the influence of climatic factors, accompanied by moistening and drying of the samples, it can occur as a monotonic increase in the mass of the samples (composition 1 - ED-20 + Etal-1440N) and its cyclical change (compositions 2, 4). The greatest cyclicity of mass change is observed for the composition ED-20 + Etal-45M. For polymers based on ED-20 epoxy resin, cured by Etal-1460 and Etal-1440N (Figure 5b), after 3 months of full-scale exposure, an increase in the elastic modulus in tension by 17-22% is observed, which is obviously also associated with embrittlement of samples. Further exposure has practically no effect on this indicator for the composition ED-20 + Etal-1460. An increase in the duration of natural exposure to more than 180 days leads to a decrease in the elastic modulus for the ED-20 + Etal-1440N composition, which does not exceed 10%. Long-term climatic exposure does not significantly affect the change in the elastic modulus of the ED-20 + Etal-45M epoxy polymer. After 10 months of full-scale exposure, the decrease in this characteristic is no more than 10% (Figure 5 b).

Analysis of the results of full-scale exposure of epoxy polymer based on low-viscosity resin Etal-370 (compositions 9, 10, 12) indicates (Figure 6a) about a higher climatic resistance in a time interval of up to 180 days in comparison with compositions No. 1, 2, 4 based on ED-20 (Figure 4). For the compositions Etal-370 + Etal-1460 and Etal-370 + Etal-45M, an increase in tensile strength was recorded, reaching 42 and 31%, respectively, compared with the control values. However, further exposure of the compositions under natural conditions leads to a sharp decrease in properties - the relative tensile strength for these polymers by 300 days is 49÷52% of the initial indicator.

The greatest decrease in deformative indicators also occurs in the time interval from 180 to 300 days (Figure 6b). After a year of full-scale exposure, the reduction in tensile elongation varies depending on the brand of hardener in the range from 3.3 to 4 times. The nature of the change in the mass of the epoxy polymer based on the modified Etal-370 resin (Figry 7a) indicates the highest sorption

moisture absorption during the winter (time interval 0 - 90 days) and autumn (270 - 300 days) periods, which, first of all, is associated with a combination of low temperature and high ambient humidity.

Natural exposure of polymers of this group is accompanied by an increase in the modulus of elasticity in tension, depending on the hardener, up to 10–32% compared to the control samples (Figure 7b).

3.2. Discussions

Compositions based on modified epoxy resin Etal-247 (Figure 8a) have the highest climatic resistance, according to the results of field tests. The maximum decrease in tensile strength after 10 months of full-scale exposure does not exceed 20% for the composition cured by Etal-45M. For polymers cured Etal-1440N and Etal-1460, the residual tensile strength after 300 days of testing is 98 and 84% of the control values, respectively. The impact of climatic factors on the composition of Etal-247 + Etal-1472 practically does not lead to a change in properties over the entire investigated time interval. Polymers based on Etal-247 epoxy resin are also characterized by the highest, compared with other studied polymers, stability of deformation characteristics (Figure 8b). In this case, the maximum decrease 101 in tensile elongation over the entire time interval does not exceed 37%, which is significantly less than for compositions obtained based on ED-20 and Etal-370 epoxy resins (Figures 4, 6).

The nature of the curves describing the change in the mass of epoxy polymers based on Etal-247 resin (Figure 9) is similar to the above graphical dependencies shown in Figures 5a and 3a. In addition, the most noticeable variation in weight depending on the duration of full-scale exposure is also observed for the polymer cured by Etal-45M.

4. CONCLUSIONS:

When analyzing the changes in the characteristics of polymer samples after exposure to climatic factors, it was found that compositions based on Etal-247 epoxy resin, cured with amine hardeners Etal-1440N, Etal-1460, Etal-1472 and Etal-45M, demonstrate the best elastic strength characteristics after one year of full-scale tests. Furthermore, the high stability of the indicators under consideration allows us to conclude that the use of Etal-247 resin as a base leads to creating of the most climate-resistant epoxy

coatings.

5. DECLARATIONS

5.1. Study Limitations

No limitations were known at the time of the study.

5.2. Acknowledgements

The authors are grateful to the leadership of the Satbayev University and the Science Committee of the ME&S RK for creating the conditions for carrying out this work.

5.3. Funding source

This research is funded by the Science Committee of the Ministry of Education and Science of the Republic of Kazakhstan and was done as part of the project AP08855714 "Thermal insulation coatings based on finely dispersed mineral granular systems" in the framework of "Grant funding for scientific and (or) scientific and technical projects for 2020-2022 with an implementation period of 27 months".

5.4. Competing Interests

The authors declare that no potential conflict of interest exists in this publication.

5.5. Open Access

This article is licensed under a Creative Commons Attribution 4.0 (CC BY 4.0) International License, which permits use, sharing, adaptation, distribution, and reproduction in any medium or format, as long as you give appropriate credit to the original author(s) and the source, provide a link to the Creative Commons license, and indicate if changes were made. The images or other third-party material in this article are included in the article's Creative Commons license unless indicated otherwise in a credit line to the material. If material is not included in the article's Creative Commons license and your intended use is not permitted by statutory regulation or exceeds the permitted use, you will need to obtain permission directly from the copyright holder. To view a copy of this license, visit <http://creativecommons.org/licenses/by/4.0/>.

7. REFERENCES:

1. Kablov E. N. Climatic aging of composite materials for aviation purposes. I. Mechanisms of aging. E. N. Kablov, O. V. Startsev, A. S. Krotov, V. N. Kirillov. Deformation and destruction of materials. Moscow, 2010. No.11. 19–27.
2. Kablov E. N. Climatic aging of composite materials for aviation purposes. II. Relaxation of the initial structural irregularity of the gradient of properties across the thickness. E. N. Kablov, O. V. Startsev, A.S. Krotov, V.N. Kirillov. Deformation and destruction of materials. Moscow, 2010. No. 12. 40–46.
3. E. N. Kablov Climatic aging of composite materials for aviation purposes. III. Relaxation of the initial structural irregularity of the gradient of properties across the thickness. E. N. Kablov, O. V. Startsev, A. S. Krotov, V. N. Kirillov. Deformation and destruction of materials. Moscow, 2011. No. 1. 34–40.
4. Startsev O. V., Krotov A. S., Golub P. D. Effect of climatic and radiation aging on properties of glass fiber reinforced plastic VPS-7. International journal of polymeric materials. 1998, Vol. 41. No. 3-4. 263-273.
5. Startsev O. V. Improving the reliability of predicting the properties of polymer composite materials during thermal and moisture aging. O. V. Startsev, L. I. Anikhovskaya, A. A. Litvinov, A. S. Krotov. Reports of the Academy of Sciences. - Moscow, 2009. Volume 428. No. 1. 56–60.
6. Kablov E. N. A systematic analysis of the influence of climate on the mechanical properties of polymer materials according to the data of domestic and foreign sources (review). E. N. Kablov, O. V. Startsev. Aviation materials and technologies. 2018. No. 2. 47-58.
7. V. P. Selyaev, V. O. Startsev, T. A. Nizina, O. V. Startsev, D. R. Nizin, M. V. Molokov. Analysis of the plasticizing effect of moisture on the climatic resistance of epoxy polymers modified with an aliphatic diluent Etal-1. Bulletin of the Privolzhsky territorial branch of RAASN. Issue 21. Nizhny Novgorod: NNGASU, 2018. 200–205.
8. V. P. Selyaev, T. A. Nizina, D. A. Artamonov, D. R. Nizin, D. I. Korovkin, D.O. Andronychev. Results of testing the

compositions of fine-grained concrete exposed under the influence of climatic factors. Construction and reconstruction. 2015. No. 3. 158-165.

11. GOST 11262-2017 (ISO 527-2: 2012) "Plastics. Tensile test method ". Moscow. Standardinform. 2018. 24.

9. Nizina T. A., Selyaev V. P., Nizin D. R., Chernov A.N., Artamonov D. A. Modeling the influence of climatic factors on the strength and decorative characteristics of modified epoxy composites. Corrosion, aging, and biostability of materials in the maritime climate: collection of reports II Int. scientific and technical. Conf., FSUE VIAM, 2016. Access mode: <http://conf.viam.ru/conf/195/proceedings>

10. V. P. Selyaev, D. R. Nizin, T. A. Nizina, A. N. Chernov, A.I. Gorenkova. Impact of seasonality on natural climatic aging of epoxy polymers. Expert: theory and practice. 2020. No. 1. 43–49.

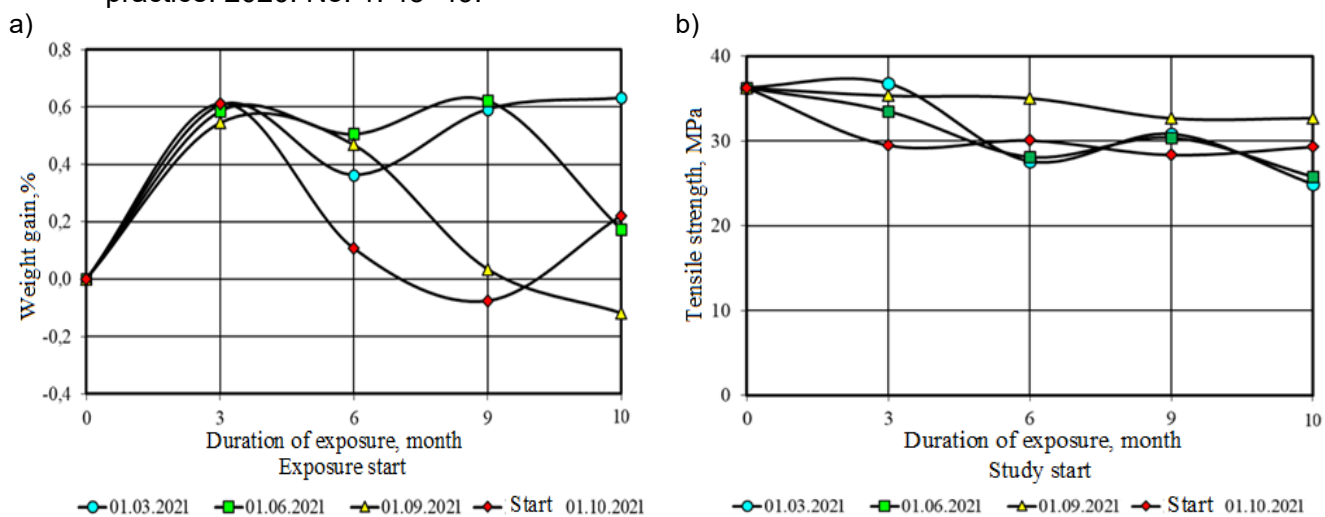


Figure 1. Change in mass (a) and tensile strength (b) samples of composition Etal-247 + Etal-45M, depending on the season of the beginning of exposure

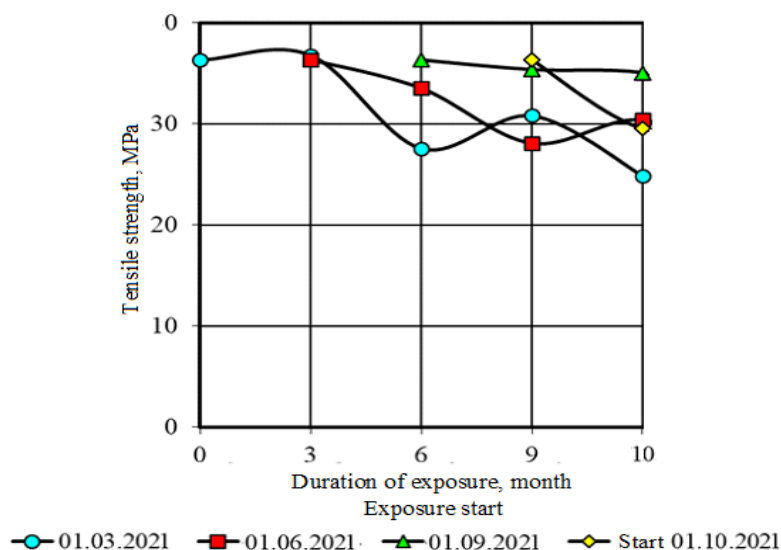


Figure 2. Change in tensile strength of specimens of composition Etal-247 + Etal-45M under tension relative to the common time axis

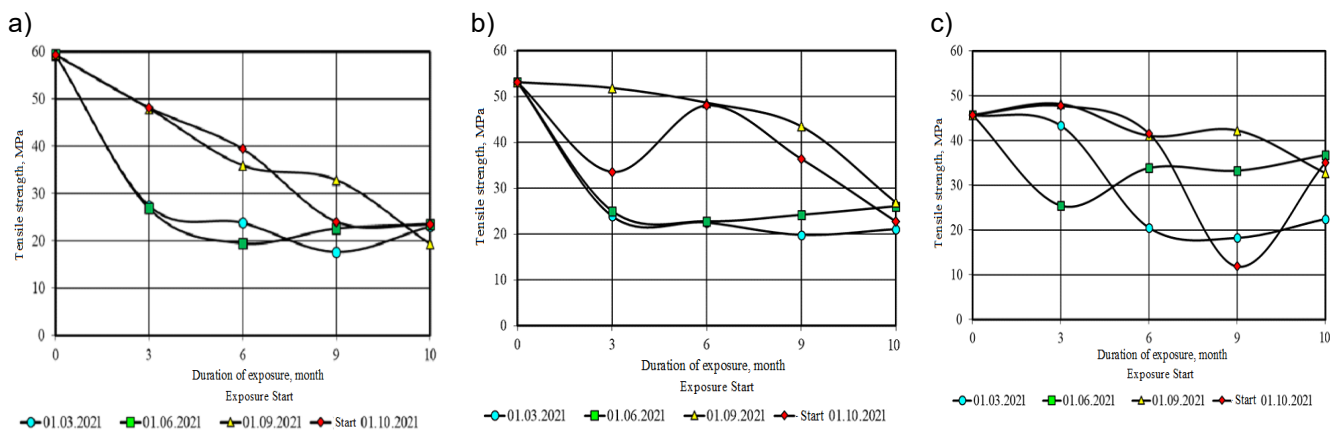


Figure 3. Change in the ultimate strength of specimens modified by Etal-1, depending on the season of the beginning of exposure (a - ED-20 + Etal-45M; b - (90% ED-20 + 10% Etal-1) + Etal-45M; c - (75% ED-20 + 25% Etal-1) + Etal-45M).

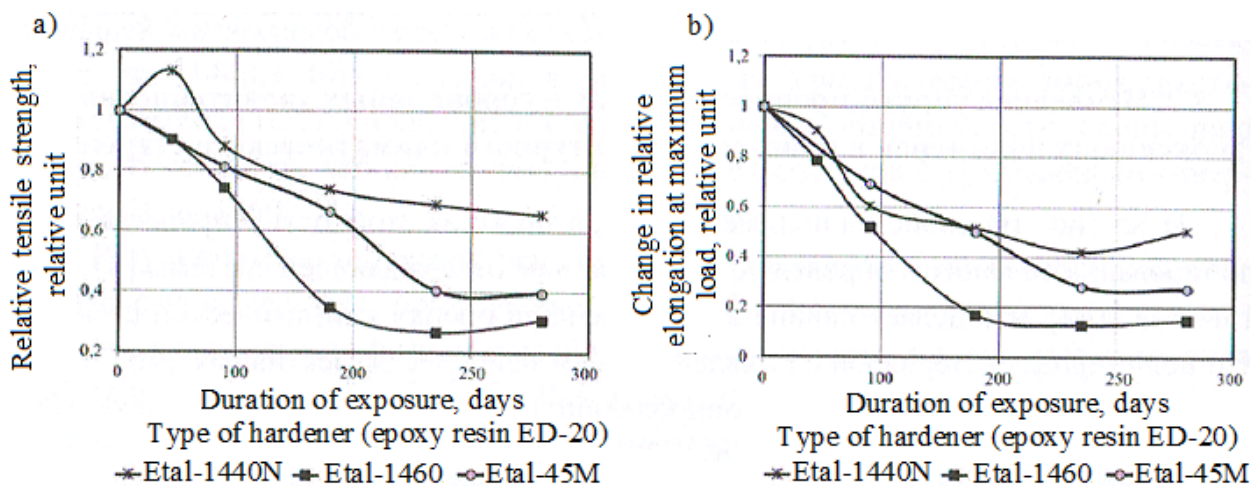


Figure 4. Change in the relative ultimate strength (a) and relative elongation (b) during stretching of epoxy polymer based on ED-20 resin, depending on the duration of full-scale exposure

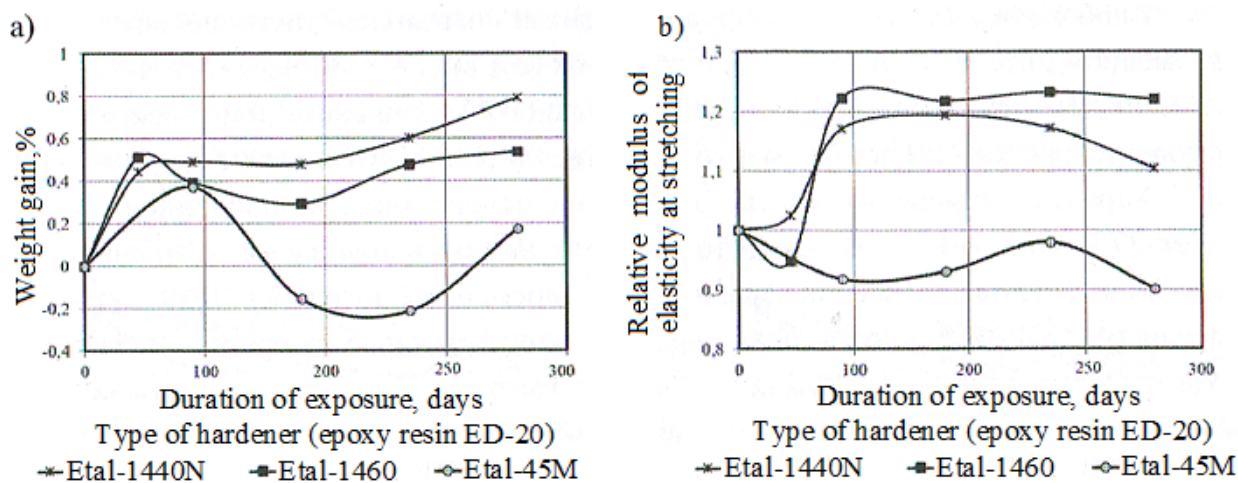


Figure 5. Change in mass (a) and relative modulus of elasticity in tension (b) of epoxy polymer based on ED-20 resin, depending on the duration of full-scale exposure

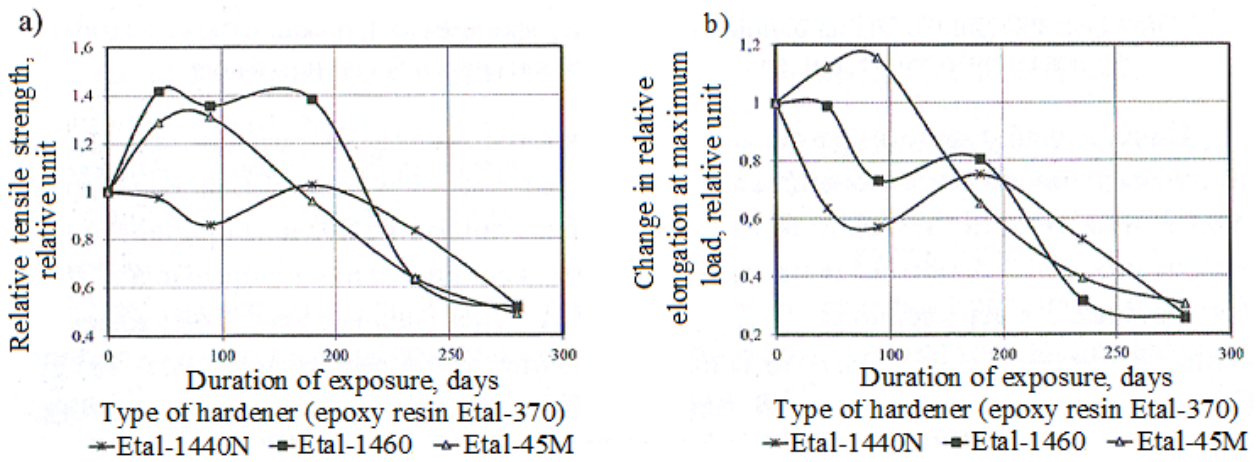


Figure 6. Change in the relative ultimate strength (a) and relative elongation (b) during stretching of the epoxy polymer based on the modified Etal-370 resin, depending on the duration of full-scale exposure

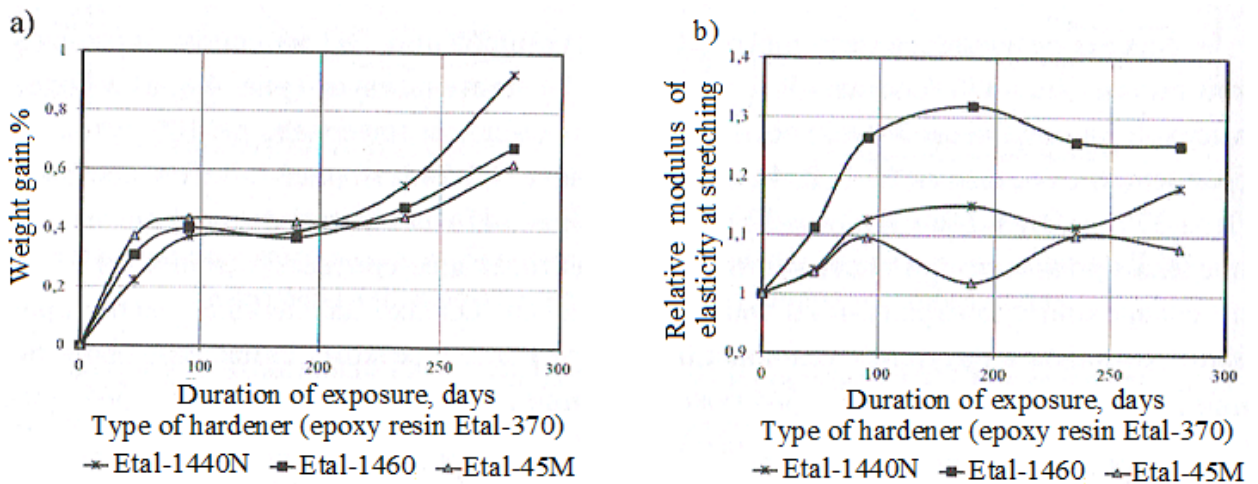


Figure 7. Change in mass (a) and relative modulus of elasticity in tension (b) of an epoxy polymer based on modified Etal-370 resin depending on the duration of natural exposure

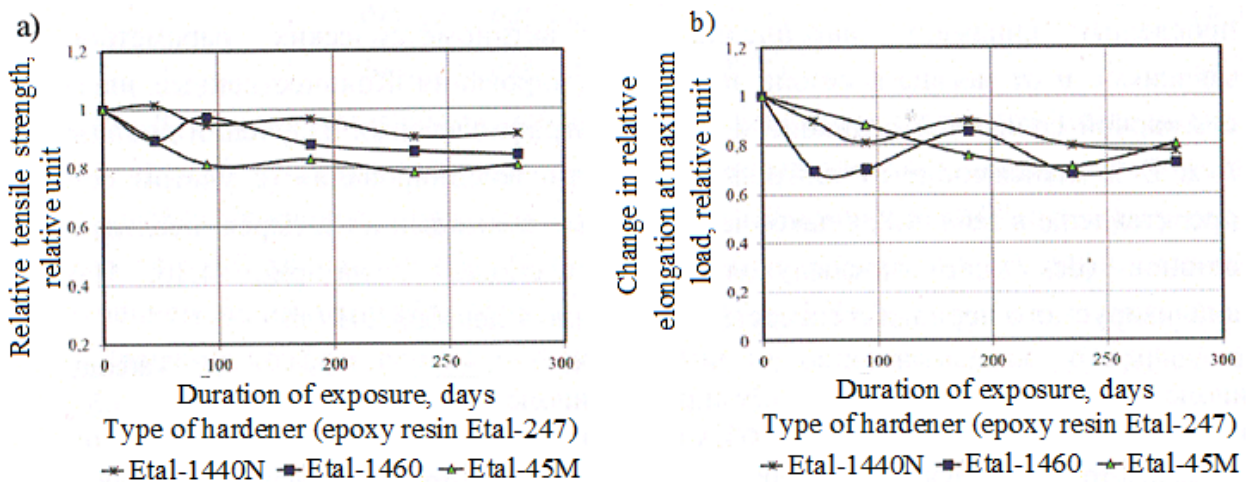


Figure 8. Change in the relative ultimate strength (a) and relative elongation (b) during stretching of an epoxy polymer based on modified Etal-247 resin, depending on the duration of natural exposure

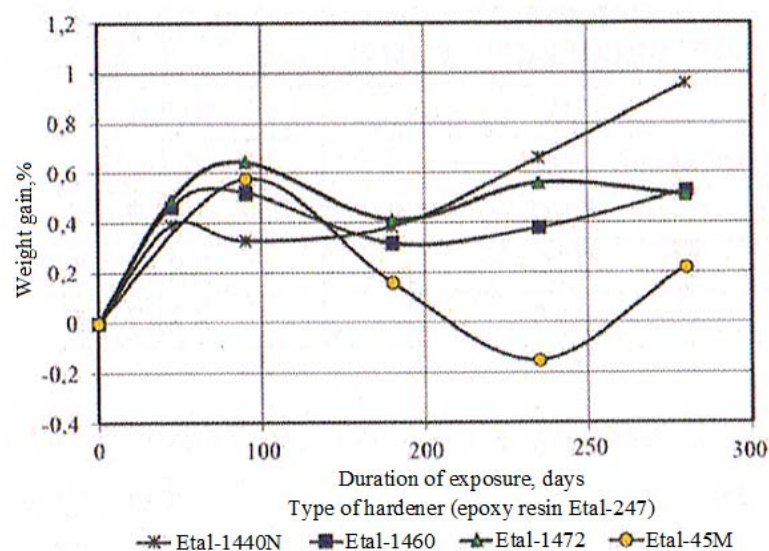


Figure 9. The weight gain of EP based on modified Etal-247 resin, depending on the duration of full-scale exposure

Table 1. Compositions of the studied epoxy polymers

No. of composition	Epoxy resin mark	Hardener mark	Resin : Hardener ratio
1	ED-20	Etal – 1440H	100÷56
2		Etal n – 1460	100÷39
3		Etal – 1472	100÷25
4		Etal – 45M	100÷50
5	Etal – 247	Etal – 1440H	100÷53.2
6		Etal – 1460	100÷37
7		Etal – 1472	100÷23.75
8		Etal – 45M	100÷47.5
9	Etal – 370	Etal – 1440H	100÷56
10		Etal – 1460	100÷39
11		Etal – 1472	100÷25
12		Etal – 45M	100÷50
13	ED – 20	Polyethylene polyamine	100÷10
14	Etal – 247	Polyethylene polyamine	100÷9.5

SURVEY ON KNOWLEDGE OF SEXUALLY TRANSMITTED INFECTIONS AND GONORRHEA: DO WE KNOW ENOUGH?

PERLBACH, Agostina¹; ROMANO, Mariana¹; DINAMARCA, Sofía^{1,2}; BUONFIGLI, Julio³; QUINTERO, Cristián Andrés^{*1,4}

¹ Universidad Juan Agustín Maza, Mendoza, Argentina.

² Instituto de Histología y Embriología (IHEM) CCT-CONICET Mendoza, Argentina

³ Poliedra, Ciudad de Mendoza, Mendoza, Argentina.

⁴ Facultad de Ciencias Médicas, Universidad de Mendoza, Mendoza, Argentina.

* Corresponding author

e-mail: cquintero@umaza.edu.ar

Received 20 April 2022; received in revised form 22 May 2022; accepted 20 June 2022

ABSTRACT

Background: Sexually Transmitted Infections (STIs) constitute an important group of infections with serious implications for public health. According to WHO, 1 million new contagions are produced daily, with more than 370 million new cases yearly. STIs can be originated from viruses, bacteria, fungi, or parasites. Regardless of their nature, they can be either cured or treated and controlled, but more importantly, they are preventable. **Aims:** The best tool to fight against STIs is prevention, which has a strong dependence on knowledge. This work aimed to assess the level of knowledge of society about STIs and gonorrhoea. **Methods:** We conducted an online survey, covering a wide range of ages and levels of education, inquiring about areas such as origin, ways of contagion, prevention, associated diseases, and treatment of STIs and gonorrhoea. We performed a statistical analysis of the answers. **Results and Discussion:** it was found that the general level of knowledge about STIs was independent of the age and level of education of the respondents. The respondent has shown better familiarity with prevention and contagion than with origin, diseases, and treatment. When the question was focused on gonorrhoea, we found a lack in the cognizance of several points. **Conclusions:** Based on our findings, we conclude it is necessary to improve sexual education programs, starting at early ages but directed to all populations, particularly about gonorrhoea.

Keywords: Gonorrhoea, STIs, *Neisseria gonorrhoeae*, knowledge, survey

1. INTRODUCTION

Sexually transmitted infections (STIs) are caused by more than 30 types of viruses, bacteria, fungi, and parasites. The STIs with the highest incidence are syphilis, gonorrhoea, Chlamydia, and trichomoniasis, which are all curable infections. The STIs caused by viruses, such as hepatitis B virus, herpes simplex virus (HSV or herpes), human immunodeficiency virus (HIV), and human papillomavirus (HPV), are all incurable but treatable infections (WHO, 2018; Workowski *et al.*, 2021). STIs can be acquired by any person, regardless of their gender, age, or sexual orientation. However, the most critical age is between 14 and 24 years old. According to a World Health Organization (WHO) report from

2018, more than 1 million people contract a curable STI every day. It is estimated that more than 376 million people aged between 15 to 49 years old acquire Chlamydia, gonorrhoea, syphilis, or trichomoniasis (WHO, 2018). In Latin America, 89 million new cases occur annually in the same age range, affecting 1 in 20 adolescents (Di Marco, Ferraris, and Langsam, 2018).

In the short term, the most observed manifestations in cases of STIs are oral lesions, genital sores, warts, itching, burning during urination, abnormal genital or anal discharge, and lower abdominal pain (Díez and Díaz, 2011). However, they can cause Pelvic Inflammatory Disease (PID), predisposition to ectopic pregnancy, neurological problems, and even

generalized infections in the long term. In more severe cases, infertility has been reported due to alteration of the upper genital tract in gonococcal or chlamydial infections, and neoplastic transformations can be induced by untreated HPV (Rodríguez, 2014). Likewise, injuries and inflammation due to some STIs increase the predisposition to infection by other microorganisms and may also increase the probability of acquiring HIV (5,6)

One of the most prevalent STIs is gonorrhea, caused by a Gram-negative bacterial pathogen, *Neisseria gonorrhoeae*. On a global scale, the WHO reported in 2018 a total of 87 million new cases of gonorrhea (WHO, 2018). In 2012, 78 million new cases occurred, and 14% corresponded to America. In Argentina, the general trend in the last five years has been continuous growth (Ministerio de Salud de la Nación Argentina, 2021).

Prevention is the best way to control STIs. In this sense, the key is the right information for society. Therefore, it is essential to have a reliable picture of the knowledge level of society.

Surveys of the state of knowledge about STIs, in general, are carried out mostly on high-risk populations, such as young populations between 16 and 28 years old (Di Marco *et al.*, 2018; Visalli *et al.*, 2019; Zin, Ishak, and Manoharan, 2019). However, although adolescents and young adults are more likely to acquire STIs, the rest of the population is not exempt.

This work aimed to survey and identify the level of knowledge that the general population has about STIs and gonorrhea in Argentina. A proportion of the people who have doubts, gaps in their knowledge, common confusions, and misconceptions were found, independent of their age and level of education. The results will allow improvements in the communication about STIs and propose new strategies that generate a responsible attitude in people, especially young people, and thus reduce the incidence of these diseases.

2. MATERIALS AND METHODS

2.1 Methods

2.1.1 Survey

A cross-sectional study was conducted through an anonymous online survey using Google Forms software on STIs and gonorrhea. It

was targeted to the general population and presented a simple language without exclusion according to age, socioeconomic level, or educational level. Its dissemination was carried out throughout Argentina via WhatsApp, Facebook, Instagram, and e-Mail. It was enabled on June 17th 2020 and closed on July 26th 2020. In total, it remained available for 40 days.

This questionnaire was prepared in neutral Spanish and structured in four blocks based on the information collected. Open and closed questions were included. In addition, they drew on existing literature to explore respondents' knowledge, attitude, and practices to STIs.

The first block aimed to acquire information about age, gender identity, place of residence, and level of education. In the second block, the questions were directed to determine the degree of knowledge about STIs: what they are, which are their causal agents, and how they are transmitted. In the third block, questions were focused on personal habits, the frequency and reason for using protection methods, exposure to risky sexual behaviors, testing for STIs and reasons to do so, and sources of information if required. A question about the respondent's opinions on current STI campaigns was also included. Finally, in the fourth block, the emphasis was exclusively on gonorrhea: what is the etiological agent, forms of transmission and prevention, if it is an eradicated disease, what is the incidence in Argentina, if there is a vaccine, how is the diagnosis and treatment, and what possible complications the disease may have.

2.1.2 Data analysis

A descriptive analysis of each block was carried out to determine the current situation of knowledge, practices, and access to information and care related to sexual life.

Subsequently, a one-way analysis of variance (ANOVA) with R was performed to verify whether age and educational level had a measurable effect according to the knowledge of the population and if there was a significant difference between the answers given at the different levels of the same factor.

The only variable or independent factor was "Age," whose levels were under 30, 30 to 39, 40 to 49, 50 to 59, and 60 years and older. We proceeded the same way with the "Education" factor: Primary education only, incomplete secondary, complete secondary, tertiary, incomplete college, complete college, and graduate degree levels. Again, correct and incorrect answers were given a particular score.

Finally, the total scores obtained corresponding to each level of education? Within the same factor were compared.

In addition, the Chi-square test was carried out to determine the association between the information collected in the main questions "What causes gonorrhoea?", "How is it transmitted?", "What complications could it produce if it is not treated in time?", "Is there a vaccine?", "How is the treatment?". "Is it an eradicated disease?" and "What STIs do you know?". A p-value ≤ 0.05 was considered statistically significant.

3. RESULTS AND DISCUSSION:

3.1 RESULTS

3.1.1 Characterization of the study population

In general, the surveys related to STIs are focused on the young population (Awang, Wong, Jani, and Low, 2014; Di Marco *et al.*, 2018; Drago *et al.*, 2016). It was aimed to perform a survey over a wider age range. A total of 803 responses were collected, mainly with answers from Mendoza and other regions of Argentina. We analyzed the age of the participants, with people younger than 30 years old representing the 55% of the participants, 20% from 30 to 40 years old, 16% from 40 to 50 years old, and 9% corresponding to people older than 50 years old (Figure 1A). On the other hand, we analyzed the level of education, finding that 97% of the subjects had completed at least high school. Among them, 29% had a university degree, and 16% had postgraduate studies (Figure 1B). As we expected, we covered a wide age range. The higher education of the participants is not fully representative of the general population, but it presented a good approach to measuring their knowledge of them.

3.1.2 transmission: ancient myths still prevail

Pathogens causing STIs are found only in fluids of the body, primarily in fluids from the genitourinary tract that are exchanged during sexual activity and in blood. STIs are transmitted from one individual to another during unprotected sexual intercourse, vaginal, anal, or oral. They can be transmitted by pre-seminal fluid, semen, vaginal fluid, and even interaction between skin and/or mucous membranes. Another possibility is through blood, after direct contact with it or by sharing sharp objects, and during pregnancy, childbirth, or lactation (1).

Regarding knowledge about transmission forms, most participants knew the most frequent modes of transmission, like vaginal, anal, and oral sex. However, a low percentage of participants answered that insect bites or displays of affection, such as hugging and kissing an infected person, can constitute transmission routes, as seen in Figure 2.

3.1.3 Knowledge of STIs: HIV and bacteria are the best known

To indagate about causal agents of STIs, we asked an open question. The most often mentioned agents were HIV, *Treponema pallidum*, and *Neisseria gonorrhoeae*, which cause AIDS, syphilis, and gonorrhoea. However, only half of the respondents named HPV, and less than 30% cited *Chlamydia trachomatis*, the most widespread sexually transmitted infection of bacterial origin in the world, as indicated in Figure 3A. Similar results were obtained previously in surveys performed on the young population in Argentina and Malaysia (3,8). Interestingly, we observed confusion with other diseases not considered sexually transmitted, such as Ebola and Zika.

As shown in Figure 3B, we observed that HIV was known independently of education. At the same time, Hepatitis B and C were better known among those who had completed secondary education. *T. pallidum* and genital herpes were less mentioned by the people with postgraduate studies. When answers were analyzed by age range, represented in Figure 3C, hepatitis was less mentioned among participants between 50-60 years old. On the other hand, the immediately previous range, 40-50 years old, were the ones who most mentioned Hepatitis B and C virus (HBV-HCV).

Confusion was observed regarding the transmission of agents and the possible secondary pathologies that they can cause, that is, between STIs and STDs. That was the case for diseases like cervical cancer and cirrhosis: almost 5% of responders (n=40) and less than 1% (n=8) reported cirrhosis as STIs. Since cervical cancer is not transmitted, HPV is the main cause of cervical cancer and genital warts. In the same sense, some participants indicated that "AIDS" is transmitted when this syndrome is caused by untreated HIV infection.

3.1.4 Known and used prevention methods

Prevention is the best way to control STIs. In this sense, the correct information about the

population is fundamental. Condoms, male and female, are the best barrier to avoiding or minimizing the pathogen transmission during sexual intercourse (Holmes, Levine, and Weaver, 2004; Wiyeh, Mome, Mahasha, Kongnyuy, and Wiysonge, 2020; Workowski *et al.*, 2021).

Concerning prevention methods, only 7% (n=56) admitted not using any protective method when having sexual intercourse, and 20% (n=161) responded to not using any effective barrier methods against STIs but only non-barrier contraceptive methods. Furthermore, 24% (n=193) of those surveyed admitted that only sometimes they use prevention methods, as shown in Figure 4. It should be noted that only the condom is a double protection method, preventing pregnancies and transmission of STIs, while the rest only have a contraceptive function.

Most of the respondents reported not having engaged in risky sexual behavior. Although only 2% (n=16) indicated having had intercourse without any type of prevention method, 35% (n=281) have used methods that only work as contraceptives or prophylactics, but not in all types of sexual practices, which indicates that 37% (n=297) of the respondents had or has risky sexual behaviors, as shown in Figure 5. Di Marco *et al.* indicated that an early start in sexual life could be associated with less knowledge about STIs and the use of contraceptive methods (3). They warned that social groups from homes with lower incomes present earlier calendars for the onset of sexual life. Likewise, they highlighted the importance of learning in care/prevention after the start of sexual life and the need to reaffirm prevention policies before starting it.

3.1.5 Do we receive enough information about STIs?

We are exposed to a large amount of information coming from several communication forms. All governments have their ways of communicating and teaching about STIs. The next question was addressed to evaluate the amount and quality of data offered through different campaigns regarding sufficient and effective information. When we asked the participants if they considered the information sufficient, just 4% (n=32) answered it was adequate and effective (not shown). When analyzing the answers concerning education level, the participants with higher degrees more often answered that the information was insufficient or effective (Figure 6A). Regarding the age, the extremes think the opposite: while among the people who answered

effective and sufficient, the older population predominated, with 43%; the young people were the majority who answered is not effective nor sufficient, with 26%, as shown in Figure 6B. Even with this level of information, it should be highlighted that 34% (n=273) of the respondents had never had medical check-ups for STIs (not shown).

3.1.6 Half of the interviewed do not know the nature of the causal agent of gonorrhoea

When inquiring in the survey about the nature of the transmitting agent of gonorrhoea, the Gram-negative bacteria *N. gonorrhoeae*, we found that half of the respondents answered correctly. On the other hand, 7% (n=56) chose viruses, fungi, or parasites among the wrong answers. The remaining 43% (n=345) indicated that they did not know, as shown in Figure 7A. Furthermore, it was observed that most of those who knew the nature of the causative agent of gonorrhoea had completed university education or postgraduate studies. In the same direction, the answer "I don't know" decreased with increasing educational level, as shown in Figure 7B. In addition, those who knew the bacterial origin of the disease did so almost regardless of age, as can be seen in Figure 7C.

When we asked about the current state of gonorrhoea and its eradication, 41% of the people answered they do not know (Figure 8A). Interestingly, a significant proportion of the people who answered affirmatively have tertiary education, and a significant proportion of those who answered negatively have the highest level of education (Figure 8B). There were no differences in the answers when stratified by age (not shown).

3.1.7 Gonorrhoea: transmission, prevention, and treatment

Gonorrhoea is transmitted in the same way as the other STIs. When the interviewees enquired about the transmission of this disease, most of them answered that sexual intercourse is one of the ways of transmission. 96% correlated it with vaginal contacts, whereas only 64% (n=514) and 68% (n=546) correlated it with anal and oral contacts, respectively. The least mentioned routes caught our attention: just 26 % (n=209) knew that it could be transmitted from mother to child, 20% (n=161) mentioned transfusions, and 10% (n=80) via transplacental transmission. Infected surfaces were the most common among the wrong answers, probably due to confusion with the

COVID-19 pandemic. The results are summarized in Figure 9.

There are no preventive vaccines for this disease (Jerse, Bash, and Russell, 2014). However, 65% (n=522) of the respondents did not know if there was a vaccine, as shown in Figure 10A.

Furthermore, even when gonorrhea has been treated with antibiotics, the bacteria constantly develop resistance (M Unemo and Nicholas, 2012; Magnus Unemo and Shafer, 2014). Nevertheless, 50% (n=402) did not know about the treatment, as represented in Figure 10B.

When asked about the possible complications that gonorrhea can cause, 72% (n=578) of those surveyed did not have this information. The remaining percentage that answered affirmatively mentioned infertility, Pelvic Inflammatory Disease, arthritis, sepsis, neonatal blindness, abortions, and abscesses, among others. This can be seen in Figure 10C.

3.1.8 General knowledge

To know the potential differences in the knowledge of the participants concerning their educational level or age, it was performed an analysis of the "correct" answers of the participants. First, the relative data were used in the one-way ANOVA using the software R. Analyzing the five age ranges as the "Age" factor, no significant differences were found. From this, it follows that the level of knowledge (independent variable) was not conditioned by the age of the respondents, as indicated in Figure 11 A. The same tendency was followed with the "Education" factor, where the level of education was not associated with knowledge about STIs and gonorrhea, as visible in Figure 11 B.

3.2 DISCUSSION

The information recovered from the survey showed a significant knowledge level about STIs, without statistically significant differences regarding the age or educational level of the participants. Although, there is a minor familiarity related to gonorrhea, particularly in details such as the nature of the disease, treatments, and complications generated during or after the disease.

In the present work, inaccurate information was found, misconceptions about which infections are mainly sexually transmitted, and the

prevalence of old myths regarding contagions.

In agreement with previous works performed in Argentina and other countries, we found that young people have low levels of knowledge (3,7,9,16). Even more, we found that the older population also lacks in their cognizance, and they have differences regarding specific points like the pathogenic agents, methods of prevention, and ways of contagion.

It concerns the small percentage recognizing Hepatitis B or C and HPV Chlamidya as STIs. A better knowledge of HIV was expected, thanks to the prevention and information campaigns about AIDS in the last years.

Regarding the prevention methods used, the most popular and used is the condom, being also a "barrier method" able to function as a contraceptive and preventive of STIs, in concordance with other studies (7,17).

Prevention and information campaigns resulted in being qualified as insufficient, non-effective, or both for most respondents. Therefore, it would be necessary to indague deeply understand the reasons for this opinion, to improve future campaigns.

Even when gonorrhea is in the top 3 of the most named STIs agents, there is low knowledge about the nature of the agent, the treatment, and the existence of vaccines. However, the prevention and transmission of *N. gonorrhoeae* are better understood due to their similarities with the rest of the STIs.

4. CONCLUSIONS:

The prevalence of gonorrhea in Argentina has increased since 2000. In the period 1992-1999, there was a statistically significant decrease in the number of cases of gonorrhea ($p < 0.05$) compared to the previous period, which was attributed to improved diagnosis, the efficacy of fluoroquinolones used for treatment, and to the increased use of protection methods by AIDS prevention campaigns (Ministerio de Salud de la Nación Argentina, 2021). Subsequently, it continued with an upward trend. Something similar happened with Chlamydia, for which there was a decrease in incidence since 1980. Still, higher frequencies of sexually transmitted viral infections appeared simultaneously. From this, it follows that the decrease in cases is due to improved diagnosis, contact tracing, and treatment rather than to the use of barrier methods of protection like condoms (Andersson-Ellström and Milsom, 2002).

Based on the data obtained, we found some ignored issues, misconceptions, mistakes, and gaps in the information regarding STIs and gonorrhea. In general, it is observed that people know that they should use STI prevention methods, although they do not know why and what to take care of. Prevention is focused on sexual intercourse without considering transfusions and transmission from mother to child. However, even when most respondents admit to using some protection method during sexual intercourse, a significant percentage do it only sometimes, or even not at all.

Knowledge is a general level about STIs. When gonorrhea was inquired to a greater extent, the greatest shortcomings in knowledge were visualized. From the nature of the disease-causing agent to effective vaccines and treatments, the information that people have is scarce. Age and educational level are not associated with knowledge about STIs and gonorrhea.

In conclusion, the results of this study indicate that institutional work should be done at different levels to increase awareness about STIs in Argentinian society, particularly about gonorrhea.

5. DECLARATIONS

5.1. Study Limitations

The present work was based on surveys of 803 participants, and they may not be fully representative of all population in Argentina. Also, the participants were residents of different cities of Argentina, with a high percentage living in Mendoza. Despite these limitations, our findings are consistent with those in the literature.

5.2. Acknowledgements

We would like to thank Dr. Mariana Ferrari and Dr. Mauricio Galiano for their critical reading of the early version of the manuscript. We also thank Dr. Walter Pelaez for his permanent support.

5.3. Funding source

The work was supported by an internal grant from Universidad JA Maza.

5.4. Competing Interests

The authors declare that they have no competing interests.

5.5. Open Access

This article is licensed under a Creative Commons Attribution 4.0 (CC BY 4.0) International License, which permits use, sharing, adaptation, distribution, and reproduction in any medium or format, as long as you give appropriate credit to the original author(s) and the source, provide a link to the Creative Commons license, and indicate if changes were made. The images or other third-party material in this article are included in the article's Creative Commons license unless indicated otherwise in a credit line to the material. Suppose material is not included in the article's Creative Commons license, and your intended use is not permitted by statutory regulation or exceeds the permitted use. In that case, you will need to obtain permission directly from the copyright holder. To view a copy of this license, visit <http://creativecommons.org/licenses/by/4.0/>.

6. REFERENCES:

1. Workowski KA, Bachmann LH, Chan PA, Johnston CM, Muzny CA, Park I, et al. Sexually Transmitted Infections Treatment Guidelines, 2021. Vol. 70, MMWR Recommendations and Reports. 2021. 1–187 p.
2. Baseline report on global sexually transmitted infection surveillance 2012. World Heal Organ. 2012;
3. Di Marco MH, Ferraris S, Langsam M. Young population, sexually-transmitted diseases, and rights. National and regional scenario in Argentina. *Cienc e Saude Coletiva*. 2018;23(9):2835–48.
4. Díez M, Díaz A. Infecciones de transmisión sexual: epidemiología y control. *Rev española Sanid Penit*. 2011;13(2):58–66.
5. Ding J, Rapista A, Teleshova N, Mosoyan G, Jarvis GA, Klotman ME, et al. Neisseria gonorrhoeae enhances HIV-1 infection of primary resting CD4+ T cells through TLR2 activation. *J Immunol [Internet]*. 2010;184(6):2814–24. Available from: <http://www.ncbi.nlm.nih.gov/pubmed/20147631>
6. Yu Q, Chow EMC, McCaw SE, Hu N, Byrd D, Amet T, et al. Association of Neisseria gonorrhoeae Opa(CEA) with dendritic cells suppresses their ability to elicit an HIV-1-specific T cell memory response. *PLoS One*

- [Internet]. 2013 Jan [cited 2013 Sep 25];8(2):e56705. Available from: <http://www.pubmedcentral.nih.gov/articlerender.fcgi?artid=3570455&tool=pmcentrez&rendertype=abstract>
7. Visalli G, Cosenza B, Mazzù F, Bertuccio MP, Spataro P, Pellicanò GF, et al. Knowledge of sexually transmitted infections and risky behaviours: A survey among high school and university students. *J Prev Med Hyg.* 2019;60(2):E84–892.
 8. Zin NM, Ishak I, Manoharan K. Knowledge, attitude and practice towards sexually transmitted diseases amongst the inmates of women shelters homes at Klang Valley. *BMC Public Health.* 2019;19(Suppl 4):1–7.
 9. Drago F, Ciccarese G, Zangrillo F, Gasparini G, Cogorno L, Riva S, et al. A survey of current knowledge on sexually transmitted diseases and sexual behaviour in Italian adolescents. *Int J Environ Res Public Health.* 2016;13(4):1–10.
 10. Awang H, Wong LP, Jani R, Low WY. Knowledge of sexually transmitted diseases and sexual behaviours among malaysian male youths. *J Biosoc Sci.* 2014;46(2):214–24.
 11. Holmes KK, Levine R, Weaver M. Effectiveness of condoms in preventing sexually transmitted infections. *Bull World Health Organ.* 2004;82(6):454–61.
 12. Wiyeh AB, Mome RKB, Mahasha PW, Kongnyuy EJ, Wiysonge CS. Effectiveness of the female condom in preventing HIV and sexually transmitted infections: A systematic review and meta-analysis. *BMC Public Health.* 2020;20(1):1–17.
 13. Jerse AE, Bash MC, Russell MW. Vaccines against gonorrhoea: current status and future challenges. *Vaccine [Internet].* 2014 Mar 20 [cited 2014 Aug 25];32(14):1579–87. Available from: <http://www.ncbi.nlm.nih.gov/pubmed/24016806>
 14. Unemo M, Shafer WM. Antimicrobial resistance in *Neisseria gonorrhoeae* in the 21st century: past, evolution, and future. *Clin Microbiol Rev [Internet].* 2014 Jul [cited 2014 Oct 9];27(3):587–613. Available from: <http://www.ncbi.nlm.nih.gov/pubmed/24982323>
 15. Unemo M, Nicholas RA. Emergence of multidrug-resistant, extensively drug-resistant and untreatable gonorrhoea. *Futur Microbiol [Internet].* 2012;7(12):1401–22. Available from: <http://www.ncbi.nlm.nih.gov/pubmed/23231489>
 16. Andersson-Ellström A, Milsom I. Knowledge about the prevention of sexually transmitted diseases: A longitudinal study of young women from 16-23 years of age. *Sex Transm Infect.* 2002;78(5):339–41.
 17. Omar Enzo Santangelo SP and AF. Knowledge of sexually transmitted infections and sex-at-risk among Italian students of health professions. Data from a one-month survey. *Ann Ist Super Sanità.* 2018;54(1):40–8.
 18. Dirección de Respuesta al VIH, ITS HV y TM de S de la N. Respuesta al VIH y las ITS en la Argentina. diciembre 2020. 2020; Available from: <https://bancos.salud.gob.ar/recurso/boletin-sobre-el-vih-sida-e-its-en-la-argentina-ndeg-37>

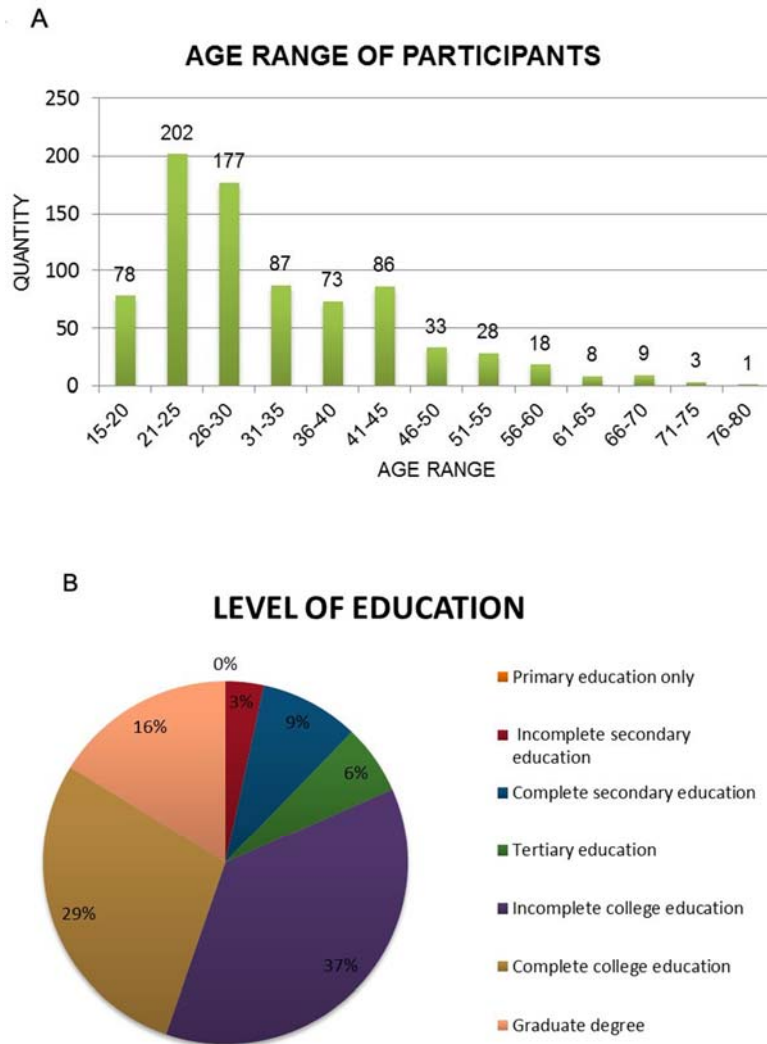


Figure 1: Characterization of the respondents according to age and education level. A- Classification of the survey participants according to age ranges. The results are shown in the number of participants. B- Classification according to the highest level of education reached. The results are shown in percentages.

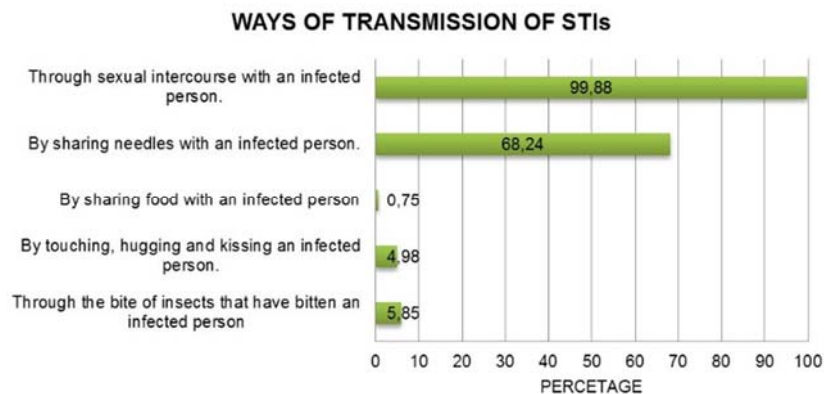
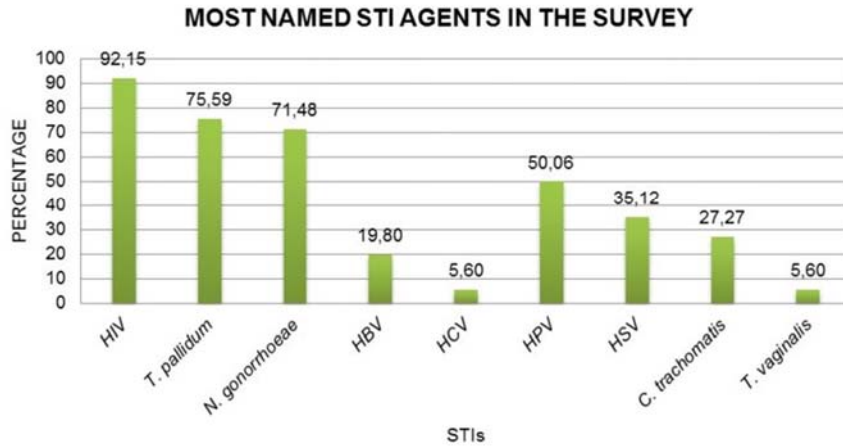
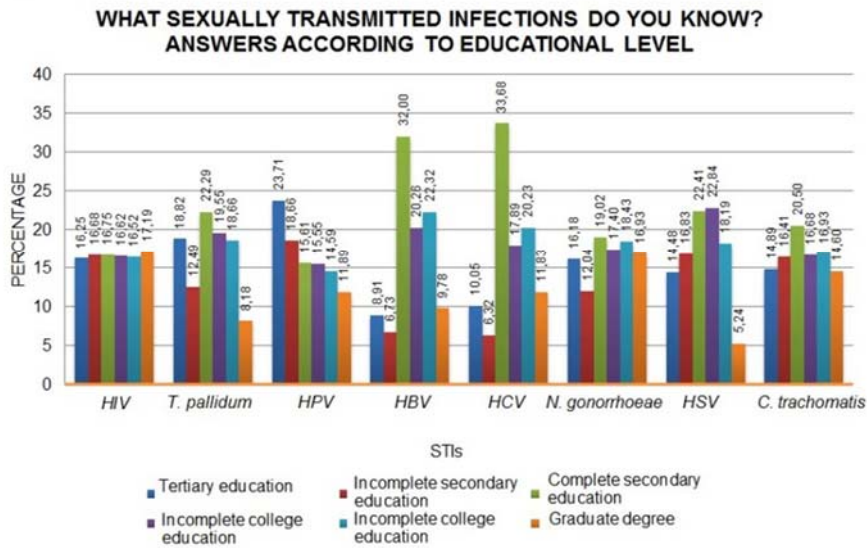


Figure 2. Ways of transmission of STIs. Closed question with the possibility to mark more than one answer. Results are presented in percentages.

A



B



C

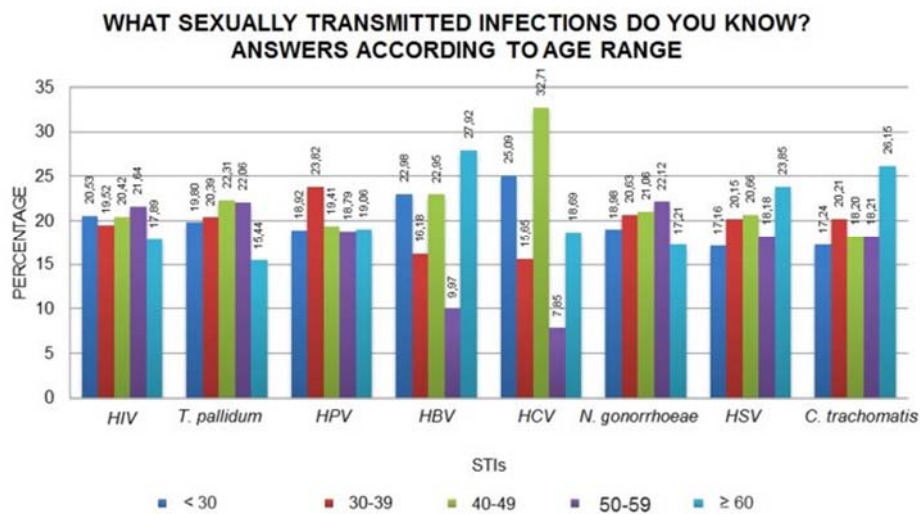


Figure 3. The most known Sexually Transmitted Infections. Open question. The graphs show the percentage of answers for each infection: A- general answers. B. Answers according to education level. C- Answers according to age.

HOW DO YOU TAKE CARE OF YOURSELF DURING SEXUAL INTERCOURSE?

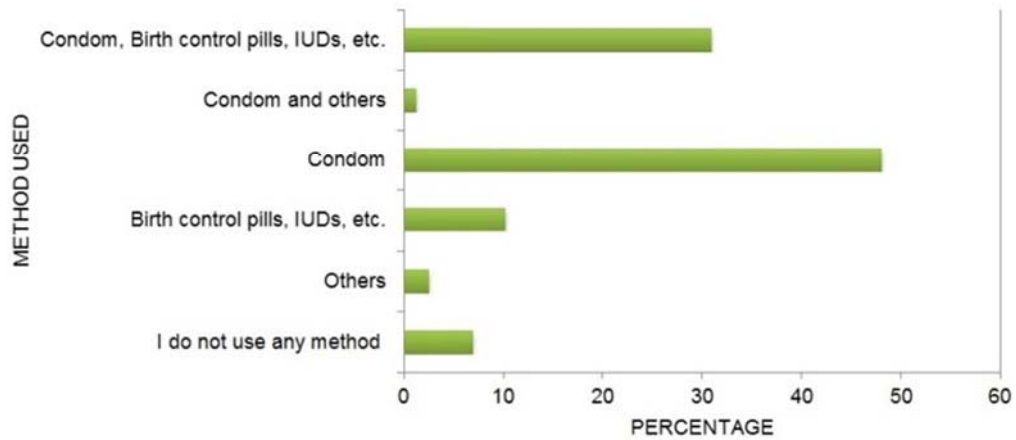


Figure 4. Methods of prevention used. Answers of participants to the question about the prevention method used during their sexual intercourse. Closed question. The results are presented in percentages.

HAVE YOU ENGAGED IN RISKY SEXUAL BEHAVIORS ?

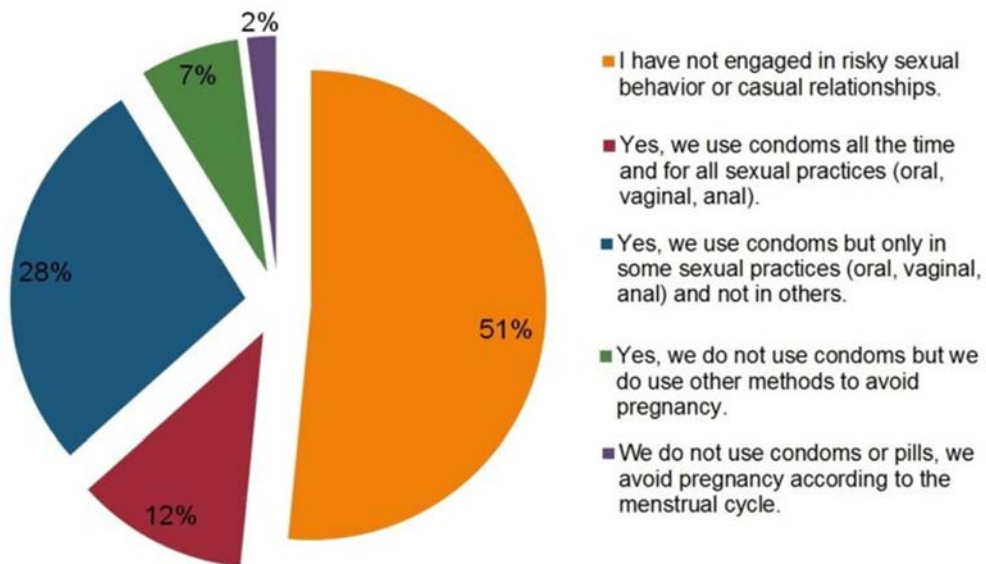


Figure 5. Risky sexual behaviors. The participants were asked about their participation in risky sexual intercourse and their behavior in those cases. Closed question. Results are presented in percentages.

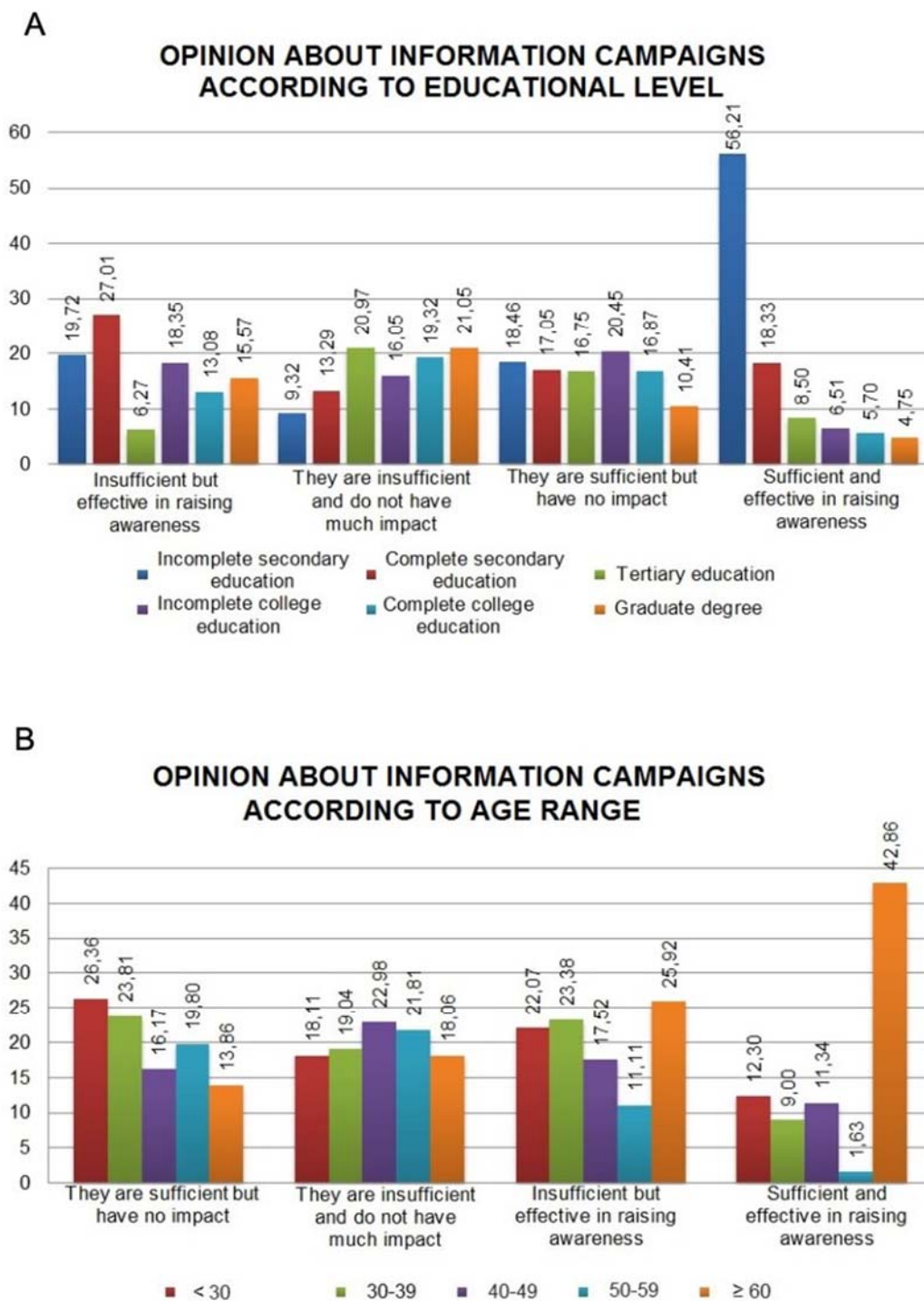


Figure 6. Level of conformity with the current information campaigns about STIs. A- Answers of participants according to educational level. B-Answers of participants according to age range. The results are shown in percentage.

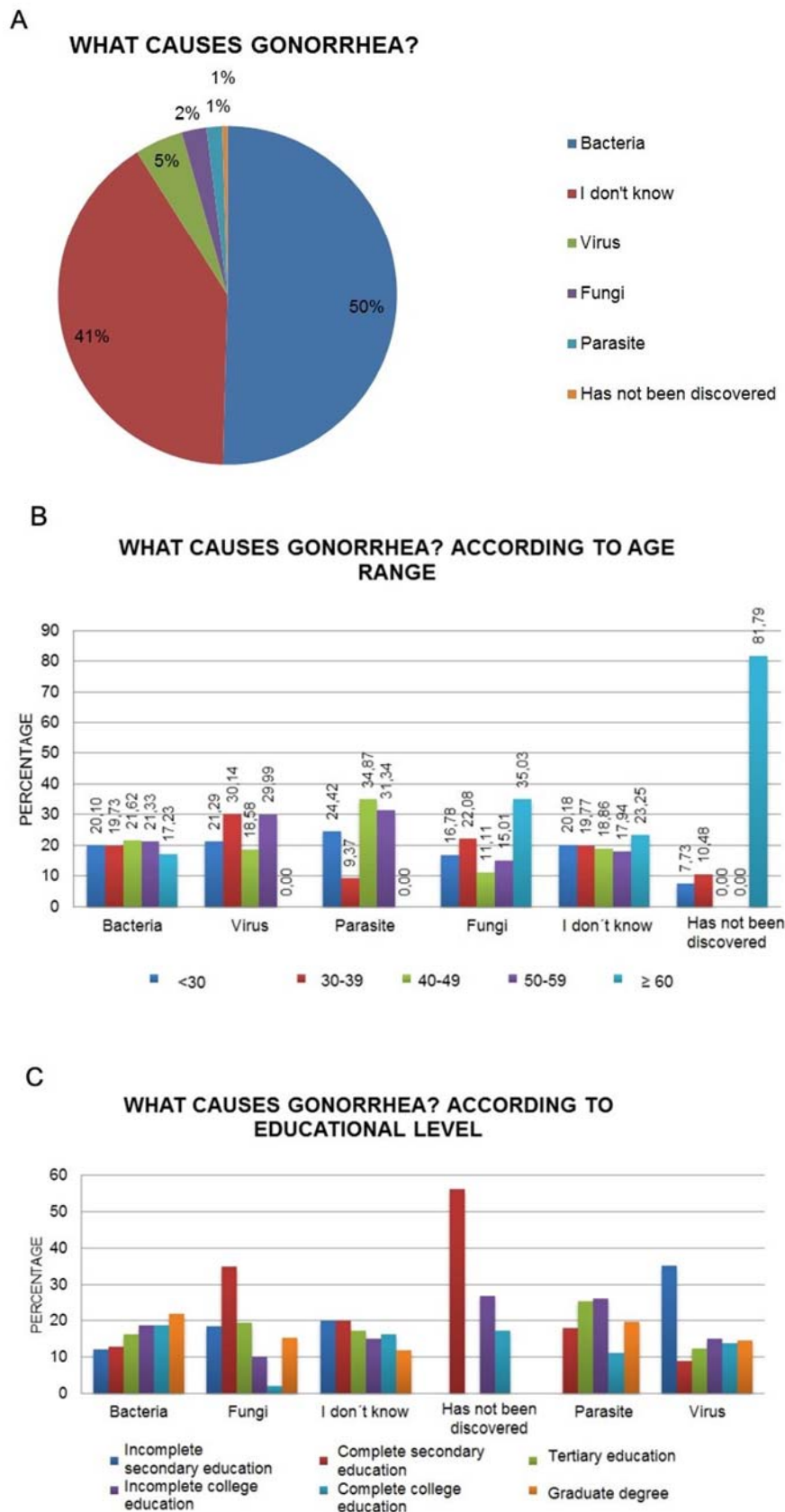


Figure 7. The nature of the agent causing gonorrhoea. The participants were asked about the nature of the agent causing gonorrhoea with a closed question. A- general answers. B. Answers according to education level. C- Answers according to age. All the results are presented in percentages.

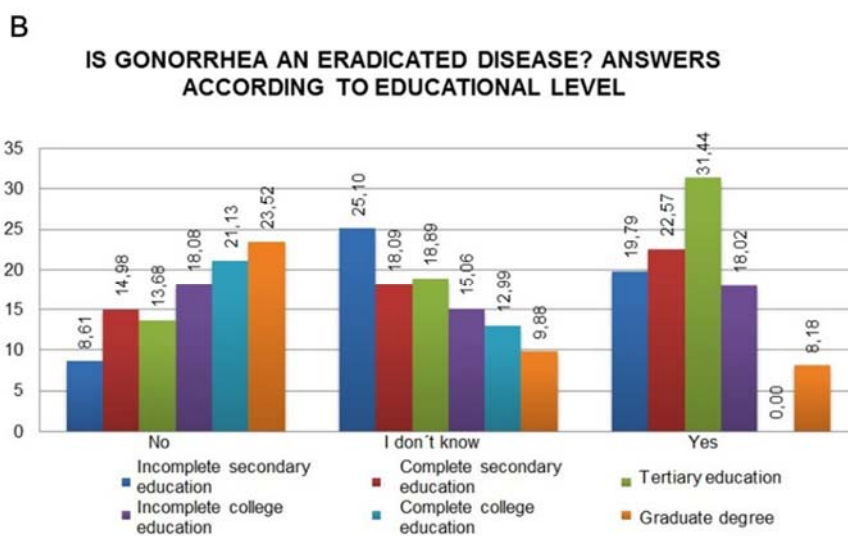
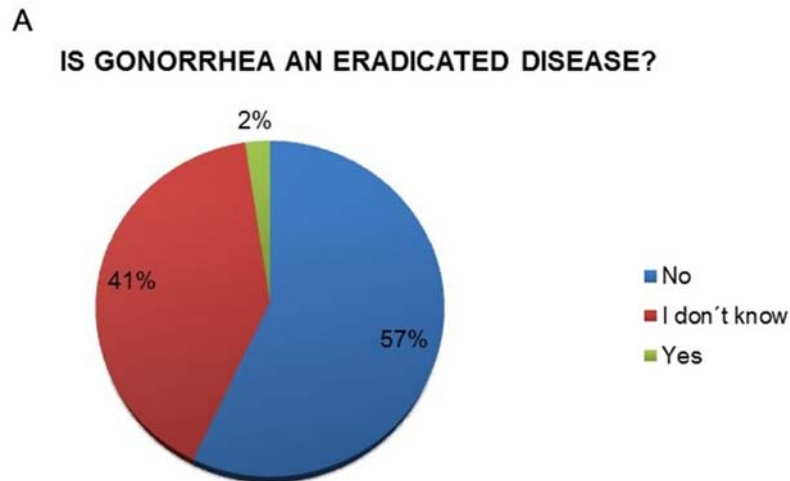


Figure 8 Current state of gonorrhoea. A- Answers about the eradication of the disease. B- Answers about the eradication of gonorrhoea according to their academic level.

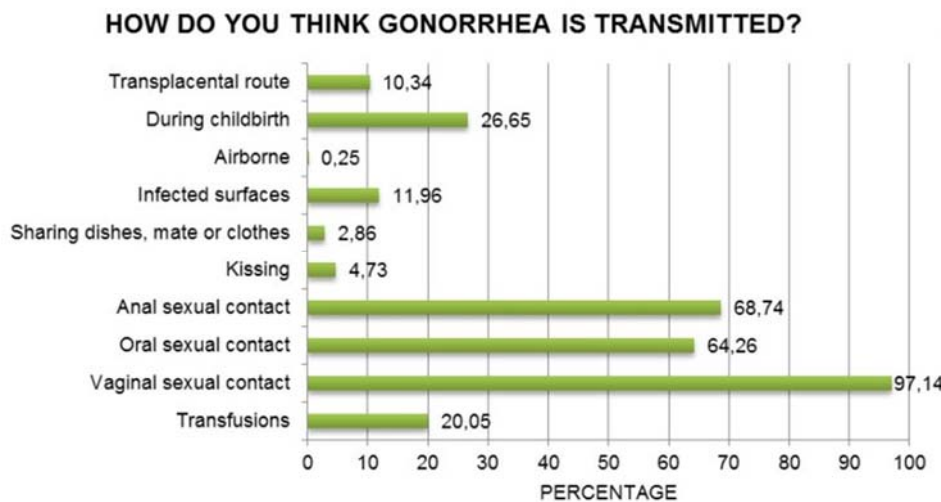
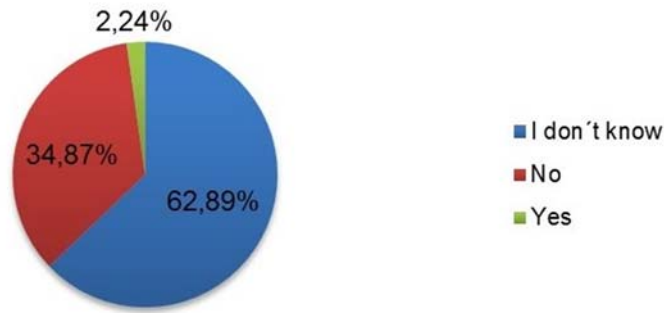


Figure 9. Transmission of gonorrhoea. The answers correspond to an open question about how gonorrhoea is transmitted. The results are presented in percentages

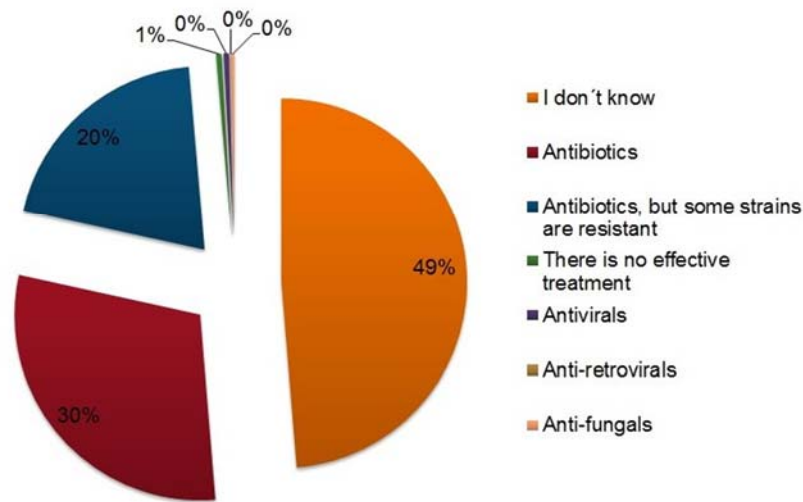
A

IS THERE A VACCINE FOR GONORRHEA?



B

HOW IS GONORRHEA TREATED?



C

WHAT COMPLICATIONS CAN GONORRHEA PRODUCE?

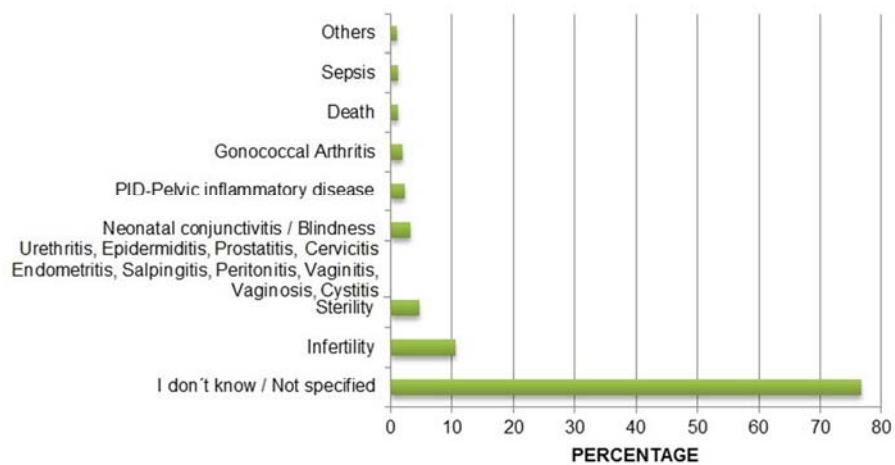


Figure 10. Prevention, treatment, and complications of gonorrhea. The answers of the participants over the questions. A- Is there a vaccine against gonorrhea? Three options to choose from. B- How is the treatment against gonorrhea? Closed question C- What are the complications that gonorrhea can cause? (open question).

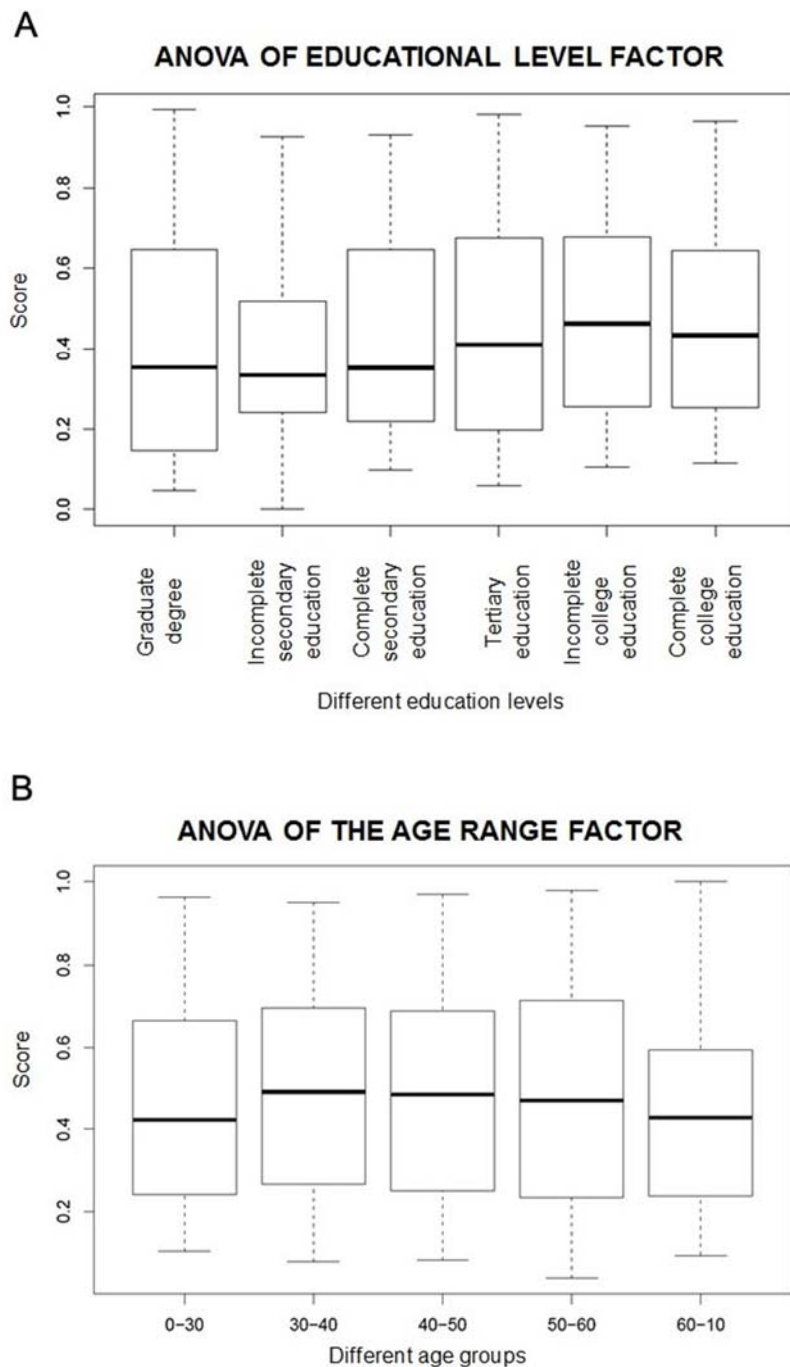


Figure 11. General knowledge of the participants, according to educational level and age. ANOVA analysis of the correct answers for selected questions. A- Analysis according to educational level. B-Analysis according to age range.

OPTIMIZATION AND KINETICS STUDIES OF THE DISSOLUTION OF DOLOMITE IN SULPHURIC ACID (H₂SO₄) VIA BOX-BEHNKEN EXPERIMENTAL DESIGNJOSEPH, Isaac Adekunle^{1*}; AJALA, Elijah Olawale¹; AHMED, El-Imam Amina²; AJALA, Mary Ajoke¹¹ University of Ilorin, Department of Chemical Engineering, Ilorin, Nigeria.² University of Ilorin, Department of Microbiology, Ilorin, Nigeria.

* Correspondence author
email: isaacchemeng@yahoo.com

Received 06 March 2022; received in revised form 28 May 2022; accepted 20 June 2022

ABSTRACT

Background: The recovery of any valuable component from dolomite as a double carbonate mineral depends on its dissolution efficiency. **Aim:** This study aimed to optimize and provide a simplified novel approach to the kinetics of dolomite dissolution in sulphuric acid solution using the Box-Behnken experimental design. **Methods:** The dolomite sample was dissolved in a sulphuric acid solution at seventeen different experimental conditions. The residue containing impurities was removed via filtration, while precipitation was carried out at the optimum conditions. **Results and Discussion:** The relationship between the independent and dependent variables best fits into the two-factor interaction model with a coefficient of determination of 0.9492, adjusted R² of 0.9187, and predicted R² of 0.7514. The total residual sum of 3x10⁻¹³ and adequate precision of 18.769 show that the predicted dissolution efficiency is much closer to the experimental values. The analysis of variance revealed that the individual effect of acid concentration, temperature, and dissolution time all positively contribute to the dissolution. The interactive effect of acid concentration with temperature and the interactive effect of temperature with dissolution time also positively influences the dissolution efficiency. Following the dissolution of dolomite in sulphuric acid, a white precipitate was formed at room temperature, which dissolved back at a temperature of 70 °C, agitation speed of 900 revolutions per minute, and within 10 minutes. A predictive approach using a two-factor interactive model was applied to generate the kinetic data. **Conclusions:** The established model equation is suitable for predicting dolomite dissolution in sulphuric acid. The application of the shrinking core model to the generated data shows that the reaction between dolomite and sulphuric acid is film diffusion control with a first-order reaction (0.6587) and activation energy of 27.5 KJmol⁻¹k⁻¹.

Keywords: Concentration, Temperature, Time, Dissolution Efficiency, Kinetics.

1. INTRODUCTION:

Dolomite is a naturally occurring double carbonate mineral of magnesium and calcium with the chemical formula MgCa (CO₃)₂ (Baba *et al.*, 2014; Pultar *et al.*, 2018; Ajala *et al.*, 2019). Dolomite ore can be used directly as an accelerating agent for cement hydration in concrete and a neutralizing agent in acidic soil (Mubaroka and Kurniawanb, 2015; Ajala *et al.*, 2019). In addition, dolomite is rich in magnesium. Hence it can be used for the production of magnesium-based compounds such as magnesite (MgCO₃), magnesium oxide (MgO), magnesium sulfate, as well as calcium sulfate, commonly known as gypsum (CaSO₄). The abundant

dolomite of Nigeria is spread across Abuja and the following states: Kogi, Oyo, Yobe, Kwara, Edo, and Nasarawa (Mookah and Abolarin, 2005).

Optimization of process variables helps to determine the best process conditions at which the process response can be determined (Umar *et al.*, 2016). Earlier studies usually employed one factor at a time for optimization studies, which is a challenge, and the interactive effects between the process variables are usually not accounted for (Baba *et al.*, 2014; Umar *et al.*, 2016). The Box-Behnken method under the response surface methodology in Design-Expert 11.0 software requires a minimal number of experimental runs to carry out regression and graphical analysis of experimental outcomes. Dolomite, as an alkaline

ore, is usually soluble in mineral acid. Different studies have investigated the dissolution of dolomite in different acid systems such as hydrochloric acid (Abali *et al.*, 2011; Baba *et al.*, 2014; Pultar *et al.*, 2018; Solihin *et al.*, 2018), nitric acid (Pultar, 2018; Are *et al.*, 2020). However, the optimization study of dolomite dissolution in sulphuric acid is yet to be reported. Therefore, this study is put forth to establish the optimum conditions for dolomite dissolution in sulphuric acid solution. The optimization study of process parameters using Design-Expert software is limited as it does not give information on the kinetics of a chemical reaction.

Kinetics study is a useful investigative tool that helps understand how a chemical reaction proceeds (Faraji *et al.*, 2020). Reaction kinetics can be used for reactor design, determination of the volume and size of a reactor, process scale-up, and determination of process variables that affect the rate of a chemical reaction (Fogler, 2016; Faraji *et al.*, 2020). As useful as kinetics is, it is very difficult to achieve due to the complex experimental work and data collection involved (Zhang, 2008; Zhao *et al.*, 2017; Zhouet *et al.*, 2018; Faraji *et al.*, 2020). A simplified alternative method was investigated to overcome this difficulty, hence the novelty of this study.

Therefore, this study aimed to investigate the use of a two-factor interactive model developed from the Box-Behnken Experimental method under surface response methodology to study the kinetics of the dissolution of dolomite in H₂SO₄.

2. MATERIALS AND METHODS

2.1 Materials

A representative sample of the dolomite used in this study was collected from Oreke village, Ifelodun Local Government, Kwara State, Nigeria. Sulfuric acid is of analytical grade (98%) from Guangdany Guanghai Chemical Factory Co. Ltd. Shanfau, Guandang, China.

2.2 Method

2.2.1 Dissolution Study

The dissolution study was carried out in a 500 ml conical flask reactor. The 300 ml of the specified sulphuric acid concentration was measured in the reactor and heated to the reaction temperature. After this, 1.5 g of the dolomite was

weighed into the reactor. The dissolution was allowed to continue until the specified reaction time was completed. The agitation speed was constant at 900 revolutions per minute (RPM). After the dissolution, the content of the reactor was filtered using Whatman filter paper, and the dissolution efficiency was calculated using Equation 1.

Dissolution Efficiency (%) =

$$\frac{\text{Mass of dissolved dolomite} \times 100 \%}{\text{Initial Mass of dolomite}} \quad (\text{Eq. 1})$$

2.2.2 Precipitation Study

Following the dissolution study, 3 g of dolomite was dissolved in 300 mL of H₂SO₄ at 78°C, 2 M acid concentration, 10 minutes dissolution time, and 900 RPM. The solution was quickly filtered when hot to separate the impurities present in the dolomite. The filtrate was then cooled down to room temperature to enhance precipitation. To know if the precipitate could redissolve, the mixture was heated, and at a temperature of 70 °C and an agitation speed of 900 RPM, a white precipitate was formed. The mixture was filtered using Whatman filter paper, and the residue was oven dry at 70 °C.

2.3 The Kinetic Study of Dissolution of Dolomite in Sulphuric Acid Using Box-Behnken Design

The different experimental conditions were imputed into the developed model equation to determine the fraction of dolomite dissolved at those conditions. At a constant temperature of 77.56 °C, the effect of acid concentration on the dissolution of dolomite was varied between 0.5 M to 3 M, and the dissolution time was also varied between 10 to 60 minutes. The effect of temperature was studied between 30 to 80 °C, while dissolution time was varied from 10 to 60 minutes at a constant acid concentration of 2 M.

3. RESULTS AND DISCUSSION:

3.1 Regression model and Statistical Analysis

In this study, three factors (temperature, time, and acid concentration) were chosen based on literature; preliminary experiments were carried out before the selections of the lower and upper limits of each of the independent variables, the codes, ranges, levels, and the type of factor studied is shown in Table 1. Table 2 shows the seventeen experimental runs generated by Box-Behnken Design. Laboratory experiments were carried out

under each of the experimental conditions. The experimental responses (dissolution efficiency) were supplied into the software for regression and graphical analysis. To determine the model that can best establish the relationship between the dependent and independent variables, four different models, linear, two-factor interaction (2FI), quadratic, and cubic, were tested for R^2 , adjusted R^2 , and predicted R^2 . The model with R^2 values close to 1 is most preferred. In Table 3, 2FI was chosen due to the highest value of predicted R^2 (0.7514) and the adjusted R^2 of 0.9187. The 2FI model was then used for the regression and statistical analysis. The predicted dissolution efficiency of the dolomite in sulphuric acid obtained from the model is much closer to the actual experimental values, with a total residual sum of 3×10^{-13} (Table 2). The plot of the predicted against the actual in Figure 1 shows that most dissolution efficiencies are above 95% while only a few are below the mark.

Table 3. Model Summary Statistics

Source	Std. Dev.	R^2	Adjusted R^2	Predicted R^2	
Linear	3.85	0.6077	0.5172	0.1819	
2FI	1.58	0.9492	0.9187	0.7514	Suggested
Quadratic	1.58	0.9647	0.9192	0.4354	
Cubic	0.0894	0.9999	0.9997		Aliased

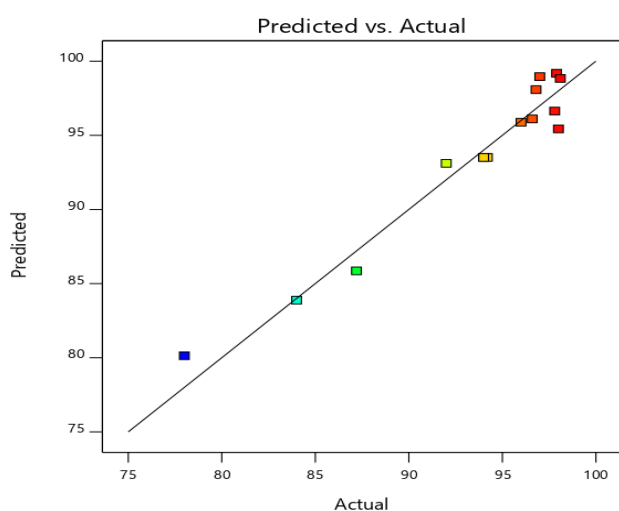


Figure 1. The plot of Predicted against the actual Dissolution Efficiency of Dolomite in Sulphuric Acid

For any given level of each element, Equation 2 in terms of coded factors and Equation

3 can be used to make predictions about the response.

Final Equation in Terms of Coded Factors

$$\text{Dissolution Efficiency (\%)} = +93.51 + 2.53A + 4.03B + 3.85C - 1.10AB - 3.25AC - 5.50BC \quad (\text{Eq. 2})$$

Final Equation in Terms of Actual Factors

$$\begin{aligned} \text{Dissolution Efficiency (\%)} = & + 49.03376 + 7.59600 \\ & \text{acid Concentration} + 0.530600\text{Temperature} \\ & + 0.820000\text{Reaction Time} - 0.035200 \text{ acid} \\ & \text{Concentration} * \text{Temperature} - 0.104000 \text{ acid} \\ & \text{Concentration} * \text{Reaction Time} - 0.008800 \\ & \text{Temperature} * \text{Reaction Time} \quad (\text{Eq. 3}) \end{aligned}$$

The Model F-value of 31.13 implies that the model is significant. There is only a 0.01% chance that a large F-value could occur due to noise. P-values less than 0.0500 indicate model terms are significant. In this case, acid concentration (A), temperature (B), reaction time (C), acid concentration and reaction time (AC), and temperature and acid concentration (BC) are significant model terms. This implies that they have measures of influence over the dissolution of dolomite sulphuric acid. Since there are not too many insignificant model terms, the model reduction was unnecessary. Adequate precision measures the signal-to-noise ratio. A ratio greater than 4 is desirable. The ratio of 18.769 indicates an adequate signal. This model can be used to navigate the design space.

3.1.1 Individual Effect of Acid Concentration, Temperature, and Reaction Time on the Dissolution Efficiency of Dolomite in Sulphuric Acid

The single effect of acid concentration, temperature, and reaction time on the dissolution efficiency of dolomite in sulphuric acid is presented in Figure 2. As the acid concentration increases from 0.5 to 3 M, the dissolution efficiency rises from 90.9 to 96%. This implies that as the acid concentration increases, the strength of the dissolution agent that can effectively react with the molecules of the dolomite also increases, thereby resulting in the increased dissolution of the dolomite (Faraji *et al.*, 2020). Hence, acid concentration has a positive influence on dissolution efficiency. Furthermore, as the temperature rises from 30 to 80 °C, the dissolution efficiency increases from 87.9 to 97.5%, implying that temperature positively affects dolomite dissolution in sulphuric acid. This is because the temperature helps the reactant molecules gain

sufficient kinetic energy for an effective collision to occur. Finally, the single effect of time shows that as the reaction time increases from 10 to 60 minutes, the dissolution efficiency increases from 89.7 to 97.3%, implying that reaction time has a positive influence on dissolution efficiency and that increasing the reaction time also enhances longer periods of contact between the ions from sulphuric acid and the molecules of dolomite.

3.1.2 Interactive Effect of the independent variables on the dissolution of dolomite in sulphuric acid

The interactive effect of the contour plot between reaction temperature and the acid concentration on the dissolution efficiency is presented in Figure 3a, while the three-dimensional plot is shown in Figure 3b. It is clear that increasing the dissolution temperature from 30 to 80°C and the acid concentration from 0.5 to 3 M increases dolomite dissolution in sulphuric acid from 90 to 97.2%. This implies that an increase in acid concentration brings about an increase in the dissolution agent, while an increase in temperature helps to increase the kinetic energy of the dissolution agent, thereby increasing its activity in dissolving the dolomite. The interactive effect between temperature and acid concentration positively influences dissolution (Faraji *et al.*, 2020; Are *et al.*, 2021).

The interactive effect of the contour plot between reaction time and the acid concentration on the dissolution efficiency is presented in Figure 4a, while the three-dimensional plot is shown in Figure 4b. It is clear that increasing the dissolution time from 10 to 60 °C and the acid concentration from 0.5 to 3 M results in an increase in dolomite dissolution in sulphuric acid from 85 to 97.2%. This implies that an increase in acid concentration brings about an increase in dissolution agents. At the same time, sufficient time is provided for the reactant molecules of the dolomite to dissolve in the sulphuric acid. Hence, an increase in the interactive effect between acid concentration and reaction time positively influences the dissolution of dolomite in sulphuric acid.

The interactive effect of the contour plot between reaction time and the temperature on the dissolution efficiency is presented in Figure 5a, while the 3D plot is shown in Figure 5b. Increasing the dissolution temperature from 10 to 60 minutes and from 30 to 80 °C leads to an increase in the dissolution of dolomite in sulphuric acid from 85 to 97.2%. This implies that as the temperature increases, the kinetic energy of the reactant molecules also increases, and sufficient time is required to attain a high dissolution efficiency of the

dolomite in sulphuric acid. Therefore, it can also be inferred that the interactive effect between dissolution time and the temperature positively influences the dissolution efficiency.

3.1.3 Optimization Constraints for the Dissolution of Dolomite in Sulphuric Acid

The point prediction of the optimum point was arrived at via the numerical optimization method. The optimization constraints (Table 5) were chosen based on economic cost, safety, and environmental considerations. For example, high acid concentration values can potentially harm humans and the environment. In addition, prolonged dissolution time can lead to overstretching of equipment and increase operational costs in an industrial setting.

Table 5. Optimization Constraints on Dissolution of Dolomite in Sulphuric Acid

Name	Goal	Lower Limit	Upper Limit
A:acid Concentration	is target = 2	0.5	3
B: Temperature	is in range	30	80
C:Reaction Time	Minimize	10	60
Dissolution Efficiency	Maximize	78	98.1

The predicted optimum point of dissolution of dolomite in sulphuric acid is presented in Figure 6. At an acid concentration of 2 M, the temperature of 78 °C, the reaction time of 10 min, and a constant agitation speed of 900 RPM, 99.2% dissolution efficiency were predicted. This is close to the 96.7% dissolution efficiency validated at the same predicted independent optimum points. Therefore, the desirability of 1 in this study is most preferred. The outcome of the dissolution in this study agrees with the report by Baba *et al.* (2014) who achieved 99.3% dissolution efficiency of dolomite in hydrochloric acid at 80 °C, 2 M acid concentration. However, the 60-minute reaction time is higher than the 10-minute dissolution time in H₂SO₄ in this study. In a similar study, are *et al.* (2021) reported 99.5% dolomite dissolution in nitric acid at 2.5 M acid concentration, 50-minute dissolution time, 55 °C, and 250 RPM.

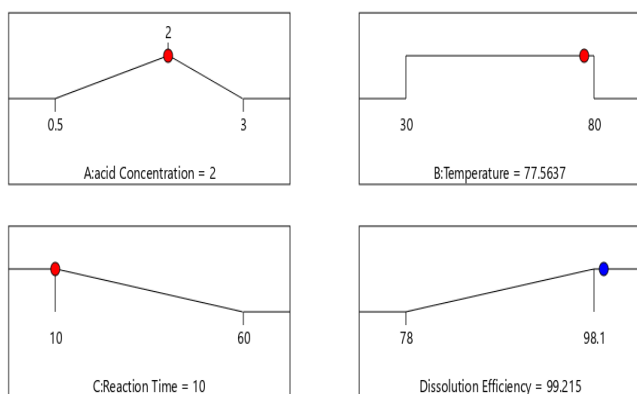


Figure 6. Predicted Optimum Point of Dissolution of Dolomite in Sulphuric Acid

3.2 Precipitation Study

Information on the dissolution of dolomite in sulphuric acid and the precipitation of any substance has not been properly documented. However, it was discovered in this study that the filtrate recovered from dolomite dissolution at the optimum point formed a white precipitate suspected to be magnesium oxide. Further precipitation attempts from the filtrate using calcium oxide and sodium hydrogen carbonate as precipitants did not result. This implies that there was complete precipitation.

3.3 Application of Box-Behnken Experimental Design in the Kinetic Study of Dissolution of Dolomite in Sulphuric Acid

The developed model equation 3 in this study was used to predict the fractions of dolomite that reacted at different experimental conditions

3.3.1 The effect of H_2SO_4 concentration on the reaction of dolomite

The results of the variation in the acid concentration from 0.5 to 3 M on the fraction of dolomite that reacted are presented in Figure 7. It can be observed that the fractions of dolomite that dissolved increase with increased acid concentration from 0.5 to 2 M and increase in dissolution time from 10 to 60 Minutes. This implies that the increase in acid concentration positively influenced the dissolution of the dolomite particles as sufficient dissolution time favors the dissolution process (Baba *et al.*, 2014; Pultar *et al.*, 2018, Are *et al.*, 2021). However, a further increase in the acid concentration from 2.5 to 3 M and an increase in the dissolution time from 10 to 60 minutes shows an inverse relationship with the dissolved dolomite fraction. This implies that the dissolution of dolomite in H_2SO_4 is not favored by an increase in

the acid concentration beyond 2 M. The heights dissolution fraction of 1 is predicted at 2.5 M acid concentration, the temperature of 77.56 °C and 10 minutes. This is similar to the 0.993 fractions of dissolved dolomite in hydrochloric acid at 2 M, 80 °C, and 60 minutes of dissolution time.

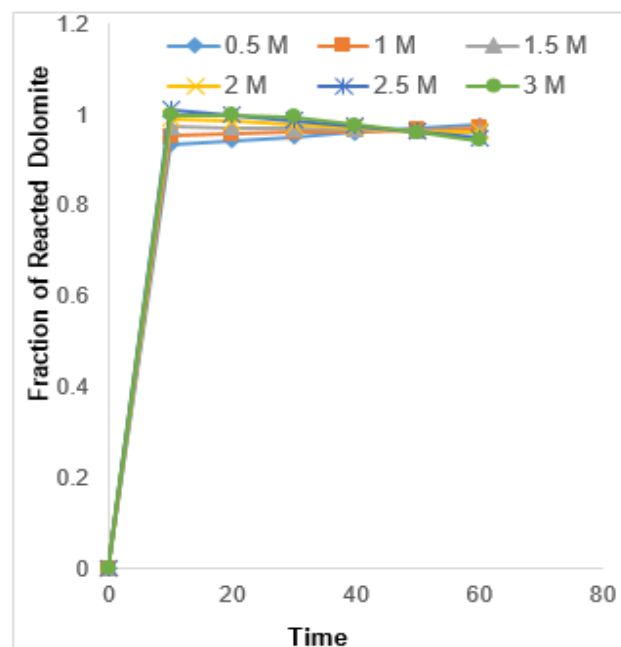


Figure 7. Effect of H_2SO_4 concentration on the kinetic study of dolomite at a temperature of 77.56 °C

3.3.2 Effect of temperature on the reaction between dolomite and H_2SO_4

There must be an effective collision between reactant molecules for a chemical reaction by the collision theory. For an effective collision to occur, there must be enough kinetic energy to drive the reactant molecules to collide with each other. The kinetic energy of a chemical reaction is a function of the reaction temperature (Are *et al.*, 2021). To understand how the reaction temperature affects the reaction between dolomite and H_2SO_4 , the effect of temperature was varied between 303 K and 352 K at reaction time variation of 10 to 60 Minutes while the acid concentration was kept constant at 2 M (Figure 8). There is a proportional increase relationship between the fraction of dolomite that reacted and the increase in the reaction temperature from 303k to 333 k. The reaction time also increased from 10 to 60 minutes. Therefore, it can be inferred that as temperature increases, the reactant molecules of dolomite and H_2SO_4 gain enough kinetic energy to overcome the energy barrier and go into reaction, resulting in a

higher fraction of dissolved dolomite. However, there is a decline in the fraction of dolomite that dissolved as the temperature increases from 343 K to 353 K. This could be attributed to higher kinetic energy gained by the liquid phase (H_2SO_4), which leads to molecular loss due to evaporation as a result of prolonging heating time.

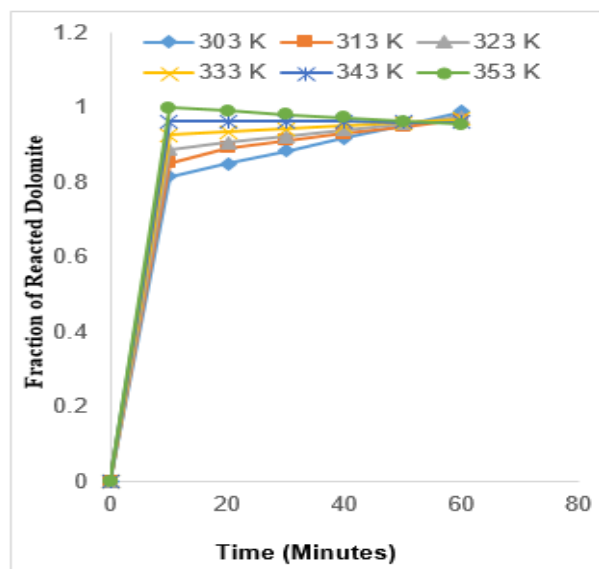
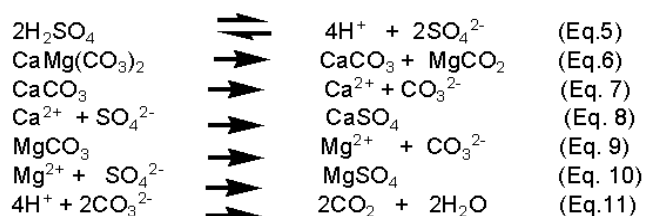


Figure 8. Effect of Temperature on the kinetic study of dolomite at 2 M and 10 minutes reaction time

3.3.3 Dissolution Kinetics of Dolomite in H_2SO_4

The dissolution of dolomite in H_2SO_4 is an exothermic reaction (equation 2) that involves the effervescence of carbon dioxide (CO_2), the formation of water, and calcium and magnesium sulfate. The magnesium ion (Mg^{2+}) and calcium ion (Ca^{2+}) from dolomite individually displace the hydrogen ion (H^+) in sulphuric acid. This agrees with the rule that cation above H^+ in the electrochemical series will displace H^+ during the chemical reaction. The amount of the sulfate ions (SO_4^{2-}) available for both Mg^{2+} and Ca^{2+} to bond with increases as the acid concentration increases. The binding of Mg^{2+} and Ca^{2+} with the SO_4^{2-} results in the breakdown of the crystal structure of the dolomite, this process is known as dissolution. The amount of the SO_4^{2-} present in the solution must be increased to increase the extent of dolomite dissolution. This can be achieved by increasing the concentration of the H_2SO_4 . The reaction mechanism developed in this study is presented in equations 4 to 11.



The rate-determining step in any reaction mechanism is considered to be the slowest step (Fogler, 2016; Faraji *et al.*, 2020). Theoretically, equation 4 could be assumed to be the slowest step since higher bonding energy is involved. The chemical structure of dolomite [$CaMg(CO_3)_2$] shown in Figure 9 has four strong ionic bonds at the point of cleavage compared to the chemical structure of magnesium carbonate (Figure 10) and calcium carbonate (Figure 11), which has two ionic bonds each at the point of cleavage. Equations 6, 7, and 8 have only one ionic bond each at the point of cleavage, while equation 1 and 9 has only weaker covalent bonds at the cleavage point. Since higher ionic bonds are present in $CaMg(CO_3)_2$, it will require higher dissociation energy to break $CaMg(CO_3)_2$ into its component. Therefore, equation 4 will require more time to go to completion, and it is therefore considered to be the slowest step.

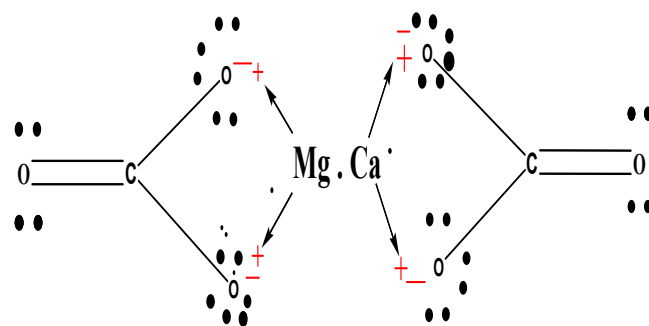


Figure 9. Chemical Structure of $CaMg(CO_3)_2$

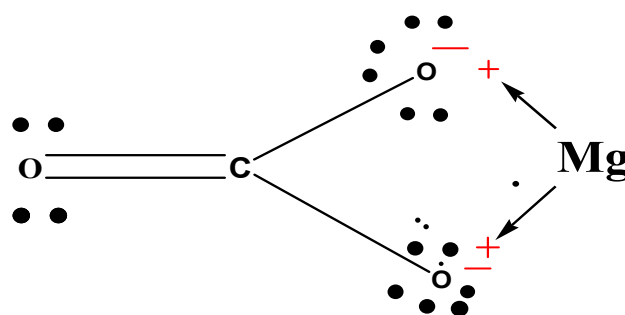


Figure 10. Chemical Structure of $MgCO_3$

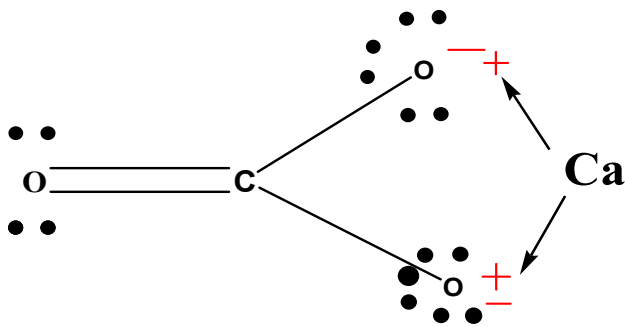


Figure 11. Chemical Structure of CaCO₃

Since equation 4 is considered to be the rate-determining step, their rate equation can then be written thus:

$$\text{Rate of disappearance} = K[\text{CaMg}(\text{CO}_3)_2] \quad (\text{Eq. 12})$$

From the rate law in Equation 12, the reaction is first order.

The shrinking model (SCM) is one of the mathematical relations used to study the kinetics behavior of reaction spherical particles in a liquid medium. The dolomite particle is assumed to be spherical, while the H₂SO₄ is in a liquid phase. Hence the use of SCM is considered suitable for this study. For kinetic model determination, the data obtained in Figures 7 and 8 are further subjected to the three model division of the SCM shown in Equations 13 to 15.

Film diffusion control:

$$X = \frac{6bDC_A}{\rho_0 R_0^2 t} = K_1 t \quad (13)$$

$$1 - (1 - x)^{1/3} = \frac{6bDC_A}{\rho_0 R_0^2 t} = K_2 t \quad (14)$$

$$1 + 2(1 - x) - 3(1 - x)^{2/3} = K_3 t \quad (15)$$

Where ρ_0 is the molar density of solid reactant (mol/m³), R_0 is the radius of a sphere (m), b is the stoichiometric coefficient of the solid, D is the effective diffusion coefficient (m²/s), and C_A is the concentration of A in the bulk solution (mol/m³), K_1 , K_2 , K_3 are rate constant for diffusion control, surface chemical reaction control and Product layer diffusion control respectively (Ajemba *et al.*, 2013; Are *et al.*, 2021). Therefore, model consideration is based on the highest coefficient of determination (R^2) value.

Table 6 shows the apparent rate constants and correlation coefficient (R^2) at various temperatures and concentrations for the three models. Model consideration is based on the highest coefficient of determination (R^2) value. Judging from the values of R^2 , it can be inferred that the mechanism of the reaction follows the order of film diffusion control > ash layer diffusion control > chemical reaction control with average R^2

values (0.9953 > 0.98175 > 0.94755) from effect of concentration and average R^2 (0.99494 > 0.98454 > 0.97186) from effect of concentration. This agrees with the report by Baba *et al.* (2014) that the reaction between dolomite and hydrochloric acid is film diffusion control. However, Are *et al.* (2021) reported that the reaction between dolomite and nitric acid is ash layer diffusion control. Figure 12 presents the film diffusion control plot with the individual R^2 value at different concentrations.

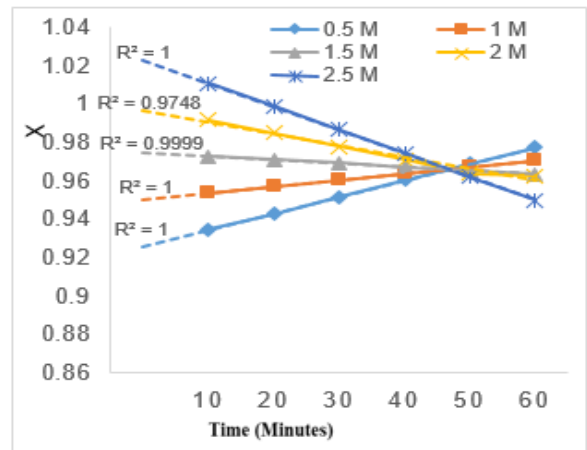


Figure 12. Plot of Film Diffusion Control for Effect of Acid Concentration

3.3.4 Order of reaction between dolomite and H₂SO₄

The speed at which a chemical reaction proceeds is judged by order of the reaction. This is determined by plot the apparent rate constant (slope of Figure 12) against the natural logarithm of the corresponding acid concentration shown in Figure 13. From the slope of 0.6587, the reaction order is first ordered with the H⁺ concentration, and it agrees with the reaction order determined by the rate law. It is also close to the 0.77 reaction order Pultar *et al.* (2018) reported for dolomite dissolution in nitric acid. However, it is below 0.9152 reaction order reported by Are *et al.* (2021).

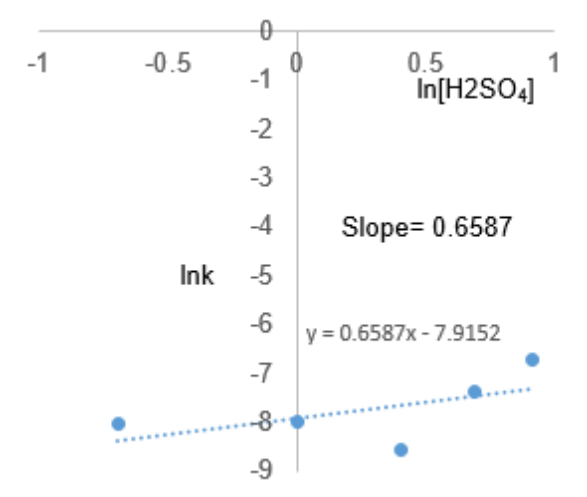


Figure 13: Plot of $\ln k$ Vs $\ln[\text{H}_2\text{SO}_4]$

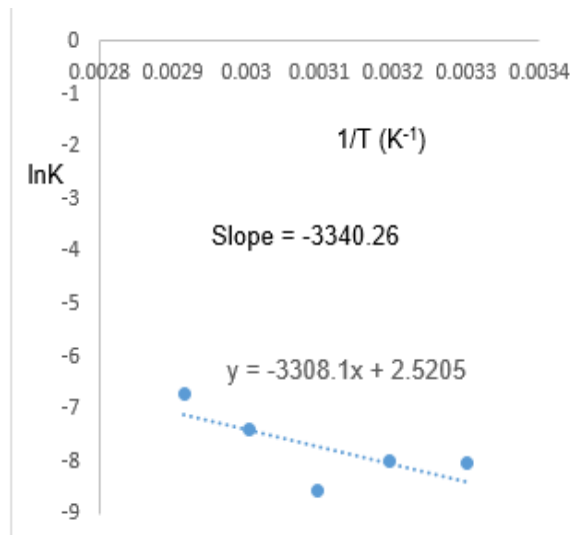


Figure 14: Plot of $\ln k$ Vs $1/T$ (K^{-1})

3.3.5 Activation Energy of the reaction between dolomite and H_2SO_4

The Arrhenius equation (equation 16) is a mathematical expression used to evaluate the amount of energy (activation energy) needed for a chemical reaction to occur.

$$k = A \exp\left(-\frac{E_a}{RT}\right) \quad (\text{Eq. 16})$$

Where K is the rate constant, E_a depicts the activation energy, 'A' stand for the frequency factor, R is the universal gas constant, and T is the temperature of the reaction

Linearizing equation 16 by taking the natural logarithm gives rise to $\ln k = \ln A -$

$\frac{E_a}{RT}$ (17) which is similar to the equation of straight-line $Y = mx + C$. A plot of the $\ln k$ against T^{-1} in Figure 14 gives rise to a slope equal to $-\frac{E_a}{R}$

Therefore, $E_a = -\text{slope} \times R$, where $R = 8.3145 \text{ Jmol}^{-1}\text{k}^{-1}$ and the slope is -3340.26

$$E_a = -(-3308.11) \text{K} \times 8.3145 \text{ J/molK} = 27505.28 \text{ Jmol}^{-1}\text{k}^{-1} = 27.5 \text{ KJmol}^{-1}\text{k}^{-1}$$

The activation energy of $27.5 \text{ KJmol}^{-1}\text{k}^{-1}$ is the amount of energy needed for the reaction between dolomite and H_2SO_4 to occur, and it can also be referred to as the amount of energy required to dissolve dolomite in H_2SO_4 . The activation energy of $27.5 \text{ KJmol}^{-1}\text{k}^{-1}$ is close to the $26.605 \text{ KJmol}^{-1}$ reported by Are et al. (2021), but it is below the 30 to $57 \text{ KJmol}^{-1}\text{k}^{-1}$ reported by Pultar et al. (2020) for dissolution of dolomite in nitric acid. However, Baba et al. (2014) reported lower activation energy of 20.77 KJmol^{-1} for dolomite dissolution in hydrochloric acid.

4. CONCLUSION:

Dolomite dissolution in sulphuric acid solution was optimized using Box-Behnken Experimental Design. The ANOVA shows that the single effects of temperature, acid concentration, and time all have positive, significant effects on the dissolution efficiency. Furthermore, the interactive effect between acid concentration and temperature and the interactive effect between temperature and dissolution time have significant positive effects on dissolution efficiency. At an acid concentration of 2 M , the temperature of $78 \text{ }^\circ\text{C}$, the reaction time of 10 minutes, and a constant agitation speed of 900 RPM , an optimal point prediction of 99.2% dissolution efficiency were established, while 96.7% dissolution efficiency was validated with the formation of white precipitate at room temperature. In the kinetic study, under the influence of acid concentration, the highest dissolution fraction of 1 was predicted at 2.5 M acid concentration, the temperature of $77.56 \text{ }^\circ\text{C}$, and 10 minutes. Under the influence of dissolution temperature, a heights dissolution fraction of 1 was predicted at 2 M acid concentration, the temperature of $80 \text{ }^\circ\text{C}$, and 10 minutes. From the rate-determining step, the reaction order between dolomite and H_2SO_4 is first order. The kinetic study also confirmed this with the value of 0.6587 , signifying a first-order reaction. The activation energy of the reaction between dolomite and H_2SO_4 is $27.5 \text{ KJmol}^{-1}\text{k}^{-1}$ and is film Diffusion Control. Hence, using two-factor interaction under the Box-Behnken Experimental Design method is a suitable novel approach to studying the kinetics of dolomite dissolution in H_2SO_4 .

5. DECLARATIONS

5.1. Study Limitations

No limitations were known at the time of the study.

5.2. Funding source

The authors funded this research.

5.3. Competing Interests

No competing interest

5.4. Open Access

This article is licensed under a Creative Commons Attribution 4.0 (CC BY 4.0) International License, which permits use, sharing, adaptation, distribution, and reproduction in any medium or format, as long as you give appropriate credit to the original author(s) and the source, provide a link to the Creative Commons license, and indicate if changes were made. The images or other third-party material in this article are included in the article's Creative Commons license unless indicated otherwise in a credit line to the material. Suppose material is not included in the article's Creative Commons license, and your intended use is not permitted by statutory regulation or exceeds the permitted use. In that case, you will need to obtain permission directly from the copyright holder. To view a copy of this license, visit <http://creativecommons.org/licenses/by/4.0/>.

6. REFERENCES:

1. Abali, Y., Bayca, S. U., Arisoy, K., and Vaizogullar, A. I. (2011). Optimization of dolomite ore leaching in hydrochloric acid solutions. *Physicochemical Problems of Mineral Processing*, 46(1), 253-262.
2. Ajala, E. O., Ajala, M. A., Odetoeye, T. E., and Okunlola, A. T. (2019). Synthesis of solid catalyst from dolomite for biodiesel production using palm kernel oil in an optimization process by definitive screening design. *Brazilian Journal of Chemical Engineering*, 36, 979-994.
3. Ajemba R. O. and Onukwuli O. D. (2012). Dissolution kinetics and mechanisms of reaction of Udi clay in nitric acid solution. *American Journal of Scientific and Industrial Research*. 3(3), 115-121.
4. Are, C. T., Suleiman, M. A. T., Jonathan, Y. I. S. A., Manase, A. U. T. A., and Joseph, I. A. (2021). Kinetic Study of Reaction between Dolomite Ore and Trioxonitrate (V) Acid (HNO₃). *GeoScience Engineering*, 67(1), 2129.
5. Baba, A. A., Omipidan, A. O., Adekola, F. A., Job, O., Alabi, A. G., Baral, A., and Samal, R. (2014). Optimization study of a Nigerian dolomite ore dissolution by hydrochloric acid. *J. of Chem. Tech. and Metallurgy*, 49, 280-287.
6. Faraji, F., Alizadeh, A., Rashchi, F., and Mostoufi, N. (2020). Kinetics of leaching: A review. *Reviews in Chemical Engineering*. 1-36.
7. Fogler, H.S. (2016). Elements of chemical reaction engineering, 5th ed. Indiana, USA: Prentice-Hall.
8. Gerald O., Nwoko C., Oguarah A, Ogwuegbu M (2012). Comparative kinetics of iron ore dissolution in aqueous HCl-HNO₃ system. *Journal of Minerals and Materials Characterization and Engineering*, 1, 153-159.
9. Moorkah, H. I., and Abolarin, M. S. (2005). Investigation of the properties of locally available dolomite for refractory applications. *Nigerian Journal of Technology*, 24(1), 79-86.
10. Mubarak, M. Z., and Adi Kurniawan, C. (2015). Synthesis of magnesia powder from East Java dolomite through leaching, precipitation, and calcination. In *Advanced Materials Research* (Vol. 1112, pp. 550-554). Trans Tech Publications Ltd.
11. Pultar, M., Vidensky, J., and Sedlarova, I. (2019). Study of the reaction between dolomite and nitric acid. *Physicochemical Problems of Mineral Processing*, 55.
12. Sivrikaya, O. (2018). A study on the physicochemical and thermal characterization of dolomite and limestone samples for use in ironmaking and steelmaking. *Ironmaking and Steelmaking*, 45(8), 764- 772.
13. Solihin, Indriani, and Mubarak, M. Z. (2018, May). Dissolution profile of dolomite in chloric acid solution: The effect of chloric acid concentration and pulp density. In *AIP Conference Proceedings* (Vol. 1964, No. 1, p. 020022). AIP Publishing LLC.
14. Umaru, M., Aris, M. I., Munnir, S. M., Aliyu, A. M., Aberuagba, F., and Isaac, A. J. (2016, October). Statistical optimization of

- biolubricant production from jatropha curcas oil using trimethylolpropane as a polyol. In *Proceedings of the World Congress on Engineering and Computer Science 2016* (Vol. 2, pp. 19-21).
15. Yildirim, M., and Akarsu, H. (2010). Preparation of magnesium oxide (MgO) from dolomite by the leach-precipitation-pyrohydrolysis process. *Physicochemical Problems of Mineral Processing*, 44, 257-272.
16. Zhang, J., Wu, A. X., Wang, Y. M., and Chen, X. S. (2008). Experimental research in leaching of copper-bearing tailings enhanced by ultrasonic treatment. *Journal of China University of Mining and Technology*, 18(1), 98-102.
17. Zhou, X., Chen, Y., Yin, J., Xia, W., Yuan, X., and Xiang, X. (2018). Leaching kinetics of cobalt from the scraps of spent aerospace magnetic materials. *Waste Management*, 76, 663-670.
18. Zhao, D., Yang, S., Chen, Y., Tang, C., He, J., and Li, H. (2017). Leaching kinetics of hemimorphite in ammonium chloride solution. *Metals*, 7(7), 237.

Table 1. Factors and boundary conditions for the dissolution of dolomite in sulphuric acid

Factor	Name	Units	Type	Minimum	Maximum	Coded Low	Coded High	Mean	Std. Dev.
A	acid Concentration	M	Numeric	0.5000	3.00	-1 ↔ 0.50	+1 ↔ 3.00	1.75	0.8839
B	Temperature	oC	Numeric	30.00	80.00	-1 ↔ 30.00	+1 ↔ 80.00	55.00	17.68
C	Reaction Time	Min	Numeric	10.00	60.00	-1 ↔ 10.00	+1 ↔ 60.00	35.00	17.68

Table 2. Experimental and predicted dissolution efficiency from Box-Behnken experimental design

Run	A: acid Concentration M	B: Temperature oC	C: Reaction Time Min	Dissolution Efficiency (%)		Residual
				Actual	Predicted	
1	1.75	55	35	94	93.51176	0.488235
2	1.75	55	35	94.1	93.51176	0.588235
3	1.75	55	35	94	93.51176	0.488235
4	0.5	55	10	84	83.88676	0.113235
5	3	80	35	97	98.96176	-1.96176
6	0.5	55	60	96.8	98.08676	-1.28676
7	1.75	80	60	96	95.88676	0.113235
8	1.75	80	10	97.9	99.18676	-1.28676
9	1.75	30	60	98.1	98.83676	-0.73676
10	0.5	80	35	96.6	96.11176	0.488235
11	0.5	30	35	87.2	85.86176	1.338235
12	3	30	35	92	93.11176	-1.11176
13	3	55	60	97.8	96.63676	1.163235
14	1.75	55	35	94.2	93.51176	0.688235
15	1.75	30	10	78	80.13676	-2.13676
16	3	55	10	98	95.43676	2.563235
17	1.75	55	35	94	93.51176	0.488235
Sum Total						3E-13

Table 4: ANOVA for 2FI model **dissolution efficiency of dolomite** in sulphuric acid

Source	Sum of Squares	df	Mean Square	F-value	p-value
Model	467.28	6	77.88	31.13	< 0.0001 Significant
A-acid Concentration	51.01	1	51.01	20.39	0.0011 Significant
B-Temperature	129.61	1	129.61	51.81	< 0.0001 Significant
C-Reaction Time	118.58	1	118.58	47.40	< 0.0001 Significant
AB	4.84	1	4.84	1.93	0.1944 Insignificant
AC	42.25	1	42.25	16.89	0.0021 Significant
BC	121.00	1	121.00	48.37	< 0.0001 Significant
Residual	25.02	10	2.50		
Lack of Fit	24.99	6	4.16	520.53	< 0.0001 significant
Pure Error	0.0320	4	0.0080		
Cor Total	492.30	16			

Adequate precision: 18.769

Table 6: Apparent rate constants and correlation coefficient, R^2 , and at various temperatures and concentrations for SCM

Process Variable	$X = k_1t$ (Film Diffusion Control)		Kinetic Equation $1 - (1 - X)^{1/3} = k_2t$ (Chemical Reaction Control)		$1 + 2(1 - X) - 3(1 - X)^{2/3} = k_3t$ (Ash Layer Diffusion Control)	
	$K_1 \times 10^{-3}$	R^2	$K_2 \times 10^{-3}$	R^2	$K_3 \times 10^{-3}$	R^2
Temp (°C)						
30	3.48	1	6.618	0.9395	9.25	0.9591
40	2.192	0.9722	3.935	0.9495	5.814	0.9927
50	1.72	1	3.725	0.9798	5.257	0.9867
60	0.84	1	2.058	0.9932	2.861	0.9958
70	-0.04	1	-0.12	0.9989	-0.16	0.9997
80	-0.9	0.9995	-6.29	0.8244	-5.54	0.9565
Average		0.995283		0.94755		0.98175
Conc (M)						
0.5	0.858	1	2.391	0.9895	3.221	0.9939
1	0.335	1	0.998	0.9982	1.332	0.9989
1.5	0.19	0.9999	0.62	0.9991	0.81	0.9996
2	0.62	0.9748	2.72	0.9388	3.22	0.9543
2.5	1.22	1	7.45	0.9339	6.59	0.976
Average		0.99494		0.97186		0.98454

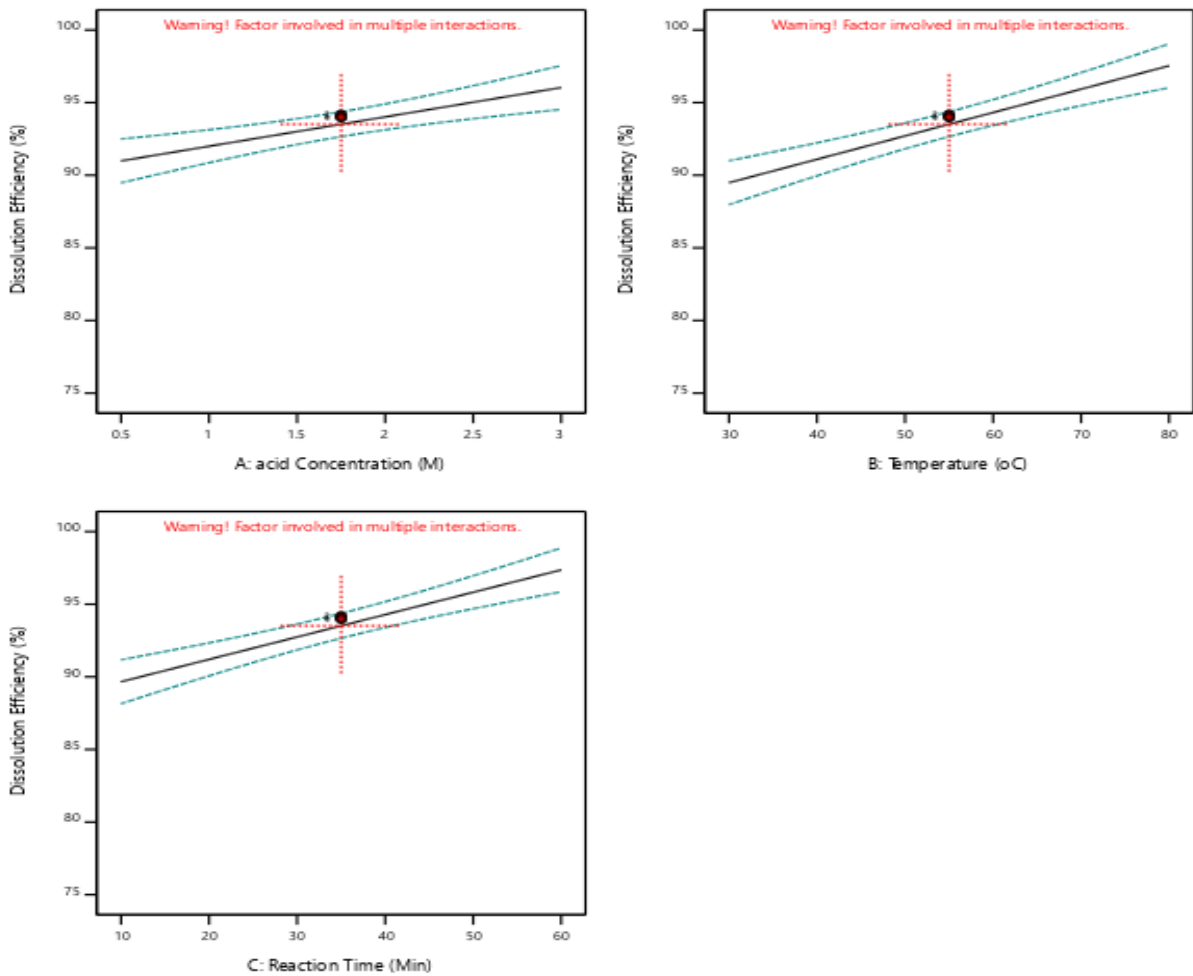


Figure 2: Single Effect of Acid Concentration, Temperature, and Reaction Time on the Dissolution Efficiency of Dolomite in Sulphuric Acid

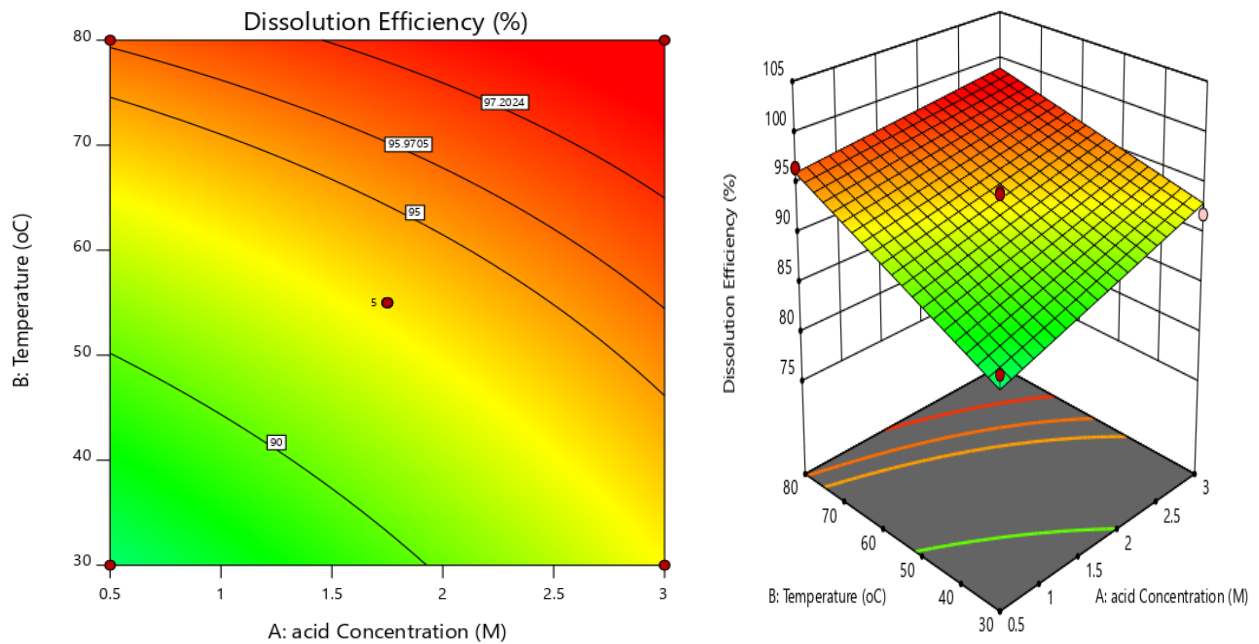


Figure 3: (a) Contour Plot; (b) Three Dimensional (3D) plot; of the interactive effect of temperature and acid concentration on the dissolution of dolomite in sulphuric acid

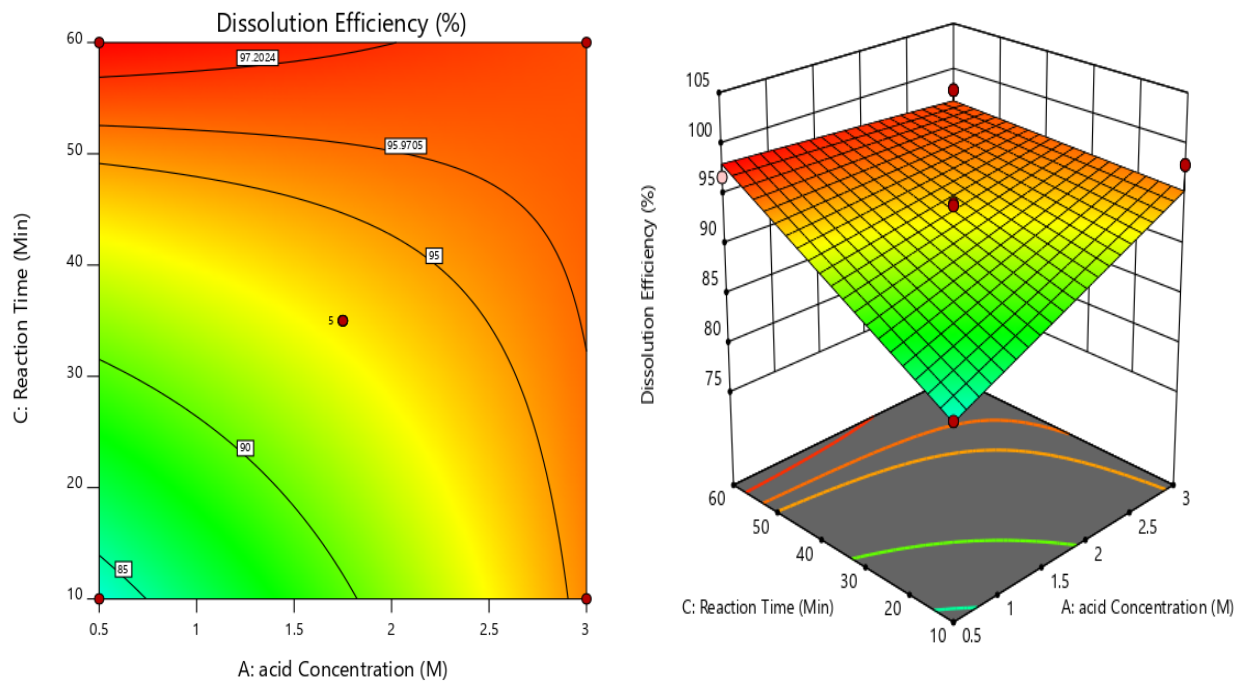


Figure 4: (a) Contour Plot; (b) 3D Plot; of the interactive effect of reaction time and acid concentration on the dissolution of dolomite in sulphuric acid.

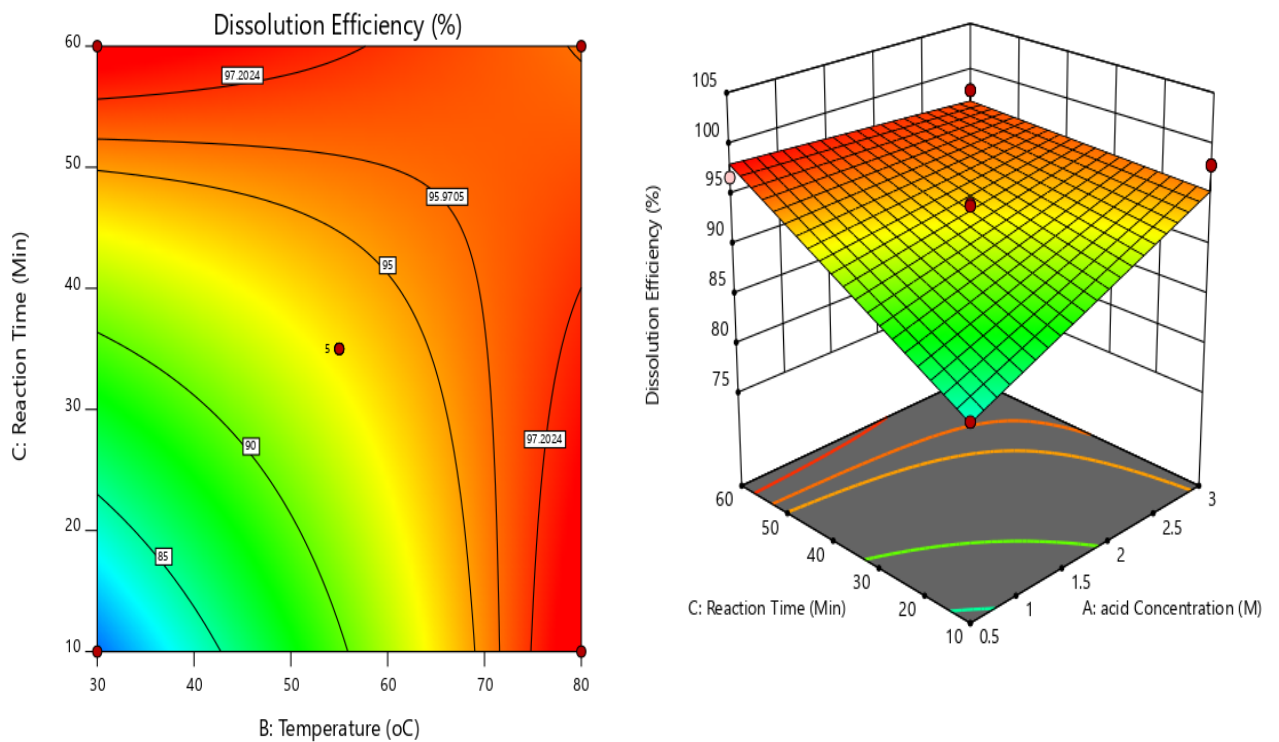


Figure 5: (a) Contour Plot; (b) 3D plot; of the interactive effect of reaction time and temperature on the dissolution of dolomite in sulphuric acid.

RESULTS OF THE 21SCON.ORG

In the first semester of 2022, a conference was realized to celebrate the 30 years of the journal formerly known as the **Southern Brazilian Journal of Chemistry**. In Brazil, it is a rare event for a scientific journal complete 30 years. As a representative of the journal staff, the former Editor-in-chief (L. De Boni) was proud to have assisted the journal.

In the history of the journal, 3 Editors were appointed, Dr. Lavinel Ionesco (founder of the journal); Dr. Luis A. B. De Boni (second editor and public server), and Dr. Walter Pelaez (current Editor-in-Chief). Dr. Pelaez is the first editor that has no deep ties with Brazil, he is from Cordoba – Argentina. Pelaez was selected for this position to increase the ties of friendship, brotherhood, and scientific cooperation, not only among Brazil and Argentina, but among the journal and the global scientific community. It is not an easy task, but he will count on the full support of the journal staff, the extremely qualified and hard work of the Argentinian scientific community, and the contributions of our dedicated authors around the world.

The conference had the honor to receive technical support of some great institutions, such as:

- Universidade de Vassouras, Brazil;
- Universidade do Estado do Rio de Janeiro, Brazil;
- Instituto Federal Sul-rio-grandense, Brazil;
- Ilia State University, Georgia;
- Universidade Federal Do Rio Grande Do Norte, Brazil;
- Instituto de Pesquisas Energéticas e Nucleares, Brazil;
- Satbayev University, Kazakhstan;
- Instituto de Investigaciones en Fisicoquímica de Córdoba, Argentina;
- Innospace, Korea;
- Universidad de los Andes, Venezuela;
- Instituto Federal do Rio de Janeiro – Campus Duque de Caxias, Brazil;
- Universidad Distrital Francisco José de Caldas, Colombia;
- Universidade Federal do Recôncavo da Bahia, Brazil;
- University Of Ilorin, Nigeria;
- I.M. Sechenov First Moscow State Medical University, Russia;
- Agência Espacial Brasileira, Brazil;
- Universidad Tecnica de Ambato, Equator;
- Facultad de Ciencias Químicas de la Universidad Nacional de Córdoba, Argentina;

- Associação Brasileira de Química - Secção Regional do Rio Grande do Sul, Brazil;
- Instituto Tecnológico de Aeronáutica, Brazil;
- Conselho Regional de Química da 5ª Região, Brazil.

The conference staff and the journal staff were proud to have received the support of such great and respectful institutions at this moment that a nice and positive page of the Brazilian scientific history was written. Thank you.

The conference would not be made possible without the dedication of its Scientific committee:

- Oana Maria Popa, Ph.D., Romania, Eurofins Romania.
- Teresa M. Roseiro Maria Estronca, PhD., Portugal, UC.
- Ketevan Kupatadze, PhD., Georgia, ISU.
- Shaima R. Banoon, MsC., Iraq, University of Misan.
- Francisco José Santos Lima, Ph.D., Brazil, UFRN.
- Carlos Eduardo Cardoso, Ph.D., Brazil, UV.
- Sérgio Machado Corrêa, Ph.D., Brazil, UERJ.
- Andrian Saputra, Ph.D., Indonesia, University of Lampung.
- Marcos Antônio Klunk, Ph.D., Brazil, UNISINOS.
- Andrey Vladimirovich Sevbitov, Ph.D., Russian Federation, Sechenov University.
- Olga D. Polezhaeva, Ph.D., Russian Federation, Russian Presidential Academy of National Economy and Public Administration.
- Daniel Ricardo Arsand, Ph.D., Brazil, IFSul.
- Élcio J. de Oliveira, Ph.D., Sweden, Luleå Tekniska Universitet.
- Rafael Rodrigues de Oliveira, PhD., Brazil, Neoprospecta.
- Masurquede de Azevedo Coimbra, M.Sc., Brazil, LACEN-RS.
- Gerzon E. Delgado, Ph.D. Venezuela, Universidad de los Andes.
- Paulo Sergio Souza, Ph.D., Brazil, Fundação Osorio.
- Danyelle Medeiros de Araújo Moura, Ph.D., Brazil, UFRN.
- Isaac Newton Lima da Silva, Ph.D., Brazil, PUCRS.
- Denise Alves Fungaro, Ph.D., Brazil, IPEN.

- Jorge Fernando Silva de Menezes, Ph.D., Brazil, UFRB.
- Cristián Andrés Quintero, Ph.D., Argentina, Universidad Juan Agustín Maza
- Fredy Hernán Martínez Sarmiento, PhD., Colombia UD-FJC.
- Rene Francisco Boschi Gonçalves, PhD., Brazil, ITA
- Gabriel Rubensam, M.Sc., Brazil, PUCRS.
- Aline Maria dos Santos, PhD., Brazil, IFRJ
- Monica Regina da Costa Marques, PhD., Brazil, UERJ.
- Alaa El Din Mahmoud, PhD., Egypt, Alexandria University.
- Zhanar Zhumadilova, PhD., Kazakhstan, Satbayev University.
- Atolani Olubunmi, PhD., Nigeria, University of Ilorin.
- Anton Timoshin, PhD., Russian Federation, Sechenov University.
- Lígia Marcondes Rodrigues dos Santos, M.Sc., Brazil, UV.
- Letícia patrão Gomes, M.Sc., Brazil, UV.
- Diana Carolina Coello Fiallos, PhD., Ecuador, Universidad Técnica de Ambato.
- Intisar Razzaq Sharba, PhD., Iraq, University of Kufa.
- Roberto Fernandez, Ph.D., Colombia, Universidad de Cartagena.
- Leandro Rosa Camacho, M.Sc., Brazil, ABQRS; CRQ-V.
- Bhavna Ambudkar, Ph.D., D.Sc., India, Dr. D. Y. Patil Institute of Technology, Pimpri, Pune (DIT).
- Roseli Gennari, Ph.D., Brazil, USP.
- Luis Alberto De Boni, Ph.D., Brazil, Retired Professor of Philosophy.
- Marco Antonio Goldani, MD. Brazil, São Lucas Hospital.
- Eduardo Goldani, Ph.D., Brazil, TQG. Chair of the conference.
- Walter José Peláez, PhD, Argentina, UNC. General Secretary
- Luis Alcides Brandini De Boni, Ph.D., Brazil, TQG. Co-Chair of the conference. Event Treasurer.

Thank you very much to all the Scientific Committee for its dedication and hard work.

It is very important to acknowledge **all the authors** that participated in the conference. In this sense it is being presented the **results of the best posters** selected by the authors' vote:

1. **Authors:** GULOTTA, Florencia A., MONTENEGRO, Mariana, DIAZ VERGARA, Ladislao, FERREYRA Nancy F., PAZ ZANINI, Verónica I.
Title: SELF-ASSEMBLED MULTILAYERS OF WATER-SOLUBLE MODIFIED-CHITOSAN AND GLUCOSE OXIDASE FOR DETECTION OF GLUCOSE IN MILK SAMPLES.
Country: Argentina.
2. **Authors:** SANTOS, Maricel del Valle, VELEZ, Alexis Rafael, MAGARIO, Ivana Maria.
Title: EFFECT OF MOLAR WEIGHT OF CARBOXYLIC ACIDS ON THE ENZYMATIC ESTERIFICATION OF GLYCEROL.
Country: Argentina.
3. **Authors:** BABATUNDE, Esther Olubunmi, ADERIBIGBE, Fatai Alade, ADEKUNLE, Joseph Isaac , ARE, Comfort Temitope, OLUWATOBI, Paul-lasisi Joshua.
Title: OPTIMIZATION OF BIODIESEL PRODUCTION FROM WASTE VEGETABLE OIL USING Zr- OXIDE CATALYST ANCHORED ON CARBONIZED MATERIAL.
Country: Nigeria.

Honorable mentions

- **Authors:** KANDASHVILI, Manana, GAMKRELIDZE, Giorgi, LORDKIPANIDZE, Tamar, NANOBASHVILI, Zaqaria, SOLOMONIA, Revaz.
Title: MYO-INOSITOL AS A POTENTIAL LOCALLY SUPPRESSING ANTI-SEIZURE THERAPEUTIC AGENT.
Country: Georgia.
- **Authors:** SAMAN, Thiago Abreu , RODRIGUES, Isabelle Medeiros, FILHO, Mário dos Santos.
Title: THE EVOLUTION OF CATARACT IN A DOG WITH TYPE I DIABETES - CASE REPORT.
Country: Brazil.

The conference had the honor of receiving extremely qualified speakers, and we are incredibly grateful.

Activity	Speaker	Country	Language
Opening Ceremony	Dr. DE BONI, Luis	HOST COUNTRY BRAZIL	EN
Stereoselective synthesis and antiproliferative activity of steviol- and isosteviol-based bi- and trifunctionalized diterpenoids	Dr. SZAKONYI, Zsolt	Hungary	EN
Overview of air monitoring in tbilisi (capital of georgia) for the period 2018-21	Dr. KUPATADZE, Ketevan	Georgia	EN
The physical chemistry behind global warming with a remembrance of my mentors, profs. E.h. Staricco and m.j. Molina.	Dr. ARGÜELLO, Gustavo A.	Argentina	EN

Development of synthesis of granular zeolite naa from coal fly ash	Dr. FUNGARO, Denise Alves	Brazil	PT-BR
Launch vehicle development in brazil (desenvolvimento de veículos lançadores no brasil)	Dr. SANTOS, Fábio	Brazil	PT-BR
Production of synthetic biofuels	Dr. DE BONI, Luis; GOLDANI, Eduardo	Brazil	EN
Pesquisa aplicada em tempos de pandemia	Dr. TRAJANO, Eduardo Tavares Lima	Brazil	PT-BR
Treating chemical residues with poas (case study)	Dr. DE BONI, Luis	Brazil	EN
Non-invasive dialysis	Dr. BHAVNA Ambudkarr	INDIA	EN
Closing ceremony	Dr. PELAEZ, Walter	HOST COUNTRY ARGENTINA	EN/ES/PT

To complete the conference, we are announcing the selected best manuscript. After a challenging evaluation process, due to the high quality of the manuscripts received it was selected the manuscript entitled "**COMPARISON OF TWO STAINING METHODS FOR ANODIZING IN ALLOY 6063 ALUMINUM PROFILES**", by PESSUTTO, Ana Carla, and JONKO, Eliena. From the *Universidade de Caxias do Sul*. DOI: 10.48141/SBJCHEM.v29.n31.2021.03_PESSUTTO_pgs_21_36.pdf. The authors will be contacted for the details.

Eduardo Goldani, Ph.D., Brazil, TQG. Chair of the conference.

Walter José Peláez, PhD, Argentina, UNC. General Secretary.

Luis Alcides Brandini De Boni, Ph.D., Brazil, TQG. Co-Chair of the conference. Event Treasurer.